ELECTROFORMATION AND CHARACTERIZATION OF Al_2O_3 EMBEDDED NICKEL MATRIX COMPOSITE COATINGS

A THESIS SUBMITTED TO
THE GRADUATE SCHOOL OF NATURAL AND APPLIED SCIENCES
OF
MIDDLE EAST TECHNICAL UNIVERSITY

BY

OLGUN YILMAZ

IN PARTIAL FULFILLMENT OF THE REQUIREMENTS
FOR
THE DEGREE OF MASTER OF SCIENCE
IN
METALLURGICAL AND MATERIALS ENGINEERING

AUGUST 2018

Approval of the thesis:

ELECTROFORMATION AND CHARACTERIZATION OF Al_2O_3 EMBEDDED NICKEL MATRIX COMPOSITE COATINGS

submitted by **OLGUN YILMAZ** in partial fulfillment of the requirements for the degree of **Master of Science in Metallurgical and Materials Engineering Department, Middle East Technical University** by,

Prof. Dr. Halil Kalıpçılar _____
Dean, Graduate School of **Natural and Applied Sciences**

Prof. Dr. Cemil Hakan Gür _____
Head of Department, **Metallurgical and Materials Engineering**

Prof. Dr. İshak Karakaya _____
Supervisor, **Metallurgical and Materials Eng. Dept., METU**

Assist. Prof. Dr. Metehan Erdoğan _____
Co-Supervisor, **Metallurgical and Materials Eng. Dept., AYBU**

Examining Committee Members:

Prof. Dr. Kadri Aydınol _____
Metallurgical and Materials Engineering Dept., METU

Prof. Dr. İshak Karakaya _____
Metallurgical and Materials Engineering Dept., METU

Assist. Prof. Dr. Batur Ercan _____
Metallurgical and Materials Engineering Dept., METU

Assist. Prof. Dr. Metehan Erdoğan _____
Metallurgical and Materials Engineering Dept., AYBU

Assist. Prof. Dr. Erkan Konca _____
Metallurgical and Materials Engineering Dept., Atılım U.

Date: 17/08/2018

I hereby declare that all information in this document has been obtained and presented in accordance with academic rules and ethical conduct. I also declare that, as required by these rules and conduct, I have fully cited and referenced all material and results that are not original to this work.

Name, Last name: Olgun Yılmaz

Signature :

ABSTRACT

ELECTROFORMATION AND CHARACTERIZATION OF Al_2O_3 EMBEDDED NICKEL MATRIX COMPOSITE COATINGS

Yılmaz, Olgun
MSc, Department of Metallurgical and Materials Engineering
Supervisor: Prof. Dr. İshak Karakaya
Co-supervisor: Assist. Prof. Dr. Metehan Erdoğan

August 2018, 103 pages

The mechanical and tribological properties of electrochemical coatings can be enhanced by embedded second phase particles to nickel matrix. Two different anionic surfactants sodium dodecyl sulfate (SLS) and ammonium lignosulfonate (ALS) were used together to adjust the wetting conditions and provide suspension of Al_2O_3 particles in a nickel sulfamate electrolyte in this study. High performance atomic force microscope (hpAFM), X-ray diffraction (XRD), X-ray fluorescence (XRF), scanning electron microscope (SEM) and deposit stress analyzer were used to characterize the composite coatings. The effects of current density and amounts of the two surfactants and alumina particles in the electrolyte on wear rate, coefficient of friction (COF), and hardness were studied. It was found that the amount of incorporated Al_2O_3 dominantly affected the properties of coatings which could be controlled by adjusting the operating parameters. Although combined effects of the surfactants and current density on mechanical and tribological parameters were unpredictable in some cases, the composite coatings possessed superior properties than pure nickel. The presence of alumina particles in the composite coating increased the residual stress. Moreover, it resulted in preferentially oriented and finer nodular grains instead of regular morphology.

Keywords: Electrodeposition, Ni/Al_2O_3 composite coating, wear resistance, friction coefficient, residual stress, crystallography

ÖZ

Al_2O_3 GÖMÜLÜ NİKEL MATRİSLİ KOMPOZİT KAPLAMALARIN ELEKTROLİZLE ŞEKİLLENDİRMESİ VE KARAKTERİZASYONU

Yılmaz, Olgun
Yüksek Lisans, Metalurji ve Malzeme Mühendisliği Bölümü
Tez Yöneticisi: Prof. Dr. İshak Karakaya
Ortak Tez Yöneticisi: Dr. Öğretim Üyesi Metehan Erdoğan

Ağustos 2018, 103 sayfa

İkinci faz parçaların nikel matrise gömülmesiyle kaplamanın mekanik ve yüzey özellikleri geliştirilebilir. Bu çalışmada, Al_2O_3 tozlarını nikel sülfamat kaplama banyosunun içinde yüzeyinin ıslanabilmesi ve askıda tutabilmek için sodyum dodesil sülfat (SLS) ve amonyum lignosülfonat olmak üzere iki ayrı anyonik eklenti kullanılmıştır. Üretilen kaplamaların karakterizasyonu için yüksek performans atomik kuvvet mikroskobu (hpAFM), X-Işını kırınımı (XRD), X-Işını floresans (XRF), taramalı elektron mikroskopu (SEM) ve iç gerilim ölçme cihazı kullanılmıştır. Akım yoğunluğu, çözeltide bulunan eklenti ve alümina miktarlarının aşınma sürtünme sertlik üzerindeki etkileri incelenmiştir. Kaplamaya giren alümina tozlarının kaplama özelliklerini önemli oranda etkilediği ve bunun deney parametreleriyle kontrol edilebildiği bulunmuştur. Bazı durumlarda parametrelerin beklenmedik etkilerinin bulunmasına rağmen, üretilen kompozit kaplamalar saf nikel kaplamalardan çok daha iyi özelliklere sahip olmuştur. Kaplama giren alümina tozları kaplamanın kalıntı gerilimini de arttırmaktadır. Bununla beraber, tozlar matrisin tane yapısında bir yönelmeye ve daha küçük aynı zamanda küresel tane yapılarına sebep olmaktadır.

Anahtar Kelimeler: Elektrokaplama, Ni/Al_2O_3 kompozit kaplama, aşınma direnci, sürtünme katsayısı, kalıntı gerilim, kristalografi

To my family, friends and Sezen

I am deeply indebted to my parents.

ACKNOWLEDGEMENTS

I would first like to thank my thesis advisor Prof. Dr. İshak Karakaya and co-advisor. Assist. Prof. Dr. Metehan Erdoğan. The door to Professors' office was always open whenever I ran into a trouble spot or had a question about my research or writing. They consistently allowed this paper to be my own work, but steered me in the right the direction whenever they thought I needed it.

Besides my advisor, I would like to thank the rest of my thesis committee: Prof. Dr. Kadri Aydınol, Assist. Prof. Dr, Batur Ercan and Assist. Prof. Dr, Erkan Konca for their encouragement, insightful comments, and hard questions. In addition, the authors acknowledge the Middle East Technical University (METU) for partial support provided through the project BAP-03-08-2017-002 and Turkish Aerospace Industries (TAI) for their financial support.

I thank my fellow labmates in TempLab: Mustafa Serdal Aras (MSA), Bilgehan Çetinöz, Esra Karakaya, Çağlar Polat, Atalay Balta, Berkay Çağan, and Elif Yeşilay for the stimulating discussions, their help and support, and for all the fun we have had in the last three years. Also I thank my friends in the department: Bersu Baştuğ and Başar Süer.

I must express my very profound gratitude to my brother/sister–like friends Latif Çandır, Dilara Doğan, Baran Kaya, İlhan Şenol, and Elif Su Tanyeri for their support and sincere friendship. I must express my very profound gratitude to Sezen Bostan for providing me unfailing support, continuous encouragement and deep love throughout my years of study. This accomplishment would not have been possible without her.

Last but not the least, I would like to thank my family for giving birth to me at the first place and supporting me spiritually and continuous encouragement throughout my life.

TABLE OF CONTENT

LIST OF TABLES

TABLES

LIST OF FIGURES

FIGURES

CHAPTER 1

INTRODUCTION

Commenting on electrodeposition, Schwarzacher argues 'Electrodeposition is a technology for the future' [1]. The history of the electroplating technology has been dated for over 200 years. Although it has been played an important role in the maintenance of the production industry such as electronic, automotive or aerospace, the physical process of the electrodeposition has no drastic changes for about 100 years [2,3]. Ni, Cu, Zn, Au, Ag, Cr, Cd, Co and additionally Cu-based and Zn-based alloys are generally used metals for commercial electrodeposition processes [4]. Among all these metals mentioned above, nickel has a huge consumption about 100,000 metric tons globally as a metal form and its salts for electroplating [5]. In other words, it is still a prevalently used and multi-functional metal for surface finishing processes. It plays a very big role in the industry. The scope of utilization of nickel electrodeposition has been divided into three categories: decorative, functional and electroforming [6]. It has some advantages as follows [7][8]:

i. High chance to produce materials having complex shape and using different substrates
ii. Less production time due to higher deposition rate with low cost
iii. Easily controlled composition for the deposition of alloys
iv. Coatings having high purity without porosity
v. Wide thickness range from *nm* to *mm*
vi. Suitable for industrial applications
vii. No treatment after deposition

If the purpose is not about the decorative, nickel and nickel based coatings such as alloys and especially nickel based composite coatings can be used to enhance wear

behavior, hardness of the coating or to modify magnetic properties or to improve other tribological properties such as surface roughness or friction behavior of the coating. The process in which dispersed small particles in the electrolyte are incorporated with deposited metal onto substrate and embedded to metallic matrix is called electrocodeposition as schematically shown in Figure 1 [9]. It is actually the combination of two processes: electrophoretic and electroplating. The particles are suspended and deposited onto substrate materials due to electric field in the electrophoretic deposition; however, the electrocodeposition process is more sophisticated, which the suspended particles in the electrolyte are deposited and incorporated with metal ions to form metal matrix composite coatings [10]. These types of coatings are typically applicable to the areas where high hardness or strength, lubricated surface, high corrosion resistance and protection against wear are needed [11–15].

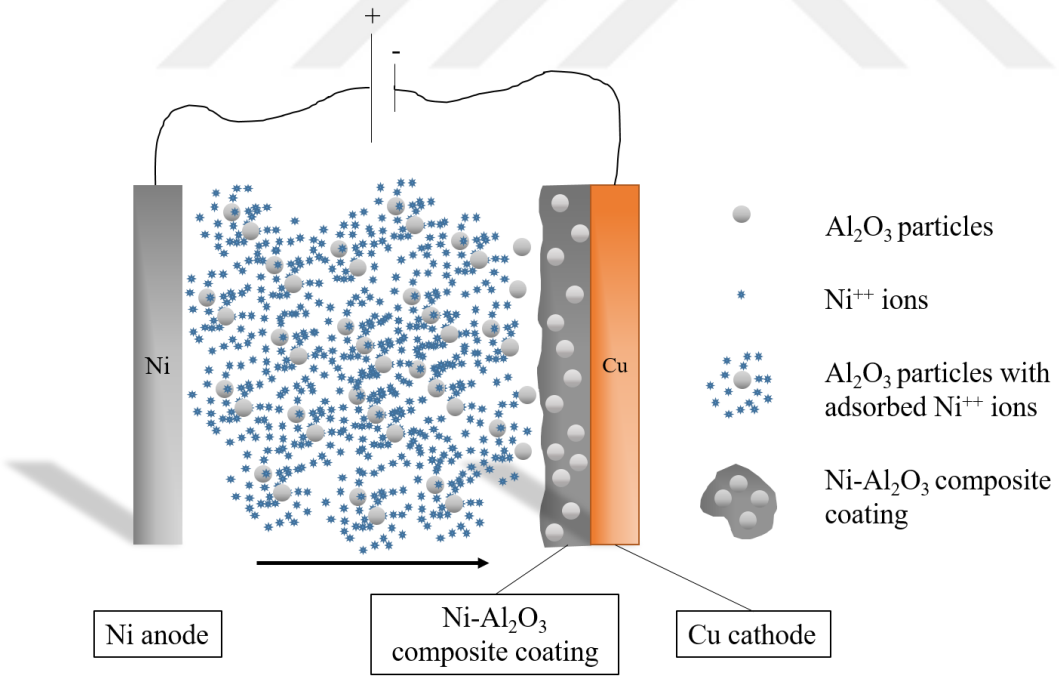

Figure 1 Schematic electrochemical cell for electrocodeposition [9]

When compared to other coating methods, electrocodeposition has several advantages which are homogeneous coating thickness even for complex shapes, decreasing waste in comparison with dipping and spraying methods, reduction of contamination, more capability of functionally-gradient material formation [9]. The composite coatings produced by electrodeposition methods are generally used in the automotive, electronics, biomedical, space and telecommunication due to their superior properties [16]. The properties are determined with respect to type, shape size and concentration of the second phase particles.

Electrocodeposition process and the properties of the composite coatings can be influenced by variable parameters such as hydrodynamics, temperature, pH, additives, bath compositions and particle type/concentration. Although many studies in the literature have been reported to figure out the effect of each operating parameters, there are often discrepancies in results. The reason of these contradictories are the interrelation of the parameters and their effect for different systems. More detailed information for the effects of process parameters and the interrelations between them will be given in the following Chapters.

The main aim of the study is to determine the effects of operating parameters such as current density, the amount and the kind of the surfactants and the amount of particle in the suspension on the mechanical and the tribological properties of the Ni-Al_2O_3 composite coatings. Surface roughness, wear resistance, friction coefficient, and hardness were the parameters investigated. Two different types of surfactants sodium lauryl sulfate (SLS, this is also referred as SDS – Sodium dodecyl sulfate) and ammonium lauryl sulfate (ALS) were used and the effects of their combination for different amounts were studied as well. The microstructural investigation and the characterization of the composite coating were done. In addition, the effects of pH, coating thickness, current density and the amount of ALS on residual stress of the composite coating was investigated so that the composite coatings having a minimum residual stress can be produced. In addition, the effect of the addition of alumina particles and the surfactant to sulfamate plating solution on the potential of nickel

deposition were studied. All experiments were designed by Minitab software using full-factorial statistical design to find the statistical results of the whole experiments.

CHAPTER 2

LITERATURE REVIEW

2.1 Fundamental Concepts and Basic Terms

The definition of *electrodeposition* indicates that the growth of layer or film is materialized onto the substrate material by the electrochemical reduction of metal ions [17]. Despite of not appearing in the cell reaction, the electron transference for *reduction* and *oxidation* always take place from one to another in the electrochemical reaction. There are three types of electrochemical reactions with respect to their oxidation states which are redox reactions, oxidation reactions and reduction reactions. In redox reactions, both reduction and oxidation reactions take place together. While it is the loss of electrons by atoms or elements in the oxidation reactions, the reduction reactions are exactly the reverse of the oxidation reactions, which means gaining the electrons by atoms or elements. Those reactions take place in the *electrolyte* which is the term of the first use by the Swedish chemist Svante Arrhenius [18]. It is the ionic conductor solution including dissociation of ions which are positively charged called *cation* (M^{Z+}) and negatively charged called *anion* (A^{Z-}). In addition to that, electrodes are used to provide metallic conduction in the conducting system. The electrode that the oxidation reaction takes place is *anode* while the *cathode* is another type of the electrode where the reduction reaction occurs. Following reactions (2.1) and (2.2) indicate the metal and nickel formation from schematic MA metal salt and a nickel sulfamate, respectively, in a neutral solution:

$$MA + ze^- \rightarrow M_{(s)} + zA^- \tag{2.1}$$

$$\mathrm{Ni(NH_2SO_3)_2} + 2\mathrm{e^-} \rightarrow \mathrm{Ni_{(s)}} + 2\mathrm{NH_2SO_3^-} \tag{2.2}$$

There are two different types of operating electrochemical cells *galvanic cells* and *electrolytic cells*. A galvanic cell includes the spontaneous cell reaction with externally connected electrodes and generally used by conversion from chemical energy to electrical energy [19]. However, an electrolytic cell needs an external electrical energy higher than the open-circuit potential of the cell for the reaction to take place [19]. Figure 2 shows the difference schematically between the systems of galvanic and electrolytic cells.

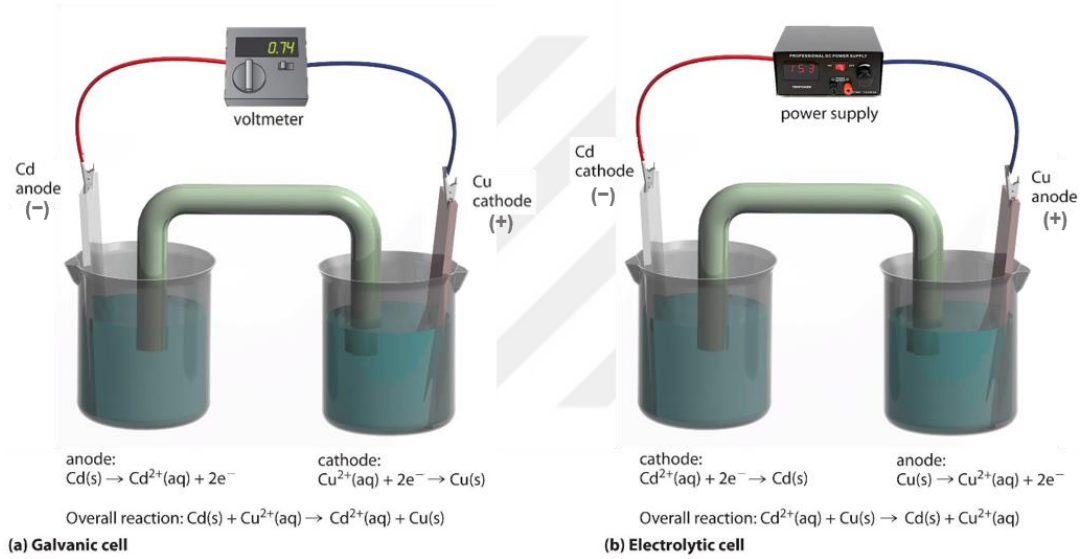

Figure 2 Schematical representation of (a) galvanic and (b) electrolytic cells

In electrolytic cells, there is a relation between faradaic current and the amount of deposition as following Eq. 2.3 [19]:

$$\frac{Q\ (coulombs)}{zF\ (\frac{coulombs}{mol})} = N(mol\ electrolyzed) \qquad (2.3)$$

where Q is the charge passed through the system (It), z is the number of electrons transferred in the electrode reaction and F is the Faraday's constant. In

electrodeposition processes, the thickness is one of the critical parameters that needs to be controlled with respect to the desired specifications of the product. In addition, above equation can be modified to determine the actual deposited weight which is related to the thickness of the coating due to using certain area and known density of deposited metal, which is following Faraday's rule:

$$W = \rho hA = \frac{MIt}{zF} \times (CE) \tag{2.4}$$

where W is the deposited weight over selected area (in grams, g), M is the molecular weight for the deposited metal, I is the average current (in amperes, A), t is the duration for deposition process (in seconds, s), z is the number of electrons transferred in the cell reaction, CE is the current efficiency which can be calculated as Eq. 2.5. The deposited weight can be calculated as multiplication of the density of metal "ρ", the thickness of the deposit "h" and the area of deposit "A".

$$Current\ Efficiency\ (CE) = \frac{W_{actual}}{W_{theoretical}} \tag{2.5}$$

The cell reaction takes place in an electrolytic cell is non-spontaneous. The nature of the cell reaction can be determined from calculation of the Gibbs energy change under constant T and P using Eq. 2.6:

$$\Delta G° = -zFE° \tag{2.6}$$

where z is the number of valance electrons, F is the Faraday's constant, and $E°$ (emf) is the difference of potentials of electrodes. However, since above potential difference is expressed for the standard states, the theoretical voltage which is required for the deposition of the metal ions onto cathode material is different. The theoretical cell potential under electrolysis conditions, E_{rxn} can be calculated by Nernst Equation in Eq. 2.7:

$$E_{rxn} = E^o + \frac{RT}{zF} ln \frac{\Pi\ a_{(ox)}}{\Pi\ a_{(red)}} \tag{2.7}$$

where E^o is the standard emf of the cell and a denotes the activities of ions in the solution. However, the applied voltage differs from theoretical voltage since the electrodes are polarized due to overpotentials. Following applied voltage in Eq. 2.8:

$$E_{app} = -E_{rxn} + IR + \eta_{act} + \eta_{conc} \tag{2.8}$$

where E_{app} is the total applied voltage, IR is voltage drop due to the ohmic resistance, η_{act} is the activation overpotential and η_{conc} is the concentration overpotential. Ohmic resistance is due to electrolyte, external connection elements and electrodes. It results in requirements of additional potential to operate the cell. It is called resistance overpotential or ohmic overpotential and it is more dominant with increase in distance between anode and cathode [20].

The reaction potential is the potential which is high enough for cell to become reversible. However, it is clearly seen in Eq. 2.8 that the reaction potential is not enough for the operation of cell due to additional resistance. In addition to this, the sign of the overpotential is positive at the anode while it is negative at the cathode as shown in Figure 3 [21].

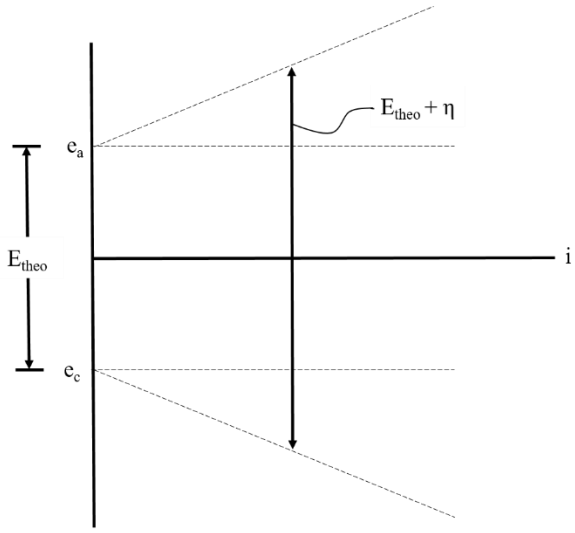

Figure 3 The overpotential of anode and cathode and the effect on theoretical cell potential

Since the metal ions are continuously reduced at the cathode, their concentration decreases near the cathode during the electrodeposition. Therefore, the reversible potential decreases and this results in the concentration overpotential expressed in Eq. 2.9:

$$\eta_{conc} = \frac{RT}{zF} \ln \frac{C_e}{C_0} \tag{2.9}$$

where C_e the ion concentration next to the electrode surface and C_0 is the unchanged ion concentration in the electrolyte. Operating condition of the electrolyte such as agitation, operating temperature, ion concentration or the geometry of cathode is very important to concentration overpotential [20]. The concentration overpotential decreases with agitation and at higher temperatures due to homogeneous ionic distribution in the electrolyte and easier ionic diffusion [20].

There is an additional kinetic barrier required to be exceeded for the reaction to proceed, which is called activation overpotential [22]. It is also a part of the total overpotential and the logarithmic function with respect to current density as shown in Eq. 2.10:

$$\eta_{act} = \frac{RT}{\beta zF} \ln \frac{i}{i_0} \tag{2.10}$$

where β is the electron transfer coefficient $(0 < \beta < 1)$, i is the current density and i_0 is the exchange current density. According to the following equation, the current density gets higher exponentially with the negative overpotential values for cathodic processes $(\eta \geq 100\ mV)$ [22]:

$$i = -i_0 e^{-\alpha z f \eta} \tag{2.11}$$

and for anodic processes meaning that overpotential is a positive value:

$$i = -i_0 e^{-(1-\alpha) z f \eta} \tag{2.12}$$

where α is the transfer coefficient and f can be calculated with respect to temperature as:

$$f = \frac{F}{RT} \tag{2.13}$$

Considering Eq. 2.11 and 2.12, if there is no overpotential, current density is directly equal to exchange current density which means that there is a constant charge exchange at the metal solution interface [22]. In addition, the logarithms of those two equations can be modified in terms of η, the Tafel equation can be obtained as following [22]:

$$\eta = a \pm b \log|i| \tag{2.14}$$

where a and b are the constants. The $\pm$ sign depends on the anodic and cathodic reactions respectively [22]. In addition, a and b constants for the cathodic processes can be expressed as:

$$a = \frac{2.303RT}{\alpha zF} \log i^{o} \tag{2.15}$$

$$b = \frac{2.303RT}{\alpha zF} \tag{2.16}$$

Figure 4 shows the Tafel plot which is a straight line for large overpotential values for the copper electrodeposition.

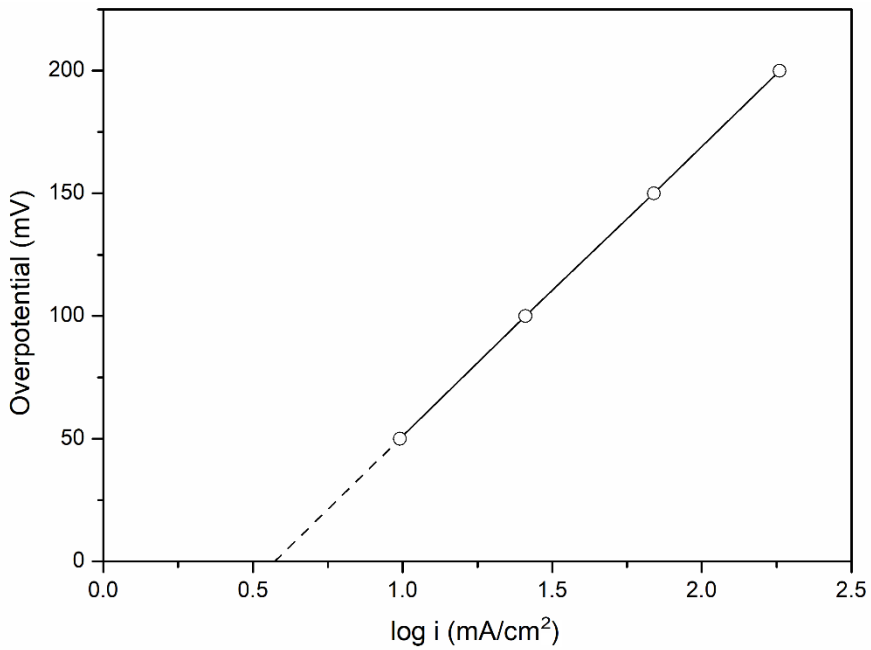

Figure 4 Tafel plot for electrodeposition of copper $\eta = f(\log i)$ [23]

2.2 Nickel Electrodeposition

The references prove that Bird in 1837 developed nickel deposition from its aqueous solution of nickel chloride and sulfate. Moreover, Shore in 1840 registered the patent of nickel deposition from its nitrate solution [24,25]. However, the well-known developer of nickel plating is Bottger and he developed the nickel and ammonium sulfates solution in 1843, which was used for about 70 years for commercial nickel plating [26]. Furthermore, the most frequently used nickel plating bath for commercial nickel electrodeposition is the Watts solution which was developed by Professor Oliver P. Watts from University of Wisconsin in 1916 [27]. It is the combination of nickel chloride, boric acid, nickel sulfate and balance water. Watts solution is popular and especially used for decorative purpose. However, the domination of Watts solution is being gradually substituted by sulfamate solution [28]. Nowadays, these both nickel plating solutions are used together for commercial nickel plating processes and for

electroforming. On the other hand, the sulfamate solution is even more popular owing to its more applicability to electroforming processes due to its lower residual stresses, higher deposition rates, and uniform distribution of metal on cathode due to higher conductivity of solution. In addition to this, among other plating solutions, the highest purity of Ni with better ductility can be obtained using sulfamate solution. Watts and sulfamate electrolytes, operating conditions and mechanical properties of deposits are shown in Table 1 [29].

Table 1 Nickel deposition solutions [6]

Composition of the Electrolyte (g/l)		
Plating Bath	Watts solution	Sulfamate solution
Nickel sulfate	225 – 400	–
Nickel sulfamate	–	300 – 450
Nickel chloride	30 – 60	30 – 45
Boric acid	30 – 45	0 – 30
	Operating Conditions	
Temperature, ℃	44 – 60	32 – 60
Cathode current density (A/dm^2)	3 – 11	0.5 -30
pH	2 – 4.5	3.5 – 5.0
	Mechanical Properties	
Tensile strength (MPa)	345 – 435	415 – 610
Elongation (%)	10 – 30	5 – 30
Residual stress (MPa)	125 – 185 (tensile)	0 – 55 (tensile)
Hardness (HV-100g load)	130 – 200	170 – 230

A typical Ni electroplating cell is shown in Figure 5. Dissolution reaction takes places at the anode while the dissolved metal ions are deposited onto cathodes due to the fact that the current which passes through the anode and the cathode [30]. The electrolyte is a conductive aqueous solution including dissolved nickel salt which is nickel sulfamate in this case. The nickel sulfamate is the main source of the nickel ions [31]. Boric acid is used to operate the solution in the suitable pH range [32] while the nickel chloride is used to maintain the anode efficiency at the optimum levels, increase the

solution conductivity and to obtain uniform metal distribution at the cathode. According to Char and Sathyanarayana, the anode efficiency is equal to 60-80% without any nickel chloride and almost 100% with the addition of 0.20 g/l nickel chloride [33]. In addition, the amount of the nickel chloride is important due to its effect on the residual stress of the coating [34]. In other words, since nickel chloride increases the solution conductivity, the residual stress resulting from the forces between deposit and impurity atoms increases as well.

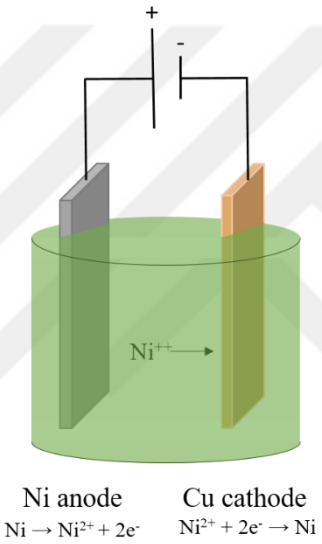

Figure 5 Schematical representation of a typical nickel plating cell

The coating thickness of the whole part which is electrodeposited depends on the current density distribution on the cathode. The distribution of the current density may strongly be influenced by the cathode geometry and the anode-cathode positions [6,35]. In other words, the current density cannot be homogeneous on the complex geometries including some sharp tips or recessed surfaces. Therefore, it can be modified and the current distribution can be homogenized by using nonconductive

shields to prevent the current density to be lower at the sharp tips or edges and by changing the anode-cathode positions using some computer modelling [35].

Other than the distribution of the current density, the cathode overpotential and the conductivity of the electrolyte have an effect on the thickness distribution of the metal [36]. The relation between all those parameters which influence the metal distributions is called *throwing power*. In other words, the higher throwing power provides the coating to have more homogeneous thickness independent from the cathode geometry. In addition, it is possible to have better throwing power with decreasing current density, and with increasing the conductivity of the electrolyte, the anode – cathode distance, pH and the operating temperature [37]. The addition of the anhydrous sodium sulfate to the electrolyte was carried out by Watson in 1960 and to modify the throwing power [38].

The adhesion of the coating to substrate is very important except for electroforming processes. It is about the crystal structure consistency between deposited metal and the substrate material. Since it is not generally seen the epitaxial growth of coating, the adhesion is typically possible because of the cohesive forces between atoms [6]. The atoms of the deposit are held to surface with covalent, ionic, metallic, polar or other bonds. To achieve good adhesion behavior, some preparation steps are standardized by ASTM [39].

Due to the standard potential of nickel and hydrogen as shown in Eq. 2.17 and 2.18, hydrogen discharge is more likely than the nickel reduction [32]. However, the nickel can be deposited since the hydrogen has a large overpotential. Moreover, during electrodeposition of nickel metal, since some of the current is consumed by the hydrogen ion in the electrolyte to discharge, cathode efficiency must be less than 100% [6,34]. In addition, the presence of boric acid in the electrolyte used as a catalyst for the nickel reduction at cathode and pH buffer reduces the hydrogen evolution [40]. The cathode efficiency increases with increase in activity of nickel ions, pH, temperature and current density [41].

In addition, hydrogen evolution results in increasing the residual stress [40] and the hydrogen embrittlement with an excess amount of hydrogen being exposed to deposited metal. Hydrogen embrittlement may take place due to the easily diffusion of hydrogen along the grain boundaries, which causes the embrittlement with ease due to hydride formation with some metals such as titanium, vanadium, zirconium, tantalum and niobium [42].

$$2H^+ + 2e^- \rightarrow H_{2(g)} \quad e^\circ = 0\ V \tag{2.17}$$

$$Ni^{+2} + 2e^- \rightarrow Ni_{(s)} \quad e^\circ = -0.25\ V \tag{2.18}$$

2.3 Deposition of Composite Coatings (Electrocodeposition)

Improvements for materials with sophisticated properties and unique characteristics have shown a forceful change after the introduction of composite materials. In addition to this, manufacturing methods for the composite materials have also shown a drastic change. Metal matrix composite (MMC) coatings can be formed by electrochemical deposition called electrocodeposition. It is an unconventional manufacturing method for producing metal matrix composites, which involves embedding of reinforcement particles into a metal matrix coating. These coatings can be used in the areas like aerospace, defense and automotive industries where improved mechanical, physical and/or tribological properties are needed [3]. Depending on the second phase particles used as the reinforcement, a particular mechanical or physical property such as corrosion resistance, stiffness, hardness, wear resistance and COF can be enhanced [43]. The second phase particles are generally incorporated with the metal matrix such as Ni, Cu, Co, Cr and their alloys [9,14]

As mentioned above, the coatings include particles whose sizes in diameter are from nano-level to 100 μm and the amount of those particles of either pure metals, or non-metallic materials such as ceramics and organic materials change from 2 to 200 g/l, which results in production of composite coatings generally having 1–10 vol.% particle content in the coating [44–48]. In general, improvements of the mechanical

properties of metal coatings are possible with the embedded hard ceramic particles or oxide particles to metal matrix. Incorporation of materials such as diamond, WC or SiC results in improvement of wear resistance of metal coatings [49–51]. The corrosion resistance of the composite coating increases with the second phase particles such as V_2O_5, TiO_2, and Cr_2O_3 [52–54]. The incorporation of the particles of MoS_2, PTFE having hexagonal crystal structure act as a solid lubricant and critically decrease the friction coefficient of the composite coating [55].

From the other researches in the literature, it is typically observed that the electrocodeposition process in its own mechanism has many parameters or variables such as current density, bath composition, pH, operating temperature, the characteristics of the second phase particle, which influence the amount of particle in the matrix. However, there are so many contradictory results from those researches for those process parameters [9]. Their effect on the composite coating is not the same and it may change with respect to the electrolyte–particle system and the cell for the deposition [9].

2.3.1 General Process Mechanisms of Electrocodeposition

The general mechanism of the electrocodeposition is very similar to that of electrophoretic deposition except for some steps [10]. In electrophoretic deposition, charged particles in the electrolyte are carried by electric field and then deposited to cathode surface by some forces such as chemical bonding or van der Waals forces [9]. On the other hand, electrocodeposition is different from the electrophoretic deposition since the particles are deposited with the metal at the same time and encapsulated particles with metal ions have better adhesion to cathode [9,56]. Furthermore, the entrapped particles are embedded to metal matrix. Martin and Williams [57] pointed out that the electrocodeposition is just the mechanical encapsulation of the particle with the metal. Moreover, Snaith and Groves [58] agree with them and they support the previous idea. Other studies claimed that the particles are adsorbed by electrodes [59,60].

Guglielmi in 1972 pursued with his further researches about two steps of this adsorption for the general process mechanisms of electrocodeposition [61]. The particles are encapsulated by the combination of adsorption of particles and then their electrochemical reduction. Guglielmi expressed a relation between the amount of particles in the electrolyte and coating as shown in following Eq. 2.19:

$$\frac{C}{\alpha} = \frac{M \times i}{z \times F \times \rho \times V_0} \exp\big(\eta(a-b)\big)\left(\frac{1}{k} + C\right) \qquad (2.19)$$

where α ($vol\%$) is the amount of particle in the codeposit, η (V) is overpotential, a and b are constants of Tafel equation (in V^{-1}) for metal and particle deposition, respectively, C ($vol\%\ or\ g\ l^{-1}$) is the amount of particle in the electrolyte, ρ ($g\ cm^{-3}$) is the density of deposited metal, F ($C\ mol^{-1}$) is Faraday's constant, i_o ($A\ dm^{-2}$) is the exchange current density, k ($1\ g^{-1}\ or\ vol\%^{-1}$) is the coefficient of adsorption, M ($g\ mol^{-1}$) is the molecular weight of the deposited metal, z is the valance of deposited metal, V_o ($dm\ s^{-1}$) is the constant for particle deposition.

Other than Guglielmi's model, various studies that applied models explaining how the electrocodeposition mechanisms work were carried out. The whole models such as Guglielmi [61], Buelens [62,63], Valdes [64] and Eng [65] cannot explain why the particles are deposited into metal matrix. They all assumed that the particles are adsorbed by ions and ions are reduced at cathode. Therefore, the particles are codeposited to metal matrix. On the other hand, Fransaer's model [66,67] had the deficiency of the descriptions but his study agreed that the reason of the codeposition is the adhesion force between particle and electrode. The additional model from Bercot in 2002 [68] was brought forward for Ni-PTFE system as the enhancement for Guglielmi's model. The difficulties in explaining the mechanisms of the electrocodeposition process are coming from the geometrical assumptions for which particles are spherical in shape and flat surfaces. However, the considerations of the heterogeneous geometries are of vital importance for modelling its mechanisms. In 2000, Vereecken *et al.* have been advanced another model for Ni-Al_2O_3 system [69]. It was indicated that the particle concentration or its transportation depended on the

convective diffusion. The effect of current density on the gravitational force and hydrodynamics of particles was explained. It is applicable if and only if particle is smaller than the diffusion layer shown in Figure 6.

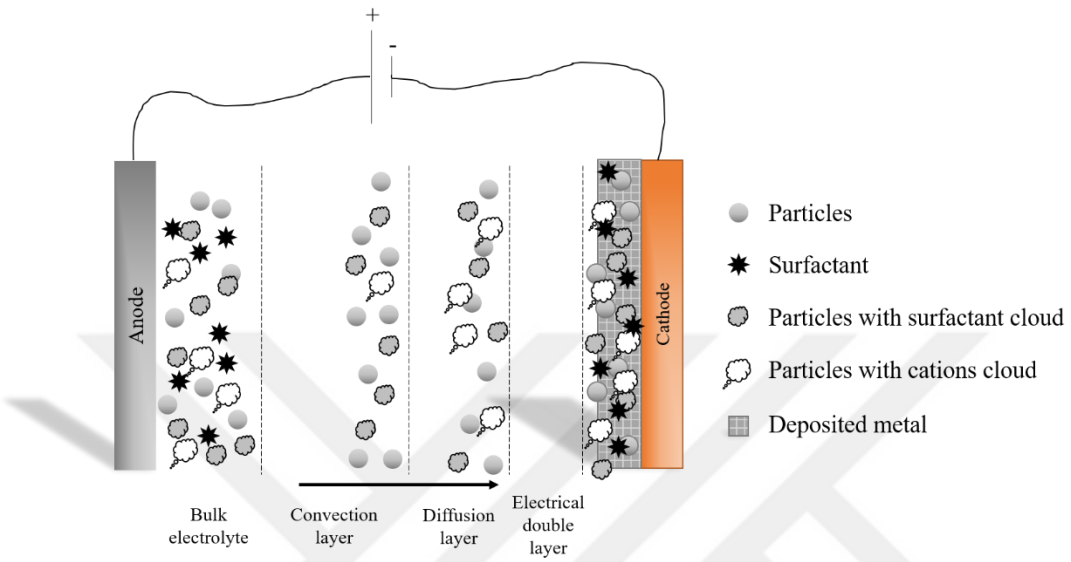

Figure 6 Schematic drawing of the general mechanism of electrocodeposition processes [70]

2.3.2 Ni-Al_2O_3 Composite Coatings

The incorporations of Al_2O_3 with metal coatings are popularly formed to enhance the mechanical, tribological and physical properties. The alumina particles embedded to nickel matrix has a critical effect on hardness, friction behavior, wear resistance and corrosion resistances. All those property changes are related to the amount of Al_2O_3 particles in the coating. In the literature, many researchers have studied on how operating parameters affect the particle content and how the particle content affects the other properties [8].

It is stated that the hydrodynamics of the electrolyte during the deposition has a strong effect on the amount of Al_2O_3 content in the coating and the distribution through the surface [71]. Inert particles have a strong tendency to agglomerate in the plating

solutions which have high ionic strength [72]. Nano-Al_2O_3 particles used with SLS as an anionic surfactant in nickel sulfamate solution increased the hardness and gave better hardness result at 0.125 g/l SLS addition to the plating bath [73]. In another study [74], the electrodeposition of Ni-Al_2O_3 composite coatings from Watts solution with a cationic surfactant hexadecylpyridinium bromide (HPB) was investigated. The zeta potential increased with the addition of HBP up to a certain concentration of HBP (150 mg/l), which resulted in a composite coating with a higher hardness and better wear resistance. However, after 150 mg/l HBP, mechanical properties deteriorated [74]. Al_2O_3 powders can be synthesized by different methods and each method yields different phases of alumina; α, γ, and δ. Better mechanical properties were obtained when α-Al_2O_3 powder was used as the reinforcement material when compared to other phases [75]. The amount of Al_2O_3 in the nickel matrix is directly related with the mechanical properties and morphology. Hardness and wear resistance increase with increasing the amount of alumina while the COF decreases which means alumina acts as a sort of solid lubricant [76]. Furthermore, increase in the amount of alumina results in decreasing grain size which is another reason for increase in hardness of the nickel coatings due to grain boundary strengthening [76].

There are several studies in the literature for electrocodeposited Ni-Al_2O_3 composite structures. Most of these studies focused on Watt's plating bath and only some of them are cited here [74,76–80]. There are comparatively fewer studies for sulfamate plating bath [73,75,81–84] and none of these studies used ALS as the surfactant agent.

2.4 The Effect of Operating Parameters

The operating parameters such as current density, pH, the amount and the characteristics of the second phase particles, additives and the hydrodynamics are critically important to produce composite coating having desired properties. The relation and interrelation between these parameters are very complicated and hard to be modelled. Therefore, a few studies are concentrated on the reproducibility of electocodeposited particle concentration of the coatings [67,85]. Some of the studies

focused on the regulation of the hydrodynamic effects by giving rotational movement to electrodes [48,86–89]. Many researchers studied on how to find the particle content in the coating by using some analytic methods such as gravimetric analysis [90,91], XRF [48], atomic absorption spectroscopy [92–94] and other microscopy techniques [95,96]. One of the studies mentioned the ability to determine the content of the particles with 0.02 wt% sensitivity and a proper accuracy [93].

2.4.1 Current Density (*i*)

The current density is probably the most researched portion of electrocodeposition [97]. The current density has so much importance on metal deposition rate and the amount of incorporated particles [98]. As mentioned in the previous parts, the effect of operating parameters depends on the type of the particle-electrolyte system and there may be contradictions between the studies for different particle-electrolyte systems. While the amount of particle incorporation increased with increasing current density in Ni-TiO_2 system [99], it decreased for Ni-diamond [100] and Ni-Cr [100]. The amount of incorporated particles has been observed as the minimum value at lower current densities when the particle concentration in the electrolyte exceeded 100 g/l for Cr-Al_2O_3 system [101]. Roos *et al.* [70] observed that when the incorporated particle content was maximum, the current density was 2 A/dm^2 for copper-γ-Al_2O_3 system, which was correlated with their model depending on the statistical determination of the particle content. It was observed in Ni-Al_2O_3 system [78] that the embedded particle content reached the maximum value upon increasing the current density to 1 A/dm^2 and then dramatically diminished to lower values with further increasing the current density. Apart from these studies, it was claimed that there was no relation between current density and the embedded $BaCr_2O_4$ content in nickel matrix [102]. Some studies have reported analyses of trends in current density and the incorporation of the particles with metal matrix that the relation between those two can be divided into three different steps; instant increasing with increase in current density followed by dramatic decrease and then coming to the stabilization and a little decreasing with further increasing of current density [86,103].

Other than the effect of current density on particle content, several studies showed that particles in suspension affects the current density itself due to polarization on cathode. Some studies stated that the presence of the particles resulted in cathode depolarization by using the same potential differences [47,88,104,105]. Furthermore, the reduction of metal ion at cathode was hindered by the presence of particles closer to cathode at low overpotentials [106]. On the other hand, the improvements of carrying of metal ions due to the existence of the particles close to cathode occurred at high overpotentials [107,108].

2.4.2 Operating Temperature and Potential of Hydrogen (pH*)*

It is argued that there was no impact of the operating temperature on particle concentration of the coating for Ni-Al_2O_3 system [105,109]. On the other hand, for other systems such as graphite and chromium matrix, the influence of the temperature was observed that increase in embedded particle to Cr matrix occurred upon heating the plating bath to 50℃ [110]. Unlike Cr-graphite system, heating to 50℃ had a negative impact on particle content for the Cr-Al_2O_3 system [111]. In addition, it was stated that the maximum particle content was achieved at 50℃ for Ni-V_2O_5 system [112]. Ouyang *et al.* revealed no temperature impact on embedded particle content for nickel - $BaCr_2O_4$ composite coating [102].

The influence of pH is not that important on the incorporation of inert particles as long as the pH is higher than the 2, which is greatly supported by many studies [118], [122], [123]. For example, dramatic decrease in particle content was resulted when pH was below 2 in Ni-Al_2O_3 system [105]. Much of the current literature on electrocodeposition pays particular attention to the effect of pH on zeta potential. Surveys such as that conducted by Man [115] in 2014 have shown that particles were positively charged at pH below pH 8 while charge of the particles was negative at pH more than 8. They also reported that the isoelectric point of alumina particles was approximately pH 7.6. In addition, it was noted that particle incorporation was hindered by more negative zeta potential. Moreover, the effect of pH on wear resistance and friction coefficient have been investigated and given in the following

parts. In addition, current efficiency critically decreases for Ni-SiC system at pH below 2 [116]. On the other hand, there was no effect of pH on particle content of the codeposited $BaSO_4$-Cu system, despite the fact that the particle concentration was increased with increasing pH in the Tl-Cu system [59].

2.4.3 Addition of the Second Phase Particles

It is stated in the literature that the particle type, shape, size, concentration and the particle concentration in the electrolyte have an influence on the incorporation of the particles with metal matrix. The amount of the second phase particle in the coating increased with increase in the amount of it in the suspension [105]. A number of researchers have reported the same results correlated with that statement for different particles and metal deposition systems [117–121]. In addition, the amount of deposition of titanium dioxide particles in Ni metal was approximately three times higher than that of Al_2O_3 with the same parameters and the same electrolyte system [117]. It was found that the α-Al_2O_3 particles had much more tendency to codeposit when compared to γ-Al_2O_3 [45]. It was also examined that the higher amount of particle concentration in the electrolyte resulted in more tendency to agglomerate and it made hard to homogenize the particle distribution in the electrolyte causing the difficulties in carrying the particles to cathode [122,123].

There are so much different results about the relation between particles size and the amount of incorporation. Several studies have argued that the particle content in composite coating increases with larger particles for different systems such as nickel based or copper based electrocodeposition processes [91,100,108,114,124]. However, it is claimed that the finer particles increases the amount of Al_2O_3 particle in the Ag matrix [109]. In contrast to these studies, it was reported that there is no important impact of particle size on the particle content of codeposit for nickel-alumina and tin-nickel alloy-silicon carbide systems [121,125].

The physical properties such as electrical conductivity of the particles have influences on the surface properties. Conductive particles act as an attraction site on cathode and

make the cathodic deposition easy; however, since it causes more metal deposition on the conductive particle, the surface roughness dramatically increases [126]. In contrast to this, it is possible to form the surface with less roughness and porosity by embedding nonconductive particles [126].

2.4.4 The Additives

Additives such as levelers, brighteners, stress relievers or wetting agents are used for different purposes in the electrolyte. The levelers are organic additives which is adsorbed by peaks on the surface and makes current densities on the grooves higher than other areas [127]. Therefore, it preferentially fills the grooves and makes possible to obtain smoother surface. The brighteners are the additives generally used for decorative purpose.

The wetting agents and surfactants have vital importance for composite coatings due to their effect on hydrodynamics and wetting conditions of suspended particles. In addition to this, the surfactants prevent particles to agglomerate in the electrolyte. For instance, the agglomeration of silicon carbide particles in nickel plating bath is possible but prevented by the addition of SDS as an anionic surfactant [128]. Mostly used surfactants are sodium dodecyl sulfate (SDS) [73], cetyltrimethylammonium bromide (CTAB) [129], saccharine [129], hexadecylpyridinium bromide (HPB) [74], and azobenzene (AZTAB) [130]. The dissolved surfactants in the electrolyte adsorb on the surface of the particles in the suspension. In addition, the surfactants make particle dispersion more homogeneous in the electrolyte and control their wetting condition by floatation in the electrolyte [131]. It acts as a wetting agent for particles and it is exclusively important to hydrophobic particles such as MoS_2. It was stated that the incorporation of MoS_2 with nickel matrix is possible using sodium lauryl sulfate as a wetting agent [132]. Moreover, because of easier reduction of azobenzene when compared to nickel ions, the amount of second phase particles dramatically increased by using azobenzene as a surfactant [130].

It has been reported that the cationic surfactants such as benzyl ammonium salt is adsorbed by MoS_2 to decrease its conductivity and resulting in more incorporation with metal matrix and homogeneous distribution through the coating [133]. On the other hand, the addition of the anionic surfactant SDS increases the amount of particle in the coating and it has the maximum codeposition with the addition of 0.12 g/l [73]. More recently, literature has emerged publications that offer contradictory findings about the surfactants. According to Weston *et al.,* there is no impact of the addition of SLS on particle incorporation, while the presence of cationic surfactant increases the amount of particle in the coating [134].

2.5 Residual Stress, Wear and Friction Behaviors

The second phase particle has dominant importance on the mechanical and tribological properties of composite coatings. The composite coatings have improved properties when compared to metals electrodeposit processes without inert particles. The enhancement of the properties depends on the type of the particle. Hard particles such as diamond, Al_2O_3, SiC, ZrO_2, or B_4C are dispersed in the metal matrix to increase the mechanical properties. In addition, the corrosion resistance, wear resistance, friction behavior, hardness and surface roughness can be improved by the incorporation of particles.

The higher wear resistance with better friction behavior and harder surface was achieved by adding nano-diamond particles to nickel cobalt alloy matrix in Watts solution [135]. Boron nitride particles provide superior lubricant behavior to nickel matrix especially at high temperatures [136]. Nano alumina particles are embedded to nickel matrix to improve mechanical properties [137]. However, nano particles has higher tendency to agglomerate and the addition of HPB as a surfactant resolved this problem and increased the amount of incorporated particles with nickel matrix. Nano particles of SiC [138], La_2O_3 [139], Al_2O_3 [140], TiO_2 [141], diamond [135], CeO_2 [142], TiC [143] are embedded to metal matrix and enhanced the mechanical, physical and tribological properties of the composite coatings. Since pH affects the zeta

potential of the particles, better mechanical properties: higher hardness, better wear resistance and finer grains were achieved at pH 5 in α-Al_2O_3 nickel matrix [115].

The internal or residual stress of the composite coatings had vital importance, especially for electroforming methods since its original shape after removing mandrel should not be distorted or it can fail due to overstress. In the literature, there are more than one theory for the reasons of the residual stress such as lattice mismatch between deposited metal and substrate or the second phase particle, the difference in thermal expansion coefficient of metal and substrate, codeposited hydrogen during deposition, the overpotential which is excess energy resulting in residual stress and crystalline joining [144,145]. There are many methods to determine residual stress in the literature. They are rigid or flexible strip, spiral contactometer, stresometer, X-ray, strain gauge, dilatometer, hole drilling, holographic interferometry [144–147]. Some steps to overcome the residual stress in the coating are to change the substrate or electrolyte, add additives or increase the operating temperature [148].

The ratio of interatomic spacing of gold and silver is about 0.17% while it is much more, about 13%, for Cu-Ag system resulting in higher residual stresses [149]. It is reported that stress reaches to the steady-state above a certain thickness [150]. In other words, residual stress decreases with an increasing coating thickness; in addition, it decreases with finer grain size for substrate material [150]. It is also stated that it is possible to obtain stress-free deposit by adjusting the phosphorous amount in the coating [151].

It is argued that the order of increasing residual stress for anions in the electrolyte is sulfamate, bromide, fluoborate, sulfate and chloride [150]. Furthermore, bromide anions prevent the pitting in the deposit [150]. The stress decreases compressively with the addition of surfactants such as aryl sulfonate and saccharin [149]. The residual stress for nickel sulfamate solution varies from 410 to 17 MPa at 40°C operating temperature respectively [16,152,153].

CHAPTER 3

EXPERIMENTAL

3.1 Preperation of Sulfamate Solution and Pretreatment Steps

The sulfamate bath shown in Table 2 was used as the nickel plating solution, which contained dissolved 350 g/l nickel sulfamate ($Ni(SO_3NH_2)_2.6H_2O$ – 63035981; Umicore, Belgium), 15 g/l nickel chloride ($NiCl_2.6H_2O$ – 7791-20-0; Selnic, France), 30 g/l boric acid (H_3BO_3 – Etibank, Turkey) and balance deionized water at 50 ℃. In addition to these, spherical alumina powder having less than 1 μm particle size shown in Figure 7 (SA1201 – Industrial Powder, USA) was used together with sodium dodecyl sulfate (SLS – Sigma Aldrich, product no: 436143) and ammonium ligno sulfonate (ALS – Tembec, ARBO 02) as surfactants at three different levels. Alumina powder has three phases containing 38.1% γ-Al_2O_3, 33.6% θ-Al_2O_3 and 28.3% δ-Al_2O_3 as shown in Figure 8. When all these ingredients were mixed, pH of the solution was measured as about 4.5.

Table 2 Composition and operating conditions of nickel sulfamate plating bath

Composition and Condition	Content
$Ni(SO_3NH_2)_2.6H_2O$ (g/l)	350
$NiCl_2.6H_2O$ (g/l)	15
H_3BO_3 (g/l)	30
Al_2O_3 powder (less than ~1 μm) (g/l)	5 : 10 : 15
Sodium dodecyl sulfate (SLS) (g/l)	0 : 0.12 : 0.25
Ammonium ligno sulfonate (ALS) (g/l)	0 : 0.12 : 0.25
Water	Balance
Current density (A/dm^2)	2 : 5 : 8
Temperature (℃)	50
pH	4.5

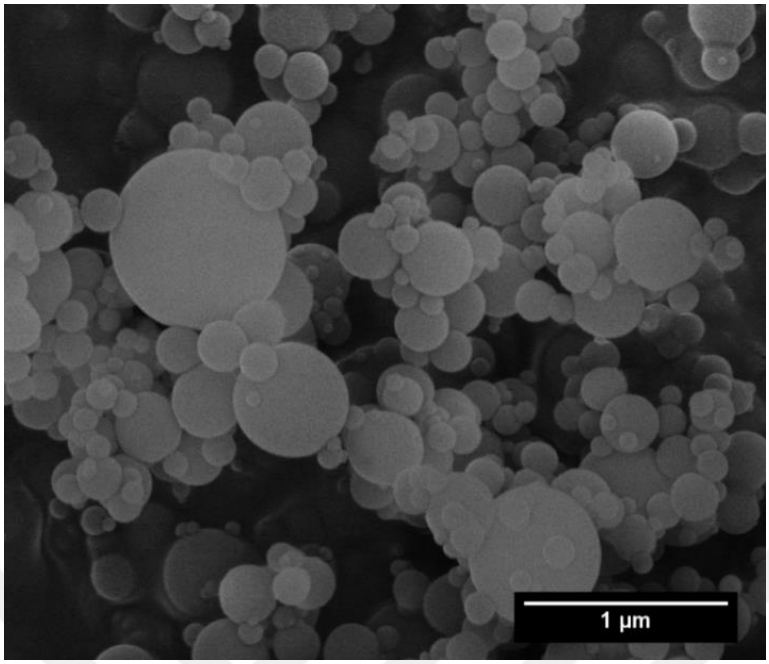

Figure 7 SEM image of submicron spherical alumina powder

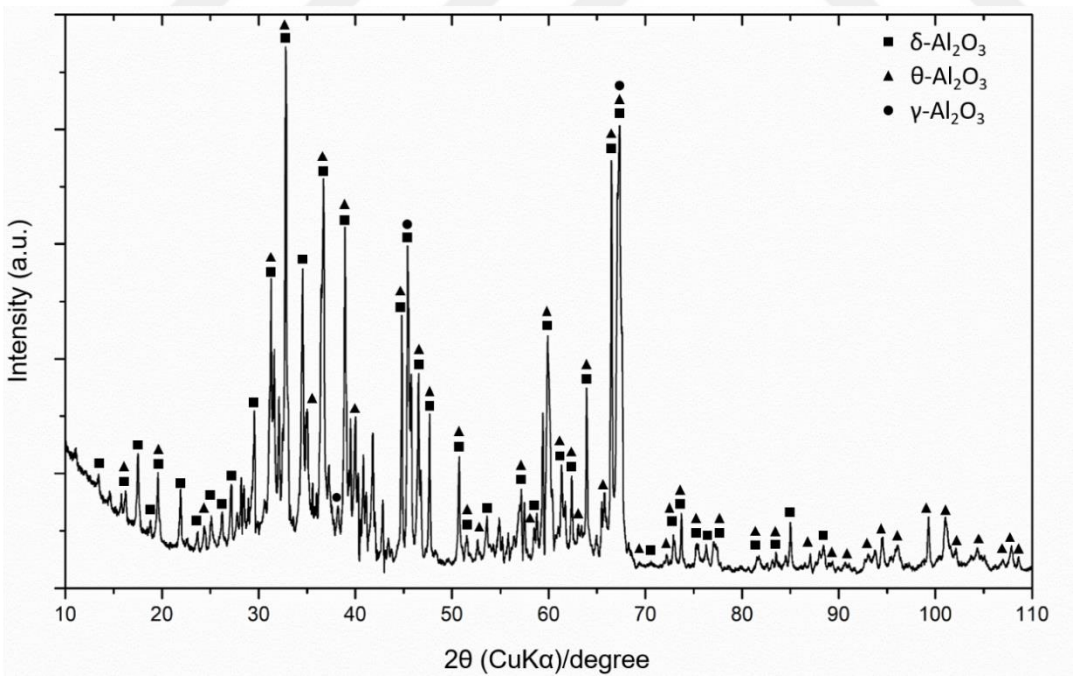

Figure 8 Xray diffraction pattern of alumina powder

Composite coatings were deposited onto rectangular copper sheet (60mm x 25mm x 2mm) cathodes. A nickel plate (Falconbridge, 99.98% Ni) having a surface area of 5 cm^2 was used as the anode. Before coating, polished copper sheets were subjected to hot water and soap to clean their surfaces. Afterwards, they were treated with 1M NaOH to clean oil and dirt from the surface and then nitric acid 25% by volume was used to activate the surface for plating. A 3M 470 electrochemical tape was used to mask the sheets so that 5 cm^2 area was left uncovered for the coating process. For all experiments, the distance between anode and cathode, immersion depth of the cathode (copper sheet), and the thickness of the coating were kept constant at 4 cm, 3 cm, and 50 μm, respectively, so as to examine the effects of ALS, SLS, current density and the amount of added alumina at three different levels as shown in Table 2. SLS and ALS were used as the surfactants to suspend alumina powders and distribute them homogeneously in the electrolyte. In addition, the solution containing the alumina powders was ultrasonically treated by Sonics Ultrasonic VCX 1500 HV for 30 minutes prior to each experiment to prevent agglomeration of the powders. Afterwards, copper substrate was deposited by Agilent B2901A Precision Source DC power supply.

The experiments were statistically designed by using full factorial design to determine the effects of current density, amounts of ALS, SLS and their combination and the amount of alumina particles in the electrolyte on hardness, wear rate and friction coefficient of coatings. As shown in Table 2, three different levels were conducted for those parameters and totally 81 experiments were done.

3.2 Simulation of Current Distribution on Cathode

Before starting the experiments, thickness distribution of the substrate materials for nickel electrodeposition on both copper plates and strips that were going to be used to measure residual stress were simulated by Comsol Multiphysics 5.2 software electrodeposition package [154]. Thickness distribution on substrate indicates the current distribution as well. Figure 9 shows that the current distribution of copper plates increases at the side and especially at the corners due to edge effect. Therefore,

all the characterization measurements for all samples were done from the central region where current density was more homogeneous compared to other parts. Moreover, copper strips have two identical arms and both arms have masks on different sides to assure deposits only on opposite sides during electroplating. Figure 10 indicates that the current distributions are almost homogeneous through the surface for thin copper strips. Very thin lines at the edges of the cathode have higher current distribution as shown in below figure. Again the characterizations related to the current distribution over the strips were done over the region where the current distributions were homogeneous.

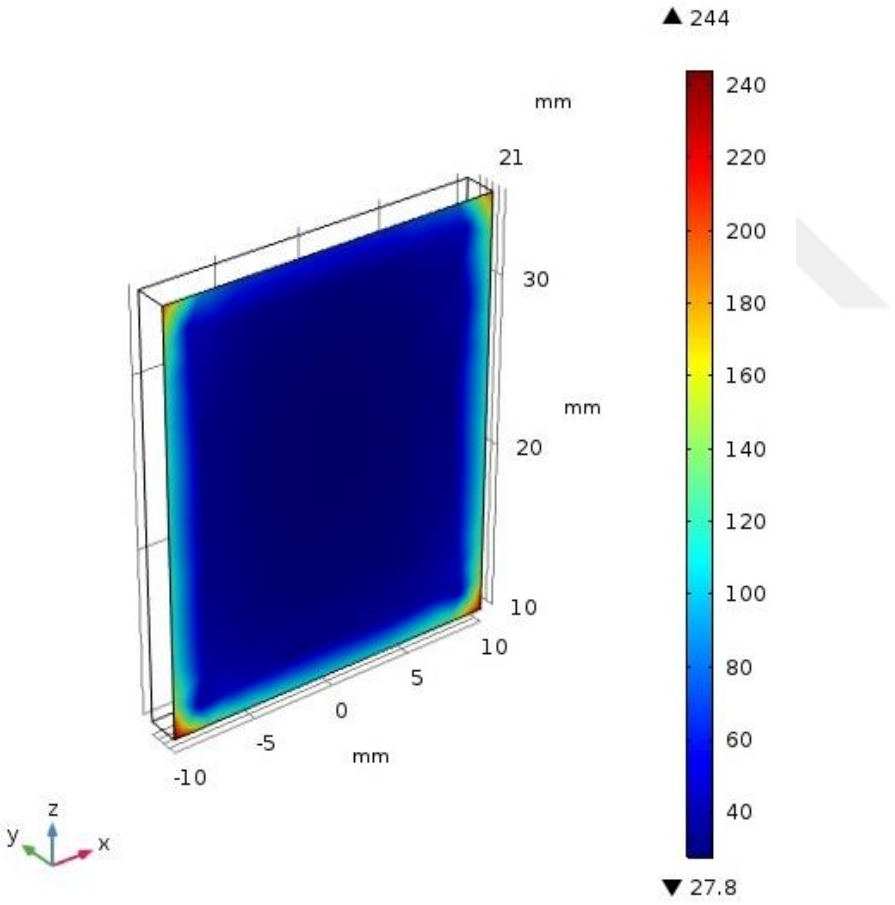

Figure 9 Thickness distribution of electrodeposited nickel on copper substrate determined by Comsol Multiphysics 5.2 software package

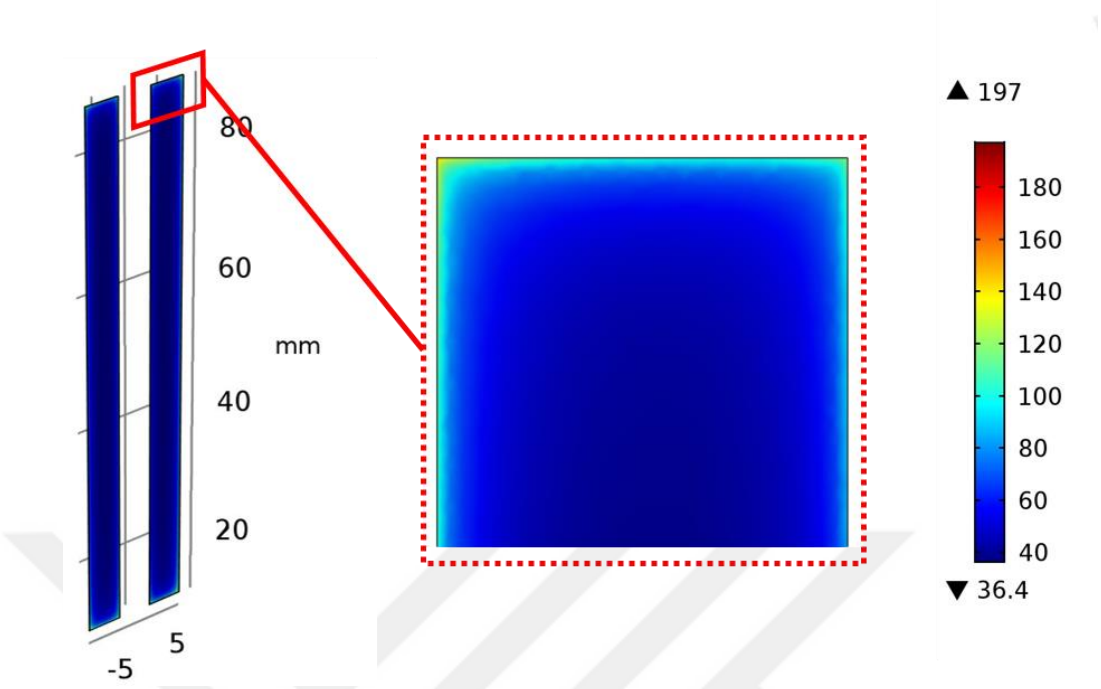

Figure 10 Calculated thickness distribution of electrodeposited nickel on copper strips used to measurements residual stress

3.3 Voltammetric Measurements

Gamry Reference 3000 Potentiostat was used to determine current density for nickel electrodeposition and the effect of surfactants and alumina powders on the nickel electrodeposition. Copper was used as cathode which is a working electrode while the nickel anode was used as a counter electrode for Ni and Ni-Al_2O_3 deposition from the cell schematically shown in Figure 11. The reference electrode was used Ag/AgCl. The cell was conducted for the potential difference between anode and cathode with respect to reference electrode. The effect of scan rate such as 25, 50, 75 and 100 mV/s on measurements were investigated up to 2 V potential difference. A similar cell was employed for electrodeposition to develop Ni-Al_2O_3 coatings for characterization studies.

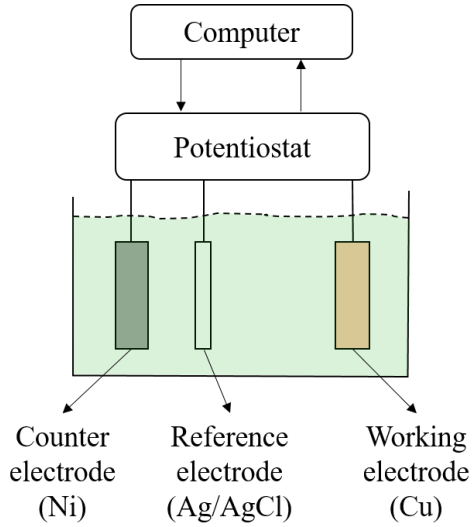

Figure 11 Schematic view of experimental setup for voltammetric measurements

3.4 Characterization Techniques for Composite Coatings

Microstructures of composite coatings were analyzed by NIKON ShuttlePix optical microscope and FEI Nova NanoSEM 430 scanning electron microscope and included EDX unit. Chemical characterization was done by Fisherscope X-Ray XDV-SDD X-ray fluorescence (EDXRF) measuring instrument and EDX analyses.

X-Ray diffraction patterns were obtained by Bruker D8 Advance X-Ray Diffractometer having Cu Kα radiation at a wavelength of 0.154183 nm and the data were collected over the 2θ range of 10° and 110° with a rate of 2°/min. In addition to this, hardness measurements were done by Shimadzu HMV- G21 Micro Vickers Hardness Tester using 1.961 N shown as $HV_{0.2}$ in the rest of this thesis.

3.5 Measurements of Tribological Properties

Ni and Ni/Al_2O_3 composite coatings were tested by CSM pin-on-disc tribometer under dry sliding at room temperature with approximately 60% humidity. A schematic view

is shown in Figure 12. Zirconia ball was used as a pin to wear the surface of the coating. In all tests, a constant load of 5 N was applied at a sliding speed of 5 cm/s. The wear track radius was 3 mm and the run lasted for 10000 laps which corresponded to a sliding distance of 183.5 m. Calibrated shear stress sensor was demonstrated COF values conducted by the amount of stress applied to sensor during measurements.

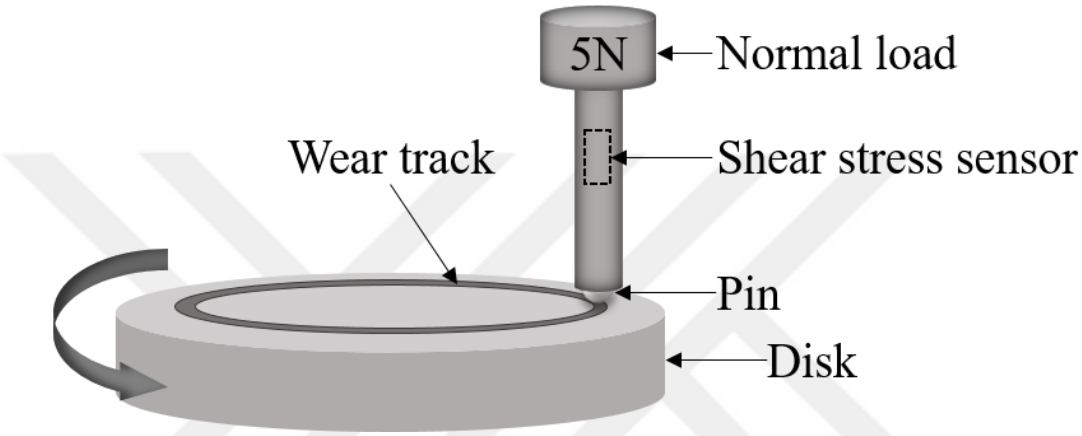

Figure 12 Schematical representation of pin-on-disk test setup

Wear volume in mm^3 can be calculated by two different methods. Firstly, it was calculated by below formula shown in Eq. 3.1 using wear track radius 'R', wear track width 'd' and pin end radius 'r'. ASTM standard G99 assumes no pin wear [155].

$$Volume\ loss = 2\pi R\left[r^2 \sin^{-1}\left(\frac{d}{2r}\right) - \left(\frac{d}{4}\right)(4r^2 - d^2)^{\frac{1}{2}}\right] \qquad (3.1)$$

Secondly, cross sectional area of wear track was calculated from the 2D profile obtained by Mitutoyo SJ-400 Profilometer Surface Roughness Tester. This area was calculated by taking the average of area determined at different points of wear track. Afterwards, the volume of the material worn out could be calculated by multiplying the area with the circumference of the wear track which was measured from the center.

Other than surface roughness, 3D surface profile was conducted by using high performance atomic force microscope (hpAFM) of NanoMagnetics Instruments. Measured area was 20x20 μm in dimensions and it was scanned at 10 μm/s rate.

3.6 Residual Stress Measurements

The instrument of Speciality Testing & Development Company called Deposit Stress Analyzer (model 683) and copper alloy test strips PN1194 as shown in Figure 13(a) were used to measure residual stress of the composite coatings. 5x5 cm nickel anode (Falconbridge, 99.98% Ni) was used to electrodeposit Ni-Al_2O_3 on copper test strips by using Agilent B2901A Precision Source to apply direct current.

The residual stress revealed by incorporated Al_2O_3 particles with nickel matrix were investigated by deposit stress analyzer. Copper strips were used to calculate residual stress via the distance between its arms which is called number of increments (U). The residual stress can be calculated as follows Eq. 3.2:

$$Res.Str.(psi) = \frac{U}{3\left(\frac{W}{D \times A}\right) \times 0.394\ inch/cm} \times K \qquad (3.2)$$

where U is the number of increments, W is the weight of deposit (g), D is the density of the deposited metal (g/cm^2), A is the plated area (cm^2), and K is the correction factor. In this case, the plated area of the strips was equal to 7.74 cm^2 and the correction factor was 1.7143.

Figure 13(b) shows position of the arms of the copper strip after electrodeposition. Each arm has plated side and resist side. The type of the residual stress tensile or compressive can be determined from the positions of arms as shown in Figure 13(b). All the samples were in tension residual stress in present case as a representative sample illustrated in Figure 13(a).

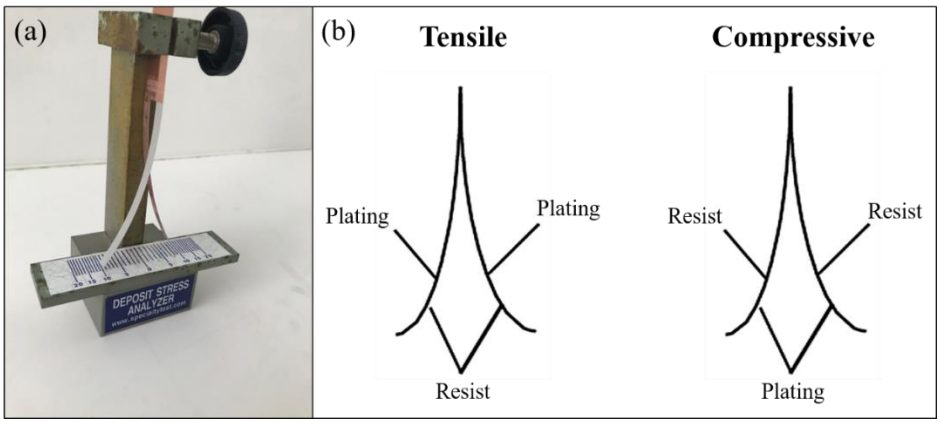

Figure 13 (a) A picture of deposit stress analyzer and copper test strip (b) Type of the residual stress with respect to the position of arms of the copper strip

The effects of current density, pH, the amount of ALS in the electrolyte were investigated by statistical full factorial design for which levels of parameters are listed in Table 3. Totally, 18 experiments were conducted to investigate the effects of above parameters on residual stress of the composite coatings.

Table 3 Parameters and their levels for full factorial design of residual stress measurements

Parameters	Level
Ammonium ligno sulfonate (ALS) (g L^{-1})	0 : 0.12 : 0.25
Current density (A dm^2)	2 : 5 : 8
pH	3.5 : 4.5

CHAPTER 4

RESULTS AND DISCUSSION

4.1 Voltammetric Studies

Linear sweep voltammetry was conducted to understand the effects of addition of anionic wetting agent and alumina powder to a typical nickel sulfamate solution. The results are given in Figure 14 and Figure 15 as positive cathodic currents. Figure 14 shows the effect of scan rate on the polarization curve between 25 and 100 mV/s. The potentials corresponding to cathode reactions are well-determined for the electrolyte containing wetting agent and Al_2O_3 powders when the potential scan rate was 100 mV/s. It can be seen in Figure 15 that reaction for deposition of nickel becomes more anodic and takes place at lower voltages due to 50 mg/l SLS wetting agent and 10 g/l Al_2O_3 powder additions to the typical sulfamate solution. When alumina powder was added to the sulfamate solution containing wetting agent, there was a shift of the reaction potential to lower values. Nickel electrodeposition shifts by about 0.1 V similar to that was reported in Watts solution [156]. If the electrolyte contains wetting agent and alumina powder, electrodeposition reaction becomes more anodic.

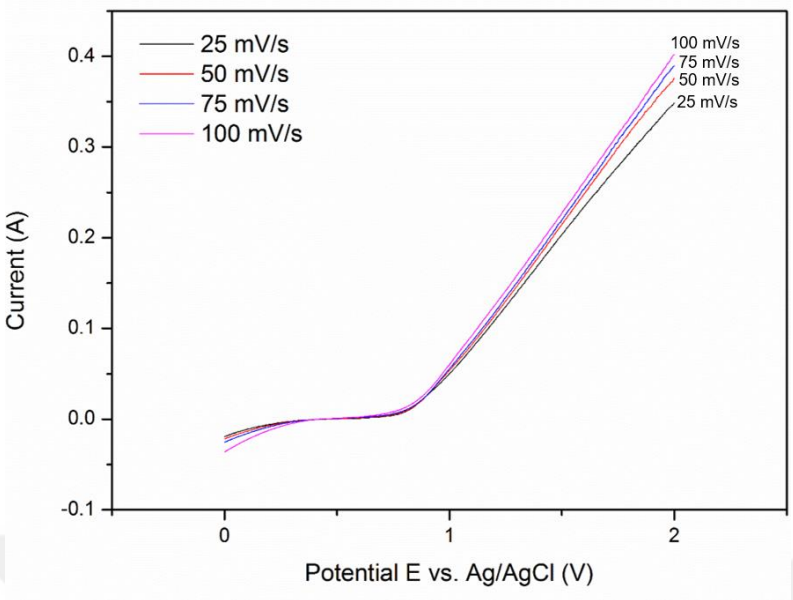

Figure 14 Linear potential sweep curves of a typical nickel sulfamate solution at different scan rates

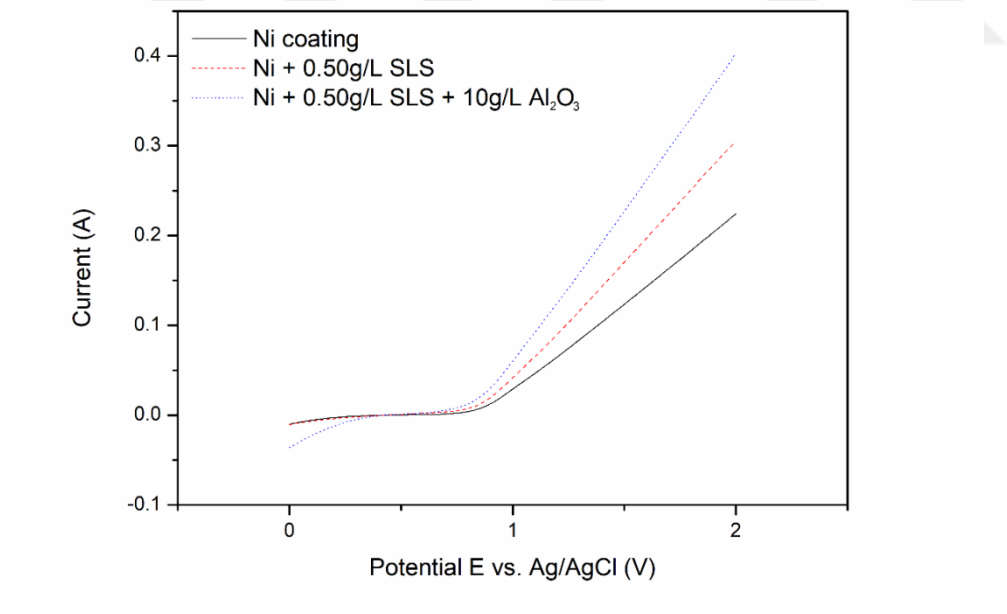

Figure 15 Linear potential sweep curves showing the effects of SLS and alumina powder addition to nickel sulfamate electrolytes

4.2 Mechanical and Tribological Investigations

All the mechanical and tribological investigation results of coatings: hardness, wear rate and COF are listed for experimental conditions determined from DOE in Table A.1 of Appendix A.

Figure 16 shows the typical cross sectional and surface images of coatings. This coating was formed at 2 A/dm^2 current density without SLS or ALS, and found to contain 9 wt.%Al_2O_3 determined by EDS taking the average of 5 different measurements one of which is shown in Figure 17. Table 4 demonstrates related Al and Ni content for the composite coating shown in below figure. As seen in Figure 16, Al_2O_3 particles were dispersed fairly homogeneously through the nickel matrix.

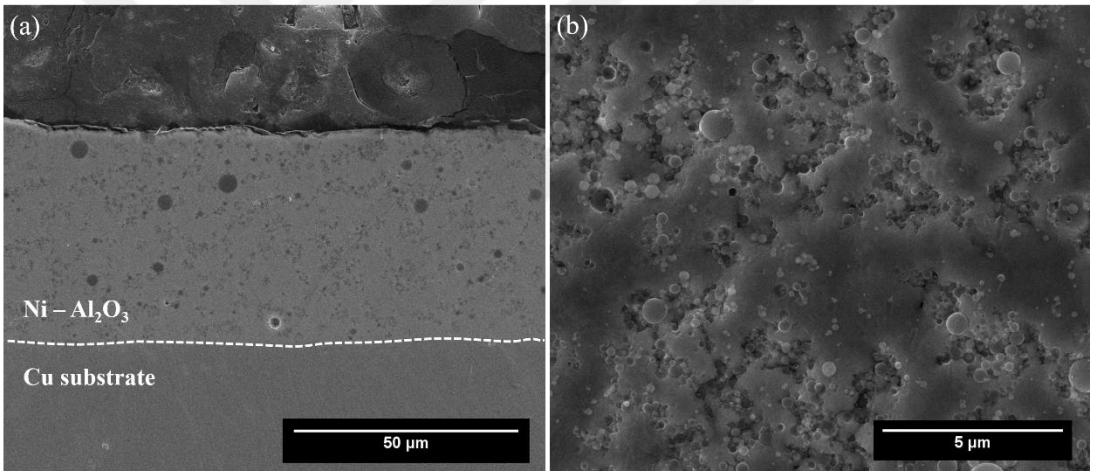

Figure 16 (a) Cross-sectional and (b) Surface images of the Ni-9 wt.%Al_2O_3 composite coating produced at 2 A/dm^2 current density without any surfactant

Table 4 Representative EDS result for Ni-9 wt.%Al_2O_3 composite coating

Elements	Ni	Al
Wt. %	97.45	2.55
At. %	94.61	5.39

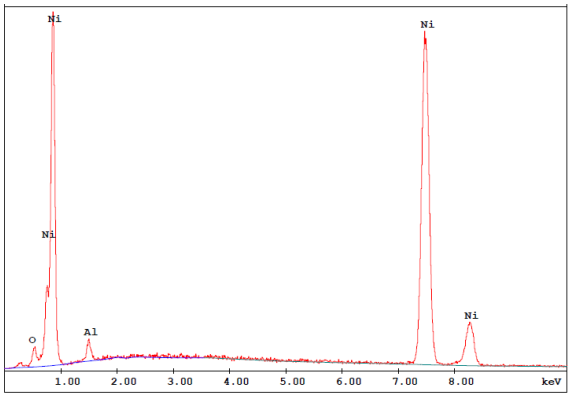

Element	Wt %	At %	K-Ratio	Z	A	F
AlK	2.63	5.55	0.0060	1.0611	0.2169	1.0000
NiK	97.37	94.45	0.9713	0.9976	0.9999	1.0000
Total	100.00	100.00				

Element	Net Inte.	Bkgd Inte.	Inte. Error	P/B
AlK	31.20	14.05	3.90	2.22
NiK	987.05	14.30	0.51	69.02

Figure 17 Representative EDS measurement for Ni-9 wt.%Al_2O_3 composite coating

4.2.1 Hardness

It is generally observed that increase in current density increases the hardness in the electrodeposition processes. As the current density increases, the nucleation rate of the metal atoms on the cathode increases and the average crystallite size of the coating decreases. This causes the grain boundary strengthening which is described by well-known Hall-Petch relationship between the strength of the material and the grain size shown in Eq. 4.1.

$$\sigma_y = \sigma_0 + k_y d^{-1/2} \quad (4.1)$$

where σ_y is the yield stress, σ_0 is a material constant for the starting stress for dislocation movement, k_y is the strengthening coefficient and d is the average grain diameter. The hardness of the nickel coatings increased with increasing current density and varied between 270 and 320 HV. As the grain size became smaller with increasing current density [157], inhibition of dislocation motion caused increase in hardness. However, the hardness of the composite coatings dominantly depends on the amount of second phase ceramic particles in the composite coatings.

The hardness of the nickel coating without surfactant had lower value at 2 A/dm^2 and higher value at 8 A/dm^2 illustrated in Figure 18a, as expected. Figure 18a shows a particular trend where hardness decreased with increasing current density independent of the amount of ALS in the case of composite coatings. This can be explained with the fact that ALS addition was more effective at lower current densities for incorporation of alumina particles into the coating; however, its presence decreased the hardness of the coating at higher current densities; e.g. 8 A/dm^2. The measured hardness values were also supported by SEM micrographs given in Figure 18b, Figure 18c and Figure 18d. As can be seen in these figures, the amount of Al_2O_3 particles present in the coating decreased with increasing current density.

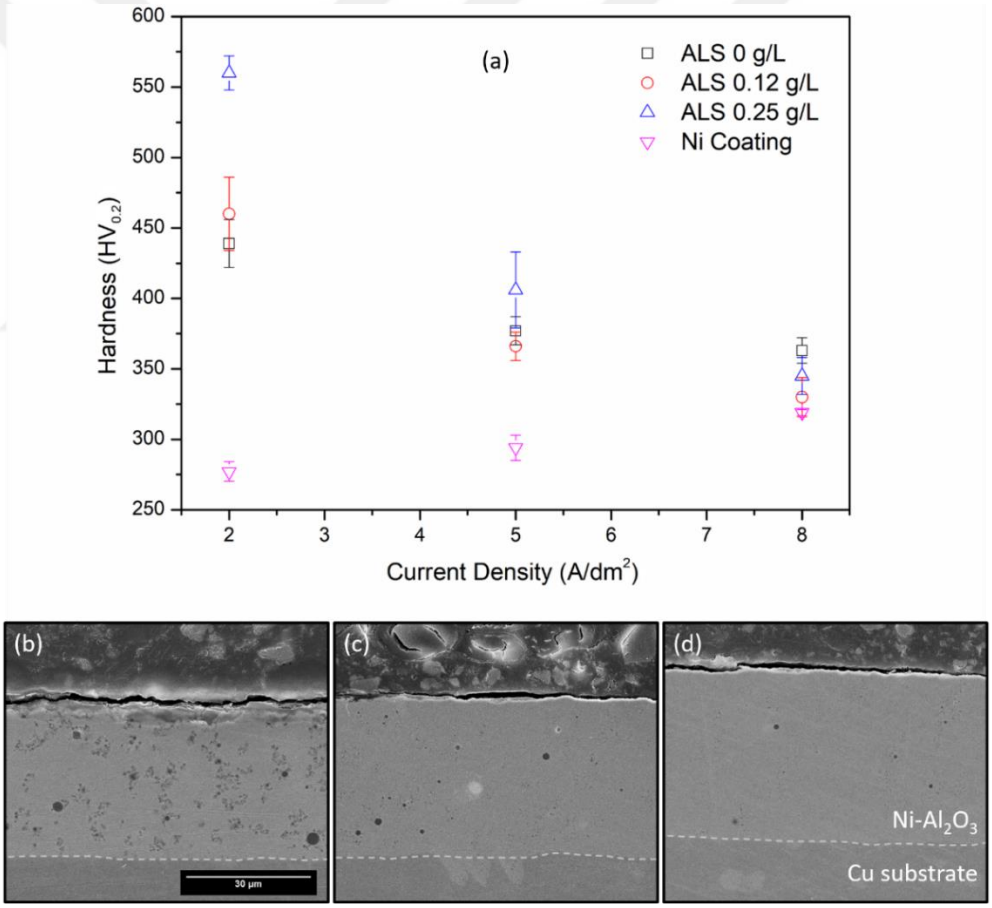

Figure 18 (a) The effect of current density with and without surfactants on hardness. Cross-sectional SEM images of the coatings with 10 g/l Al_2O_3, 0 g/l SLS and 0.25 g/l ALS at (b) 2 A/dm^2, (c) 5 A/dm^2 and (d) 8 A/dm^2

The regression equation on hardness, calculated from results given in Table A.1 of Appendix A in terms of parameters covered in this study is shown in Eq. 4.2:

$$HV_{0.2} = 430 - 1.5\,A - 19\,B - 110\,C + 470\,D \qquad (4.2)$$

where A is the amount of second phase particles in plating bath (g/l), B is the current density (A/dm^2), C is the amount of SLS addition and D is the amount of ALS addition to the plating bath (g/l). According to Eq. 4.2, the ALS addition has a dominant effect on hardness with a factor of 470 while the SLS addition has a negative effect with a factor of 110. Similar to Figure 18a, the regression equation shows that the increase in current density decreases the hardness of the composite coatings. In addition, the amount of second phase particles in plating bath has negligible effect on hardness with a factor of 1.5. The statistical significance of the fit was not critisized here because it was not attempted to include possible cross-correlations of the parameters on hardness.

Figure 19 shows the interrelations between all parameters on hardness. The interrelation between ALS addition and current density was also given in Figure 18. However, the relation given in Figure 20 differs from the given interaction plot, because interaction plots show average values of hardness measured at given current density and ALS amonunts regardless of the other parameters. Small effect of the amount of second phase particles in the electrolyte can also be seen in Figure 20. The effect of SLS cannot easily be identified since its effect depends on others as well.

The mean effects of all parameters on hardness of coatings calculated from the results of 81 experiments given in Table A.1 of Appendix A are shown in Figure 20. Each point in this plot represent the average of 9 data points from the interaction plot given in Figure 19. The amount of the second phase particles in an acidic sulfamate solution does not have much influence on hardness values. The amount of second phase particles in plating bath generally affects the particle concentration in the coating; however, it may not be considered as being in general due to interrelation effects of four parameters that affect all the properties of composite coatings. In addition, composite coatings have higher hardness when they are formed in electrolyte without

SLS. Progressive addition of SLS decreases the hardness first and then increases. Consequently, increasing order of the effects of parameters on hardness with respect to mean values are in accord with Eq. 4.2.

.

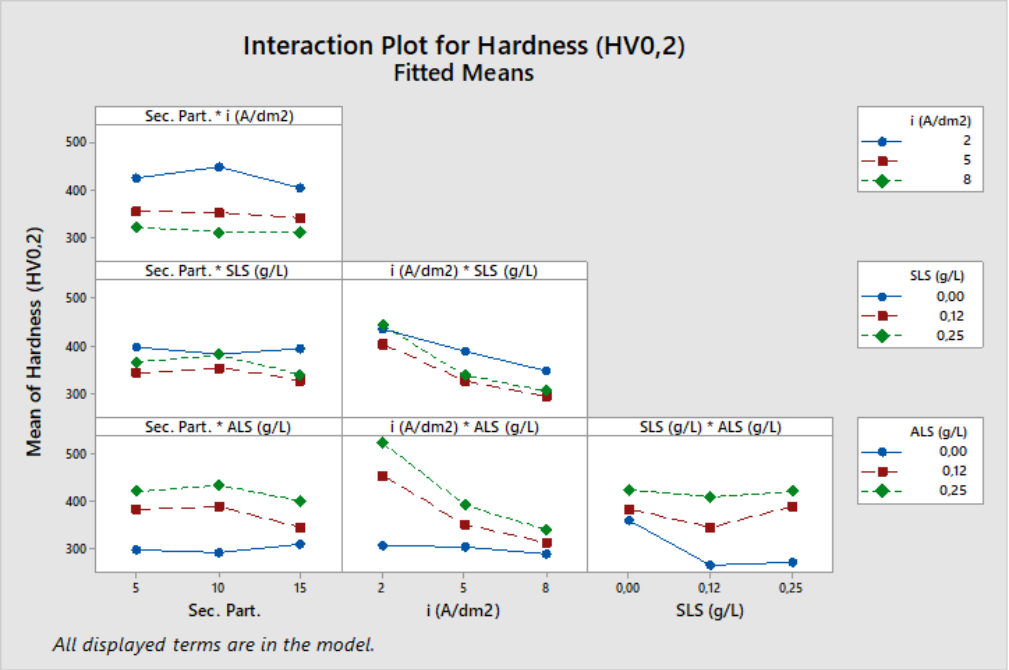

Figure 19 Interaction plot for hardness

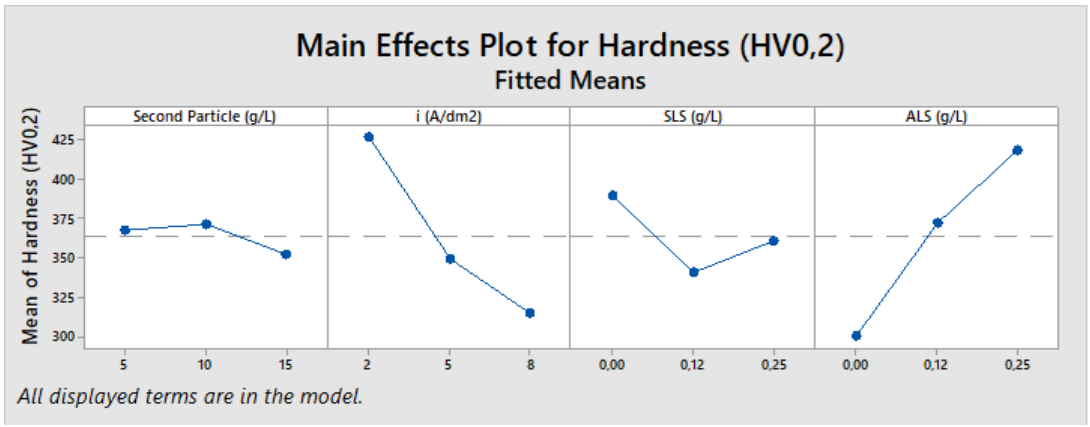

Figure 20 The mean effects of design parameters on hardness of the composite coatings

Considering the effects of current density and the addition of ALS, on hardness, it was seen that hardness of the composite coatings become higher at lower current densities and higher amount of ALS addition. Therefore, this is in agreement with the observations that amount of alumina particles in the coatings reaches the maximum values at current densites of 2 A/dm^2 and 1 A/dm^2 for copper and nickel matrix, respectively, which is supported by modelling of incorporated particles in nickel matrix [70,78]. Furthermore, extrapolation of the interactions between all parameters are given as area counter plots for hardness measurements in Figure B.1 to Figure B.6 of APPENDIX B.

4.2.2 Wear Rate

Hardness of the composite coatings without surfactants slightly decreased with increasing current density. Similarly, the wear rate for those coatings did not change to a significant extent with current density as shown in Figure 21. On the contrary, addition of ALS had a profound effect on the wear rate. The wear rate was higher at lower current densities without surfactants and with the addition of 0.12 g/l ALS. However, further addition of ALS and the combination of ALS with SLS, the lower current densities resulted in a lower wear rate for the composite coatings (see Figure 21 and Figure 22). In Figure 18, the highest hardness value was achieved at 2 A/dm^2 and 0.25 g/l ALS. It is seen in Figure 21 that this coating also had the lowest wear rate.

Figure 22 shows the effects of the amount of SLS on wear rate when the amount of ALS was constant at 0.25 g/l. Similar to ALS, the addition of SLS first decreased the wear resistance at all current densities. However, when the amount was increased to 0.25 g/l, wear resistances increased to levels attained at zero SLS. The lowest wear rate was measured as 0.0210 mm^3/N/m when the addition of 0.25 g/l SLS was combined with 0.25 g/l ALS at 2 A/dm^2.

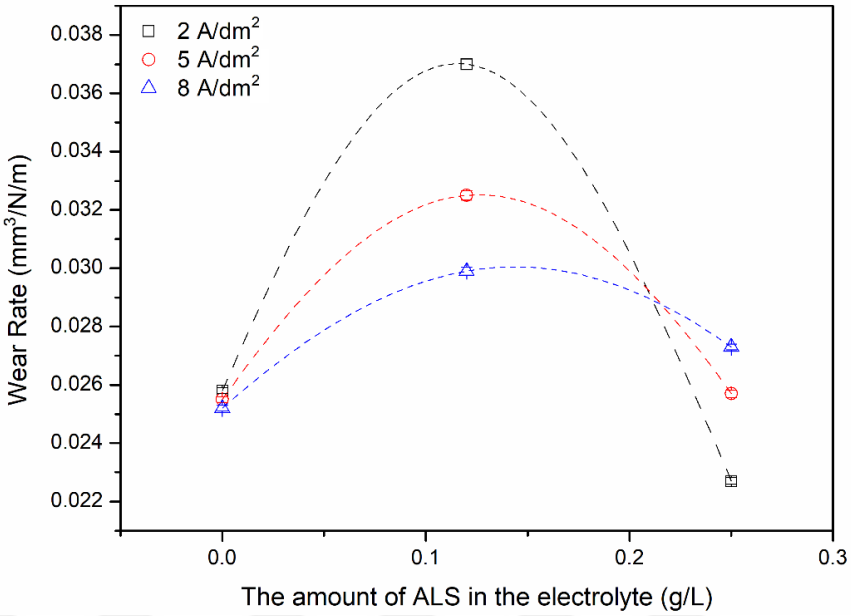

Figure 21 The effect of current density and the amount of ALS on wear rate

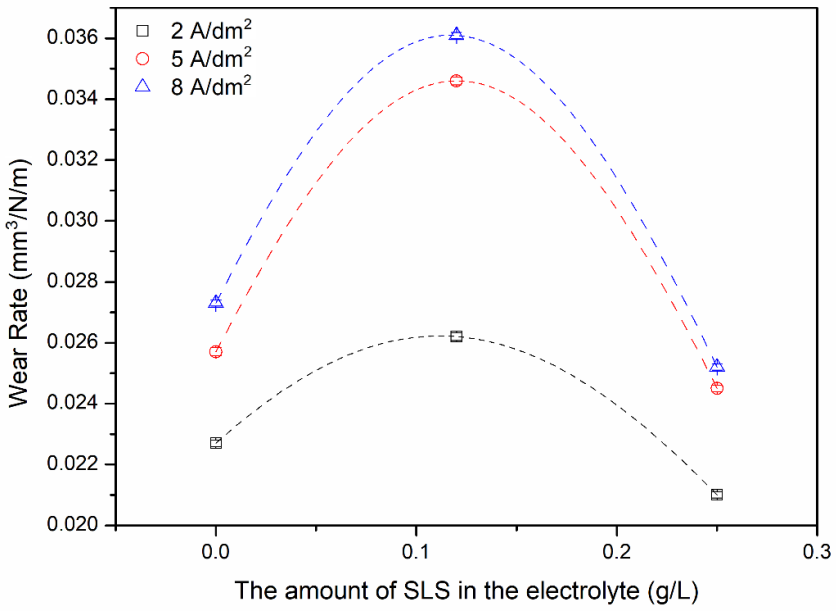

Figure 22 The effect of current density and the amount of SLS combined with 0.25 g/l ALS on wear rate

As mentioned above, the main purpose of the addition of the surfactants was to adjust the amount of uniformly distributed Al_2O_3 particles through the coating, because the amount of Al_2O_3 particles superiorly affects the hardness, wear rate and COF. Figure 23 shows the importance of the amount of Al_2O_3 on wear properties. The weight loss and the corresponding wear rate of composite coatings diminished to about half of the nickel coating when Al_2O_3 content was close to 9 wt.%.

Figure 24(a), (b) and (c) indicate the differences in width of the wear tracks and their depths from surface profiles for coatings at current densities of 8, 5 and 2 A/dm^2, respectively. It can be noted that the width of the tracks gets narrower and shallower, which indicates higher wear resistance at lower current densities. This also supports the wear results calculated by using width of the tracks from SEM images, since the cross-sectional area of the tracks became smaller with decrease in current density.

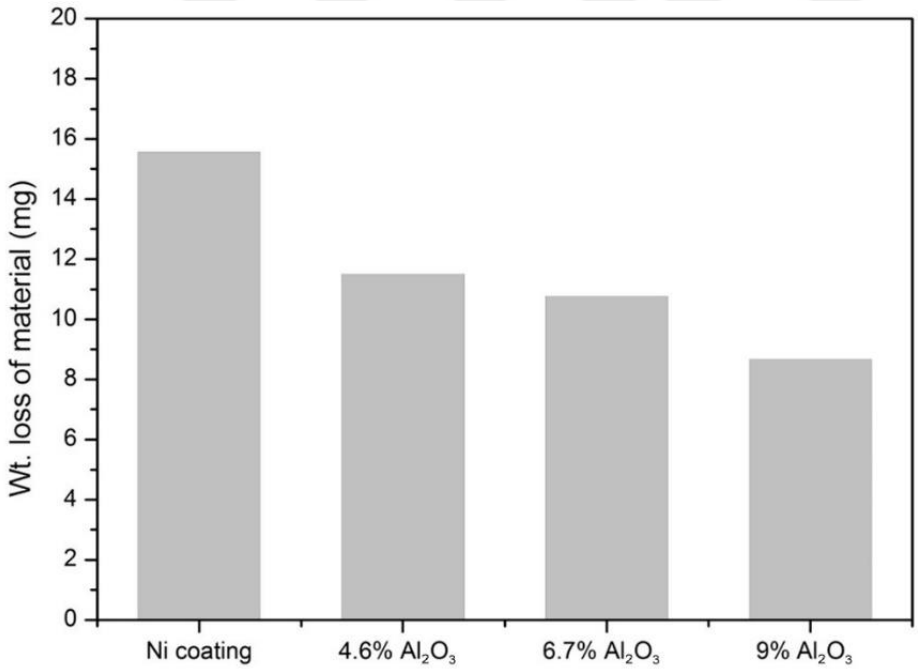

Figure 23 The effect of Al_2O_3 content on weight loss of coating after 183.5 m sliding distance

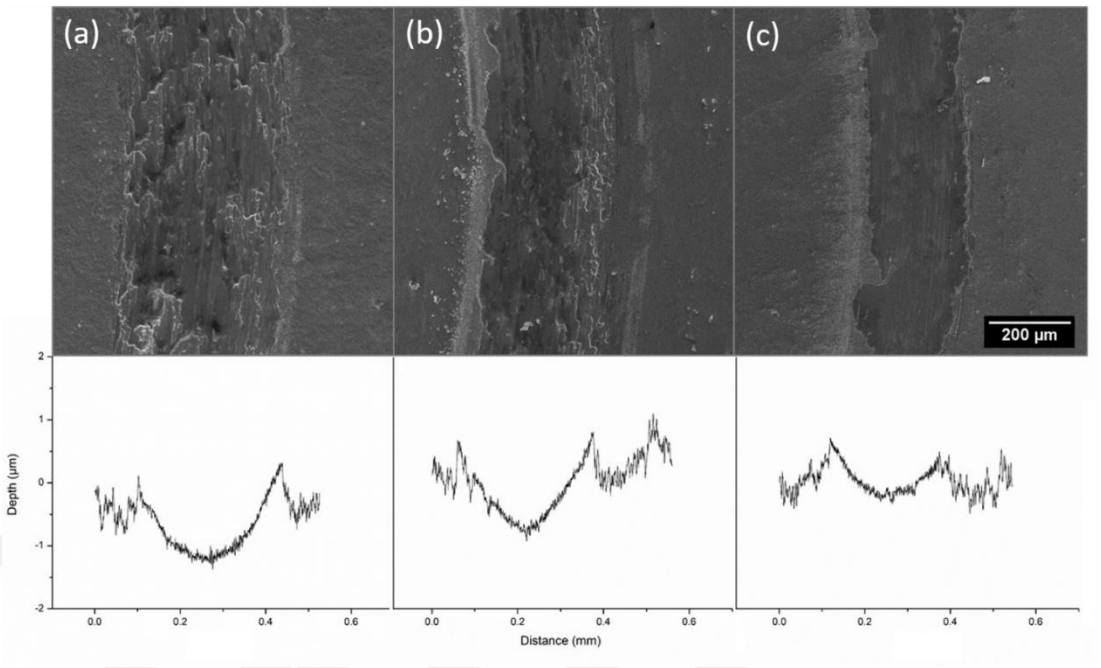

Figure 24 SEM images and surface profiles of the wear track of the composite coatings at current densities of (a) 8 (b) 5 (c) 2 A/dm^2 with 0.12 g/l SLS and 0.25 g/l ALS

The regression equation on wear rate, calculated from results given in Table A.1 of Appendix A in terms of operating parameters is shown in Eq. 4.3:

$$Wear\ rate \times 10^3\ (mm^3/N/m) = 27.7\ + 0.2\ A \\ -0.1\ B - 2.7\ C - 6.7\ D \tag{4.3}$$

where A is the amount of second phase particles in plating bath (g/l), B is the current density (A/dm^2), C is the amount of SLS addition and D is the amount of ALS addition to the plating bath (g/l). As shown in Eq. 4.3, all the constants are small due to small amount of wear determined for the samples. However, small decreasing effects of all parameters except amount of second phase in the electrolyte can be seen in this equation. The negative effect on wear rate means higher wear resistance. On the other hand, SLS addition has a negative important effect on wear rate with a factor of 0.0027. Since the results for wear rate are more complex than hardness and the amount of wear recorded were small, the statistical significance of the fit was not critisized. On the

other hand, although the factors are not accurate, it may be used to show the effects of parameters on the wear rate.

It should give more understandable perspective by analyzing the parameters one by one as the previous findings for wear rate of coatings (see from Figure 21 to Figure 24). However, the effects of operating parameters are more explicable for some parameters when the counter plots are examined. For example, the composite coatings having better wear resistance meaning lower wear rate are formed at higher ALS concentration, lower SLS concentration, lower current density and lower amount of particle in the electrolyte as seen in Figure B.7 to Figure B.9 of Appendix B. In addition to that, it is generally related to hardness values. Composite coatings having higher hardness has the higher wear resistance. The higher hardness may cause less wear from the surface because it cannot penetrate to harder surfaces easily during measurements.

Figure 25 shows that mean results of 81 experiments which is the average of 9 different results from interaction plot in Figure C.1 of Appendix C, when higher amount of alumina particles were present in the electrolyte, the wear rate increases. There is not a substantial effect of current density for the mean results and the wear rate changes between 0.0282 - 0.0277. In addition, the wear rate decreases with increasing the amount of SLS. On the other hand, the ALS has more dominant but similar effect on wear rate to SLS.

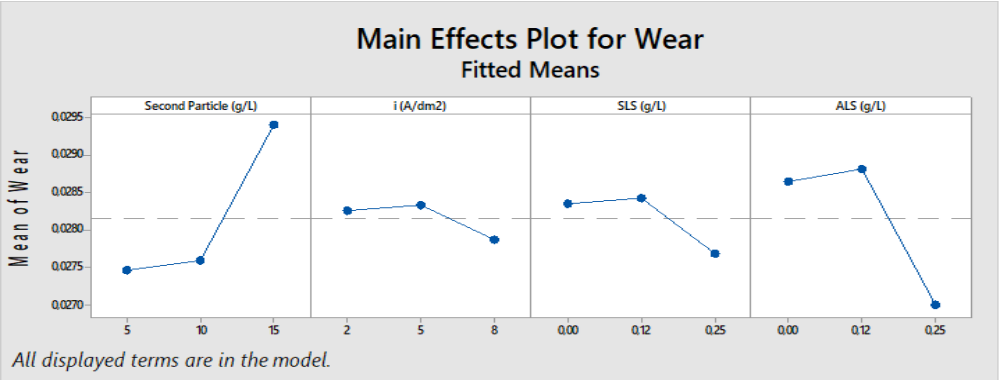

Figure 25 The mean effects of design parameters on wear rate of the composite coatings

4.2.3 The Coefficient of Friction

Figure 26 shows variation of the COF with the current density at ALS concentrations of 0, 0.12 and 0.25 g/l. The effect of ALS concentration on COF was very small at 2 A/dm^2 current density. However, COF showed higher deviations at 5 and 8 A/dm^2 when more ALS was added. Increasing the current density to 8 A/dm^2 yielded a decrease in COF values for 0 and 0.12 g/l but an increase for 0.25 g/l ALS. The COF values for 0, 0.12 and 0.25 g/l ALS were approximately 0.425, 0.489 and 0.511, respectively, at the current density of 5 A/dm^2. The measurements recorded during these tests are displayed in Figure 27 as a typical example. Other measurements showing the effect of current density and the amount of SLS addition are given in Figure C.3 and Figure C.4 in APPENDIX C.

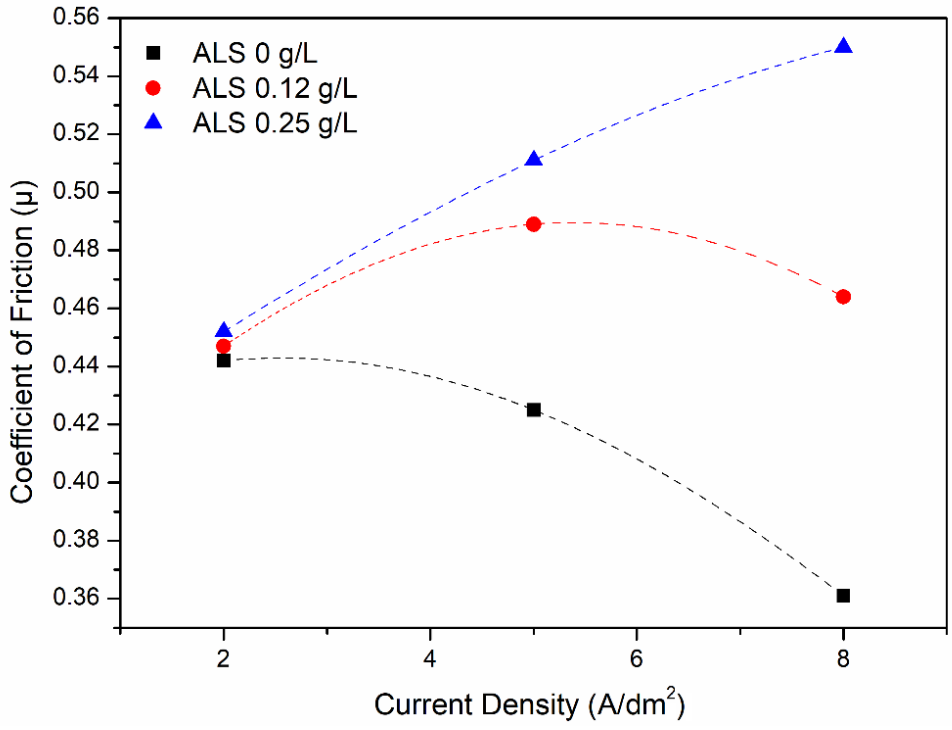

Figure 26 The effect of current density on COF at three different levels of ALS without SLS

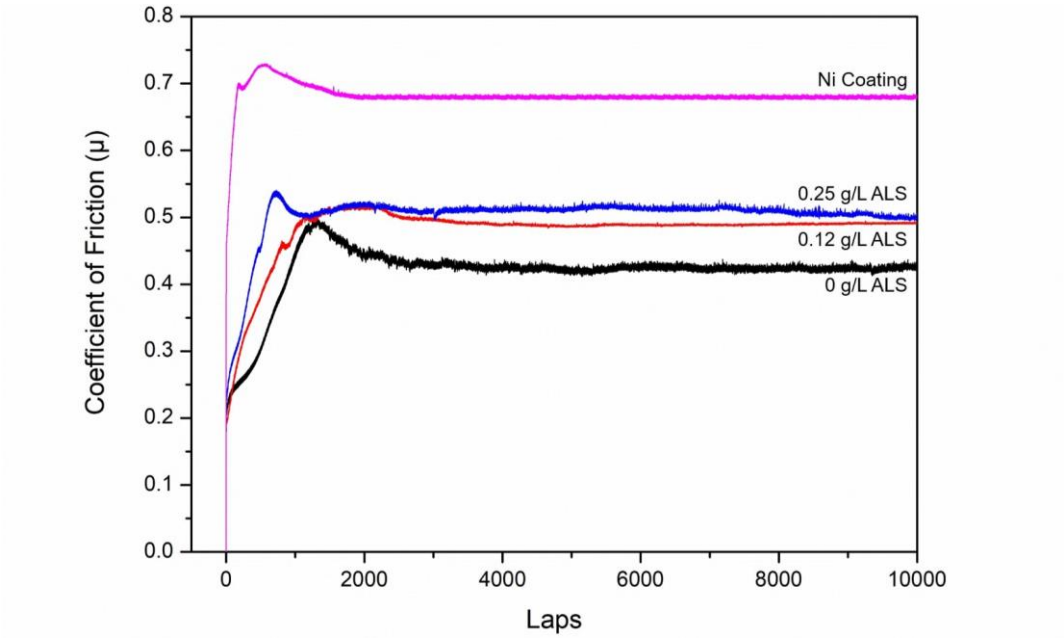

Figure 27 Recorded COF values during measurements at 5 A/dm^2 current density without SLS

The regression equation on the coefficient of friction calculated from results given in Table A.1 of Appendix A in terms of operating parameters is shown in Eq. 4.4:

$$COF = 0.481 - 0.003A - 0.001B - 0.074C + 0.104D \qquad (4.4)$$

where A is the amount of second phase particles in plating bath (g/l), B is the current density (A/dm^2), C is the amount of SLS addition and D is the amount of ALS addition to the plating bath (g/l). According to Eq. 4.4, the increase in ALS gives rise to the COF with a factor of 0.104. On the other hand, other parameters have smaller negative effects on COF. The extrapolated results for all interactions between the operating parameters are given as counter plots in Figure B.10 to Figure B.15 of APPENDIX B. On the other hand, although the equation does not have a good fit with the results, it still indicates which one is more effective on COF than the others.

SLS combined with 0.25 g/l ALS at three different levels strongly affected the properties of coatings. It is clearly seen in Figure 28 that COF increases with increasing

the current density if the only surfactant is 0.25 g/l ALS. This trend was completely reversed and COF decreased with increasing current density when 0.12 g/l or 0.25 g/l SLS was combined with 0.25 g/l ALS. It is also seen that the coating having the lowest COF value, among the present results, was obtained when the amount of SLS was 0.12 g/l.

As mentioned in above figures related to COF, the parallel results were obtained from main effects plot in Figure 29. The main effects plot show mean COF values of the interaction plot shown in Figure C.2 of Appendix C. In addition to these results, when the amount of second phase particles in the electrolyte was 5 g/l, the COF of the composite coating became higher. COF increases with an increase in ALS addition to electrolyte since it increases the alumina concentration in the coating as well.

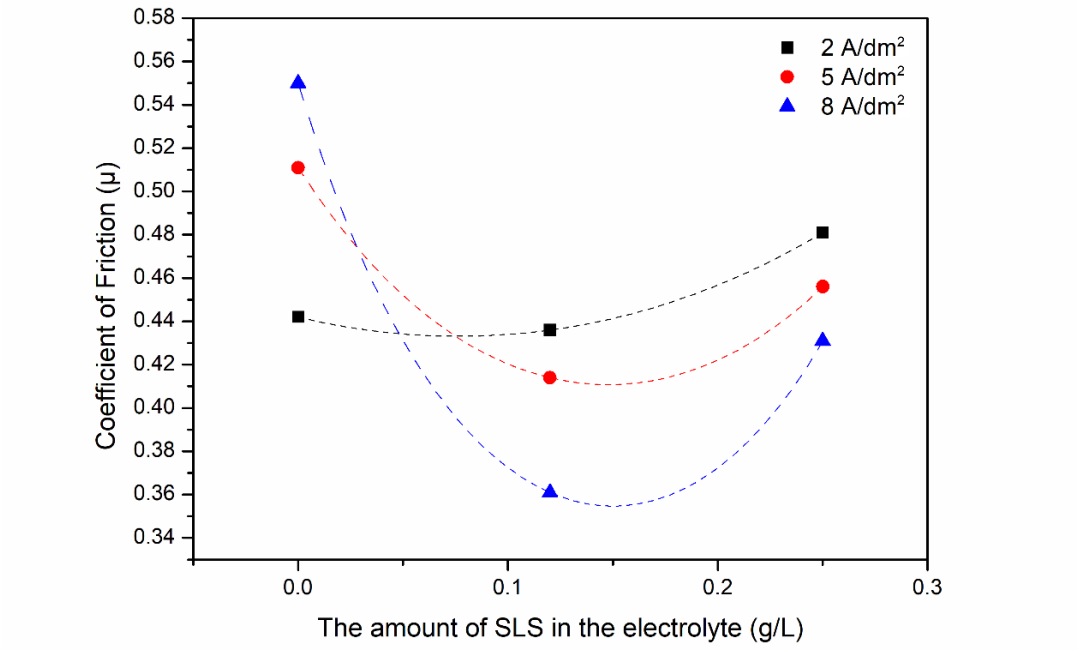

Figure 28 The effect of SLS concentration combined with 0.25 g/l ALS on COF at three different current densities

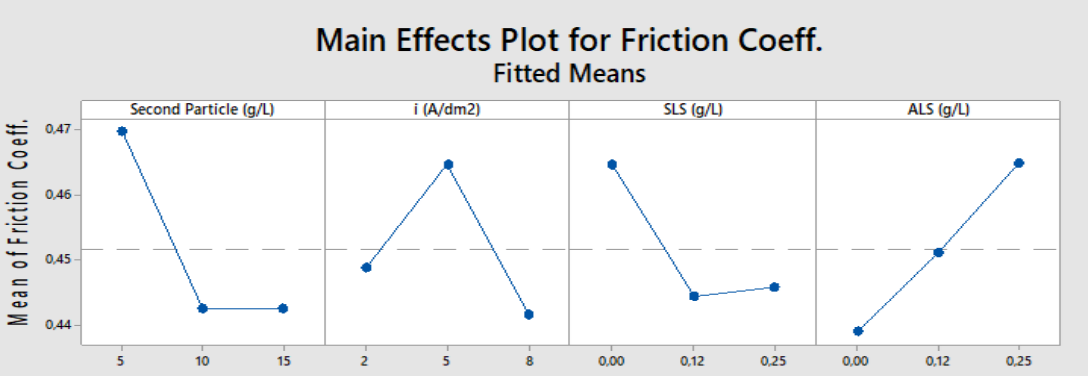

Figure 29 The mean effects of design parameters on friction coefficient

Considering the pure nickel coating having a COF of 0.678 measured at the identical conditions shown in Figure 27, composite coatings have generally lower COF due to the presence of alumina particles in the nickel matrix. It is reported that the reason of this lower COF may be due to good interfacial bonds between matrix and alumina particles, finer surface morphology resulting in decreasing the stress between the friction couples and the effect of spherical alumina powders during measurement on pin-on-disk [158,159]. It is also stated that the COF strongly depends on the type of the current, the current density and sliding speed. The COF drops below 0.2 at higher sliding speed for the nickel-alumina system [160]. Furthermore, the addition of SiC to nickel matrix lowers the COF value compared to pure nickel coatings since the hard ceramic particles acts as a barrier and decrease the direct contact between abrasive surfaces [138].

4.2.4 Surface Roughness

Since the conducting particles acts as a deposition site on cathode, they can be easily trapped by matrix when compared to non-conductive particles such as Al_2O_3 [126]. Due to this electrostatic attraction of conducting particles at cathode, they increase the surface roughness while non-conductive particles decreases [126]. Measurements were conducted to understand the change in the surface roughness. Increase in alumina

content of the composite coating slightly decreased the surface roughness as shown in Table 5 because alumina is a non-conductive ceramic particle. Topographical analysis was done to determine decreasing effect of incorporated alumina particles on surface roughness [158].

Table 5 Average roughness results in terms of alumina content in the coating

Coating	Ni	Ni-4.6%Al_2O_3	Ni-6.7%Al_2O_3	Ni-9.0%Al_2O_3
R_a (μm)	0.49 ± 0.01	0.47 ± 0.01	0.42 ± 0.01	0.37 ± 0.01

4.3 Residual Stress of Composite Coatings

All residual stress experiments were done in electrolyte containing 10 g/l alumina particles. The effect of ALS, current density and pH on residual stress of the composite coating were studied by 18 experiments as shown in Table 6 and it was designed by full-factorial statistical design of experiment for three factors. Coating thickness on copper strips was approximately 15 μm for all measurements.

Table 6 Operating parameters and measured residual stress values

ALS (g/l)	i (A/dm^2)	pH	Res. Str. (MPa)
0	2	3.5	17.47 ± 1.93
0.12	2	3.5	83.29 ± 1.97
0.25	2	3.5	175.08 ± 2.86
0	2	4.5	6.03 ± 0.61
0.12	2	4.5	66.18 ± 1.72
0.25	2	4.5	153.8 ± 4.19
0	5	3.5	35.31 ± 2.06
0.12	5	3.5	62.26 ± 2.07
0.25	5	3.5	94.13 ± 2.07
0	5	4.5	15.81 ± 0.61
0.12	5	4.5	44.5 ± 1.40

Table 6 (continued) Operating parameters and measured residual stress values

0.25	5	4.5	84.94 ± 4.08
0	8	3.5	41.15 ± 2.10
0.12	8	3.5	70.28 ± 2.13
0.25	8	3.5	85.14 ± 2.11
0	8	4.5	16.79 ± 0.66
0.12	8	4.5	29.12 ± 0.63
0.25	8	4.5	86.03 ± 4.14

The regression equation for residual stress calculated from above table in terms of operating parameters is shown in Eq. 4.6:

$$Res.Str.(MPa) = 115 + 365\,A - 4.8\,B - 18\,C \qquad (4.6)$$

where A is the amount of ALS (g/l), B is the current density (A/dm^2) and C is the pH. ALS addition has a positive and dominant influence on residual stress with a factor of 365 while current density and pH have negative effects with smaller factors of -4.8 and -18 respectively, when compared to ALS addition. The statistical analysis of above regression equation showed a fit with an R-square value of 0.802.

Since the properties of the composite are considerably influenced by the residual stress, it is better to be under control [161]. The residual stresses for composite coatings arise from the difference between lattices of matrix and the second phase particles, the difference in thermal expansion coefficient between matrix and substrate and stress due to plating bath or its conditions [162]. In general, Ni-based coatings such as alloys or composite coatings have the residual stress in tension [163–167]. However, it is reported that the residual stress can be in tension or compression with respect to type or composition of plating bath or operating parameters [158,162,163]. In this study, all the residual stresses were in tension. The interrelations of the parameters are shown in Figure 30. It is clearly seen that the residual stress decreased with increase in pH and current density. As mentioned above, more alumina could be deposited at lower current densities because deposition rate of the nickel coating was lower at lower

current densities. Therefore, those coatings had better hardness, wear resistance, lower COF and smoother surface. The more alumina content at lower current densities and higher ALS addition resulted in higher residual stress due to higher amount of alumina particles in the composite coatings. In addition, ALS addition had a little impact on residual stress without alumina particles and it may make the coatings more brittle. The sulfamate plating bath typically provides lower residual stress but addition of ALS and alumina particles caused higher residual stresses. The reason for increase in residual stress may be larger crystal structure of alumina particles than nickel. The alumina particles may distort the nickel crystal structure resulting in higher residual stress.

The counter plots, statistically extrapolates the residual stress results for the values within the design parameters as shown in Figure B.16 to Figure B.18 of APPENDIX B. The effects of operating parameters such as pH, the amount of ALS in the electrolyte and the current density on residual stress can be followed from these graphs.

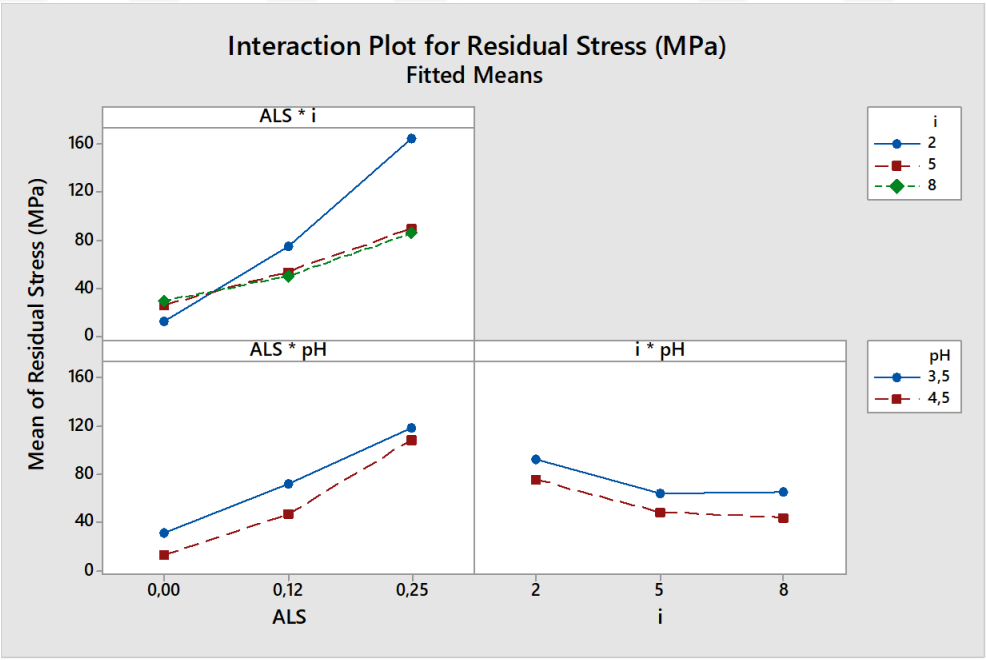

Figure 30 Interaction plot for residual stresses

The main effects plots shown in Figure 31 were determined by taking the average of 9 points for related parameter from the interaction plots in Figure 30. It is concluded that the residual stress is lower at lower ALS addition, higher current density and higher pH values.

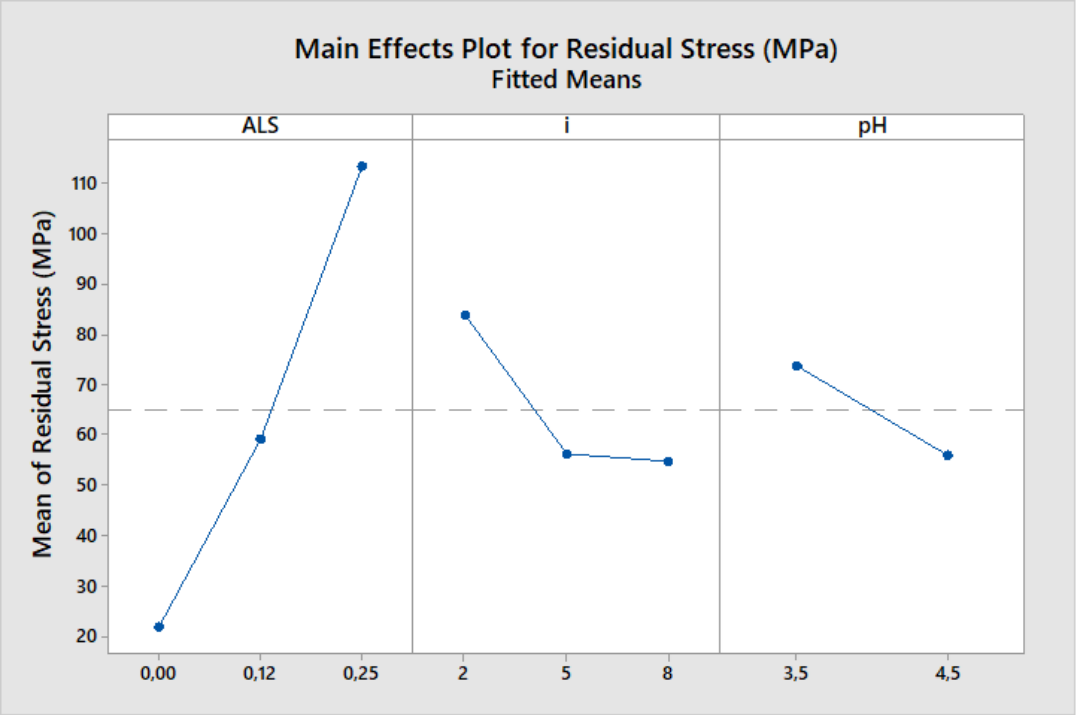

Figure 31 The mean effects plot for residual stress

Other than operating parameters, another parameter that affects the residual stress is the coating thickness. The residual stress decreases with increase in thickness as shown in Figure 32 due to the distribution of the residual stress resulting from the lattice mismatch between alumina particles and nickel matrix over a larger area [40,167,168].

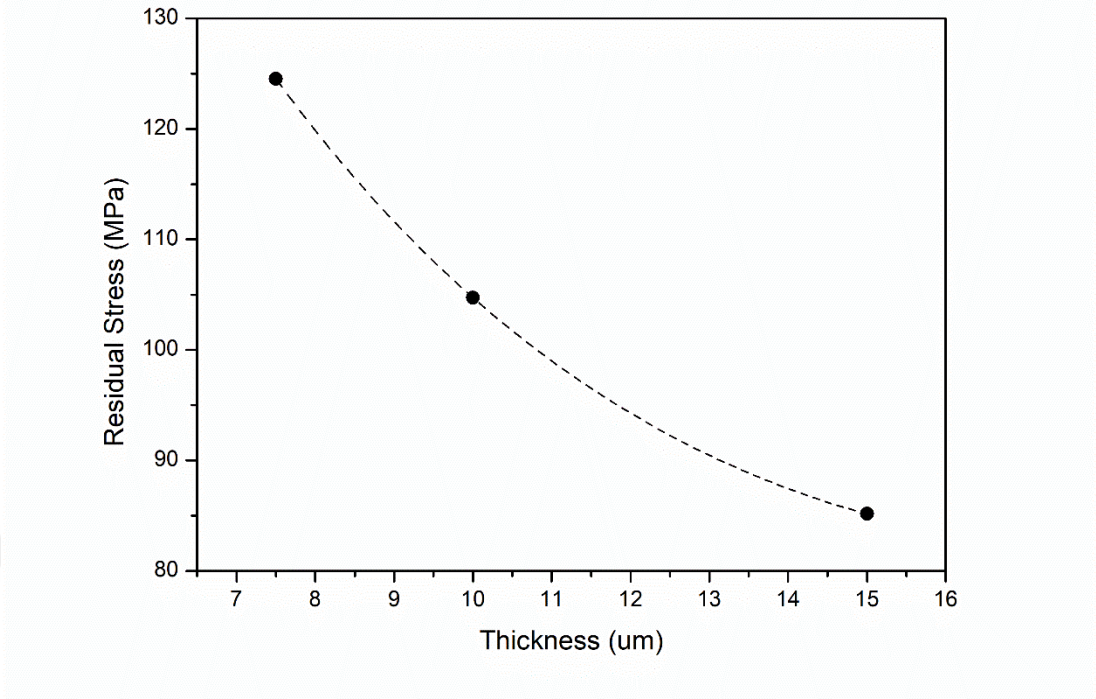

Figure 32 The effect of coating thickness on residual stress at pH of 3, the addition of 0.25 g/l ALS and the current density of 8 A/dm^2

4.4 Morphological and Crystallographical Investigations

In previous parts, it was discussed that increase in Al_2O_3 content of composite coatings decreased the surface roughness. Figure 33 indicates that the composite coatings deposited at lower current densities had quite smoother surface compared to deposits at higher current densities. The results could be related to alumina content as well since the composite coatings had higher hardness values at lower current densities with ALS addition due to incorporation of more Al_2O_3. The presence of alumina particles in the nickel matrix inhibits the growth of matrix on the particles due to its non-conductive behavior. For more detailed analysis, some measurements were conducted via AFM to study on morphology and surface roughness of composite coatings shown in Figure 33 and it supported the other results mentioned above.

The grain size of the pure nickel coatings depends on the nucleation rate of the deposition; in addition, nucleation rate increases with increasing current density. Therefore, the grain size becomes finer when more nickel nucleates at limited growth rate. On the other hand, the growth of the grains is inhibited by the presence of the second phase particles for Ni-Al_2O_3 system. Higher alumina content at lower current density shown in Figure 34 may be the result of lower grain size at lower current densities. It also represented the morphology of the composite coatings. It is clearly seen that the nodular grains nucleated and grew on copper substrate at lower current densities with the addition of anionic surfactants. Surface analysis conducted by AFM also supported this result as shown in Figure 34. In the literature, it is argued that the nodular morphology was revealed due to low Co content for Co-Ni-Al_2O_3 system [169]. They also stated that the morphology was regular not nodular without the presence of alumina particles. Therefore, it may be said that the composite coatings having nodular grains have more alumina content, which is the idea supported by higher hardness values at lower current densities.

The morphology and the crystallography of the composite coatings can be influenced by the current density, type of the current, the second phase particles, the additives, and the bath composition [169–171]. It is stated that the surface roughness decreases when the nucleation rate decreases. The reason for this argument may be the finer grains with limited growth rates resulting in the smoother surface. It is also reported that the cathodic polarization become higher due to the interaction between Al_2O_3 particles and cathode and this makes the grains finer [169]. However, Shakoor et al. stated that the Al_2O_3 addition indicates the increase in surface roughness for Ni-B-Al_2O_3 system [170]. The reason of opposite effect of alumina particles on roughness between Ni-B-Al_2O_3 and the present study may be the presence of boron together with nickel or the difference in the particles size of the alumina.

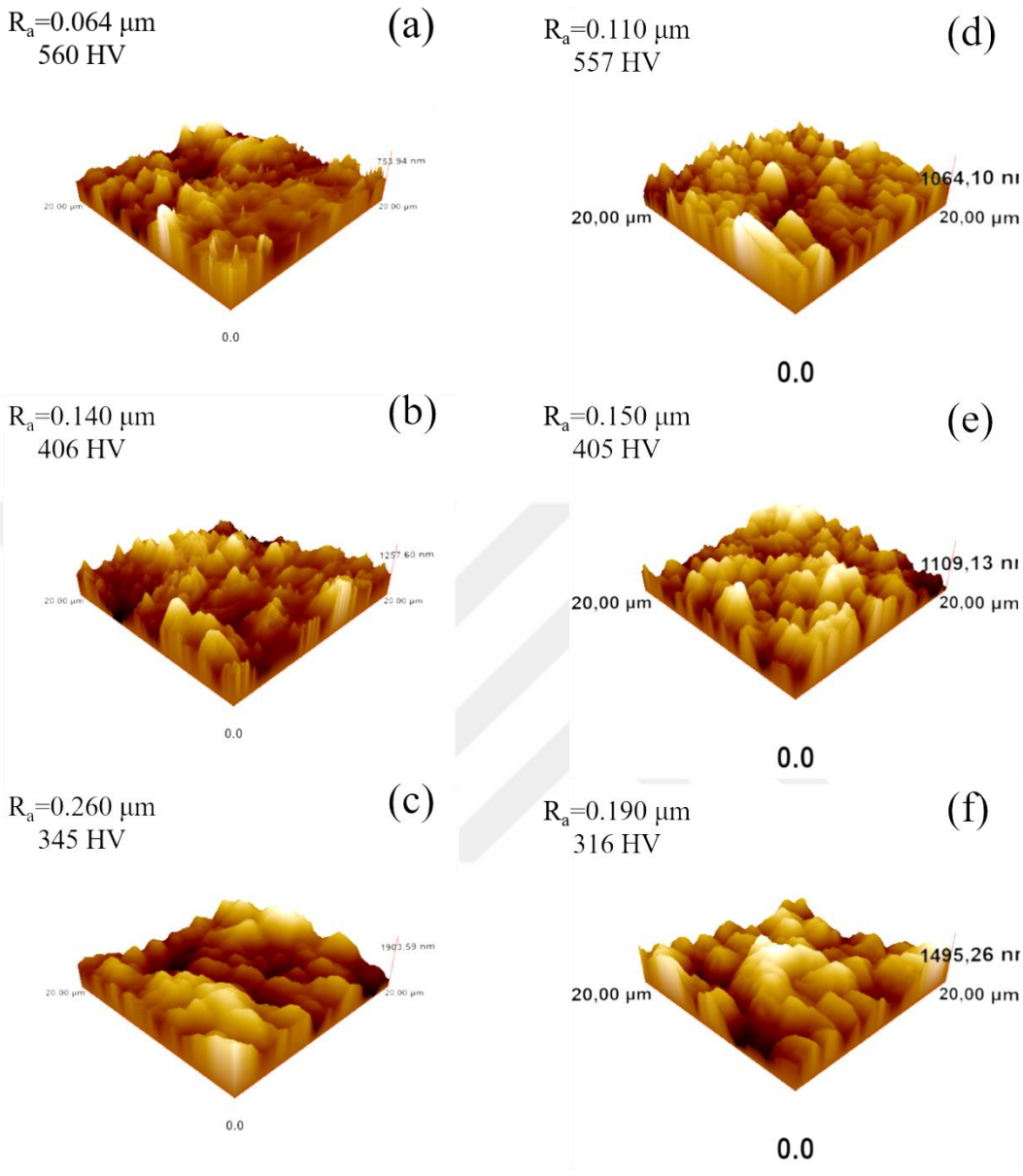

Figure 33 Surface analysis via AFM to understand the effect of current density of (a) 2, (b) 5 and (c) 8 A/dm^2 at 0.25 g/l ALS addition, (d) 2, (e) 5 and (f) 8 A/dm^2 at 0.12 g/l SLS combined with 0.25 g/l ALS and 10 g/l Al_2O_3 in the electrolyte

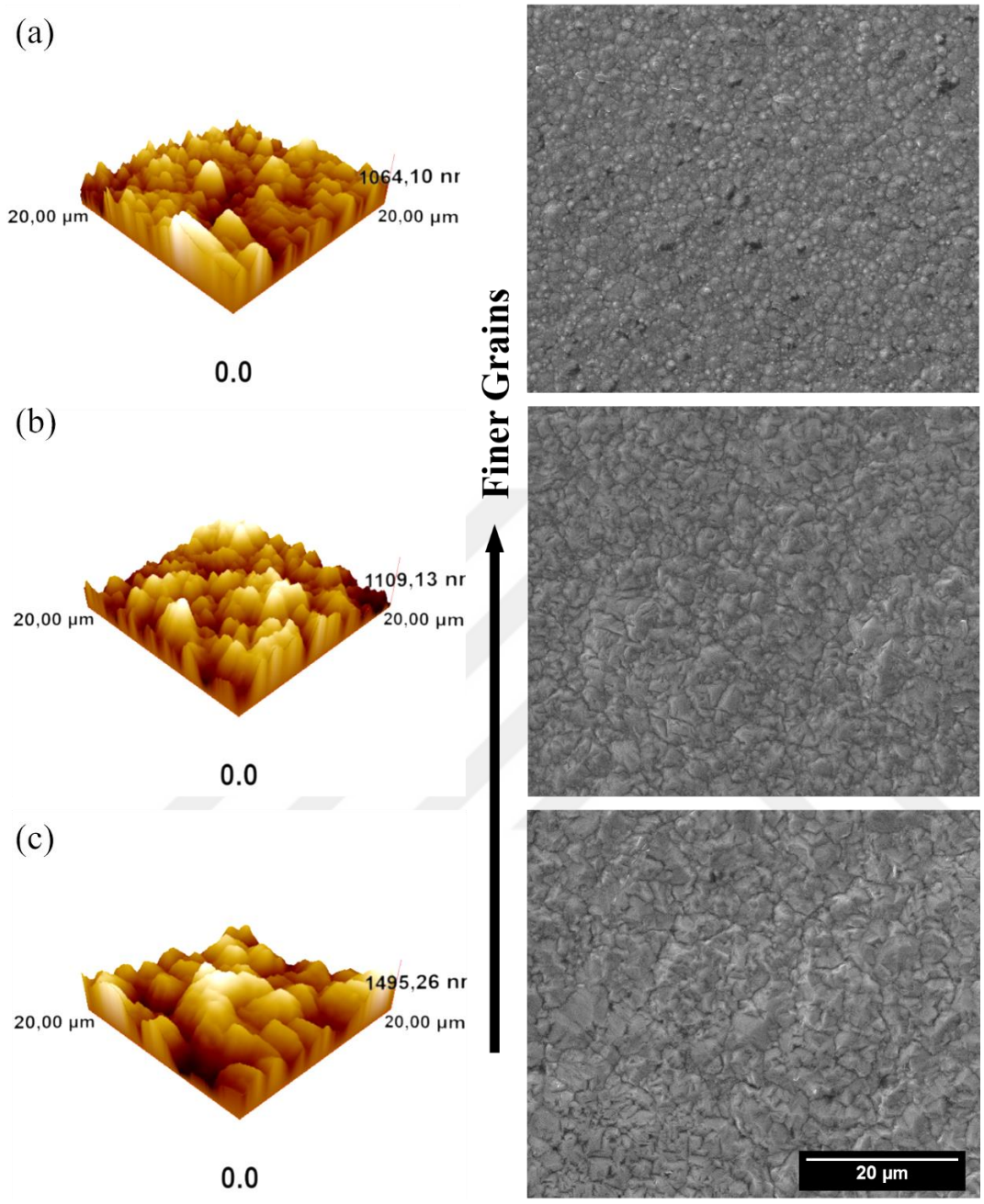

Figure 34 Surface analysis via AFM and SEM images of composite coatings at (a) 2, (b) 5 and (c) 8 A/dm^2 at 0.12 g/l SLS combined with 0.25 g/l ALS and 10 g/l Al_2O_3 in the electrolyte

Figure 35 and Figure 36 demonstrates the comparison of XRD patterns of composite coatings deposited from electrolytes of different concentrations of surfactants at different current densities. Previous results given in Figure 33 and Figure 34 indicated that the nodular grains were formed at lower current densities. When the grains were preferentially oriented on (111), (220) and (311) instead of (200) along with weak (111) as same as the Ni coating as shown in Figure 37, they were grown as nodular at lower current densities with the addition of surfactants, which is supported by some studies in literature for Ni-Al_2O_3 systems [75,172,173]. Crystallographic orientations of composite coatings were affected by bath compositions, additives, and the second phase particles [40,174]. It is reported that growth on (200) plane was favored for nickel coatings, and this tends to have lower residual stress [40]. Moreover, growth on these planes makes the coating more ductile, softer and less residual stress [51,175,176]. Nickel coatings generally oriented on (200) and (111) diffraction planes while the addition of SiC to nickel matrix reinforced the (111), (220) and (311) planes [138].

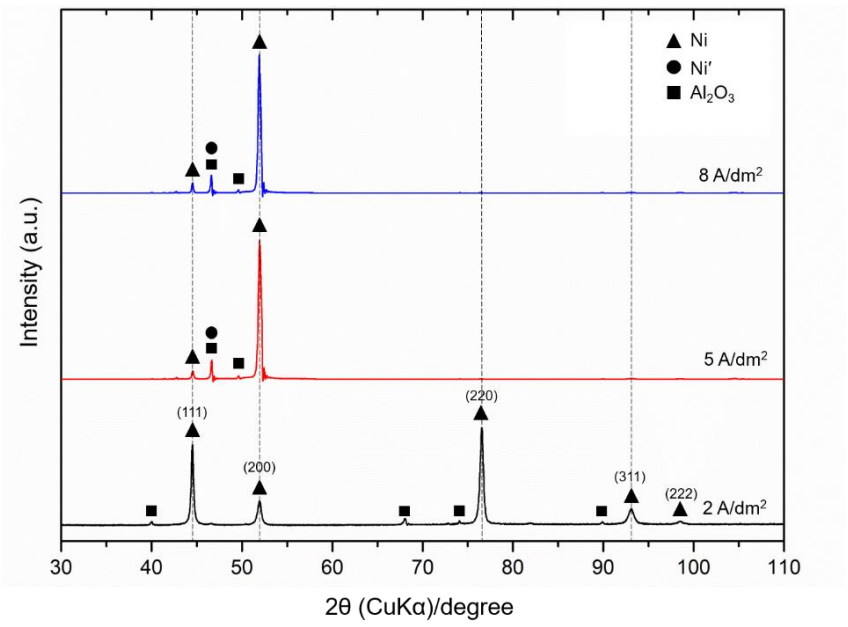

Figure 35 XRD patterns showing the effect of current density on crystallography of composite coatings at 0.25 g/l ALS

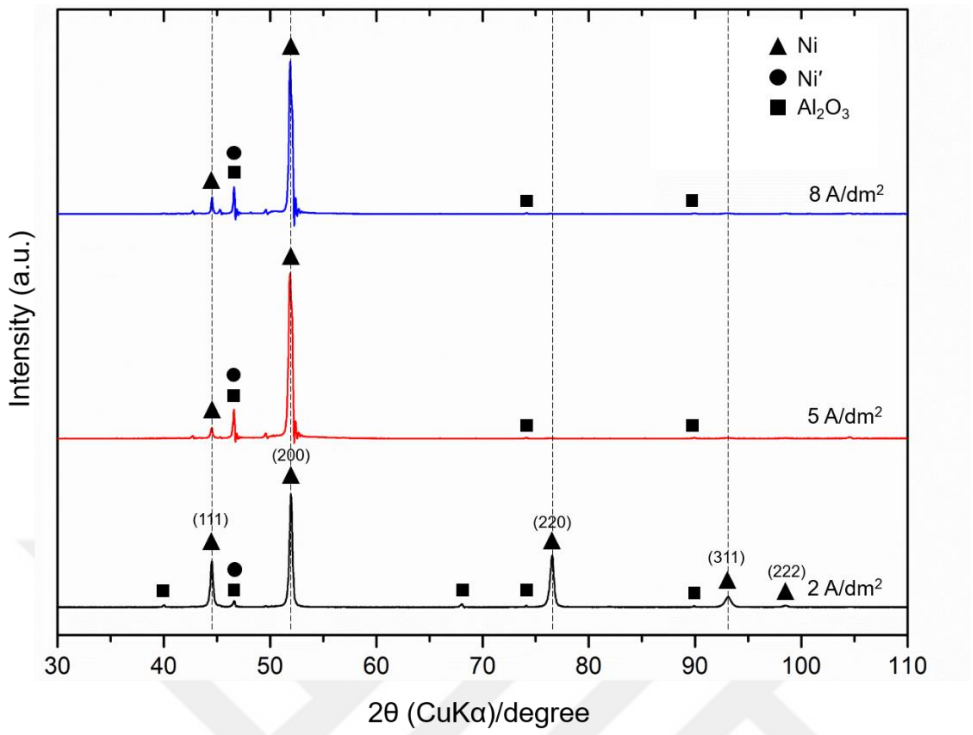

Figure 36 XRD patterns showing the effect of current density on crystallography of composite coatings at 0.12 g/l SLS combined with 0.25 g/l ALS

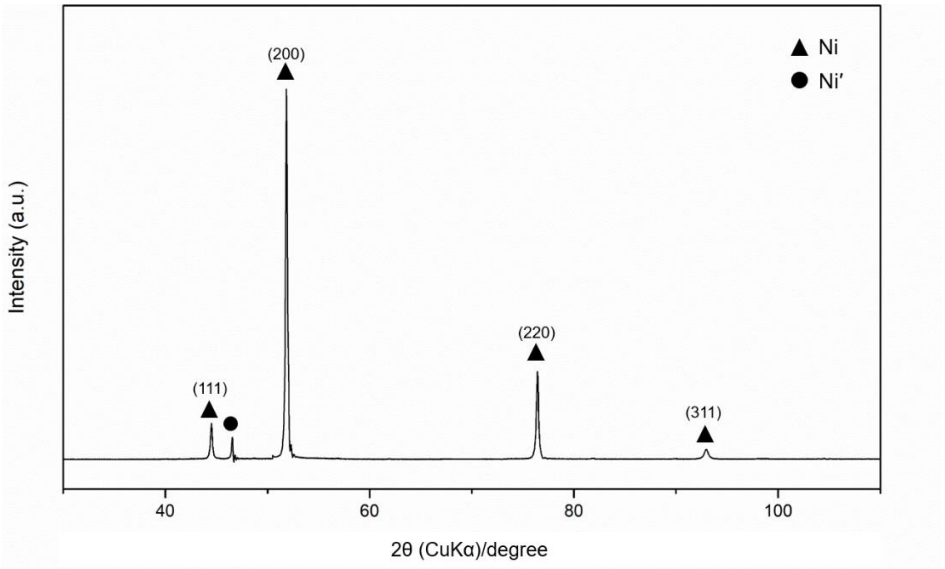

Figure 37 XRD pattern of Ni coating at a current density of 2 A/dm^2 without surfactant

Metastable BCC Ni′ phase was grown on copper substrate as shown in Figure 35, Figure 36 and Figure 37 [177–179]. It can be seen that the metastable phase can be grown in the composite coating or the pure nickel deposition process. It is more favorable at higher current densities while suppressed or not grown at lower current densities with the presence of anionic surfactants as shown in Figure 35 and Figure 36. It is also reported that metastable BCC nickel phase was grown on (001) plane of iron [177]. This metastable BCC phase of nickel has a lattice parameter of 2.76 Å [179].

CHAPTER 5

CONCLUSION

Nickel matrix composite coatings incorporated with submicron alumina particles were electrodeposited using acidic sulfamate solution.

Addition of anionic surfactants caused the reaction for electrodeposition of nickel to more anodic values. Furthermore, addition of alumina powder to sulfamate bath with wetting agent provided the reaction to be more anodic as well.

As opposed to typical nickel coatings, the hardness decreased with increasing current density with the addition of ALS and SLS combined with ALS. COF values also decreased with an increase in current density without surfactants. The addition of ALS at a constant current density increased COF. When SLS was combined with ALS, COF values first decreased and then increased with further addition of SLS.

Wear resistance of the composite coatings had a more complex relation with current density and surfactants. Wear resistance was higher at higher current densities and lower amounts of surfactants. However, better wear resistance values were obtained at lower current densities, when the amounts of ALS and SLS were progressively increased. Furthermore, it was found that wear behaviors of the composite coatings strongly depended on the amount of deposited alumina particles.

The presence of alumina powders in the composite coatings increased the residual stress. As for other process parameters, residual stresses decreased at lower pH, higher current density, lower ALS addition and higher coating thickness.

The preferred orientations became (220) and (311) at lower current densities with the presence of anionic surfactant additions when more alumina particles were present.

Nodular instead of regular shape grains grew at that preferred orientation. Nodular grains had better mechanical and tribological properties but higher residual stress.

Some studies might be suggested for further investigation of the Ni-Al_2O_3. For instance, zeta potential measurements to understand the deposited mechanism of alumina particles and their effect on the properties, the effect of pulse or pulse-reverse current on the properties and deposited alumina concentration and deposit mechanisms of different alumina phases such as α-, β-, γ-, δ- and θ-Al_2O_3 might be studied to understand the deposition mechanism of alumina particles into the nickel matrix deeply.

REFERENCES

[1] W. Schwarzacher, Electrodeposition: A Technology for the Future, Electrochem. Soc. Interface. 15 (2006) 32–35. http://www.electrochem.org/dl/interface/spr/spr06/if_spr06.htm.

[2] F. Endres, A. Abbott, D. Macfarlane, Electrodeposition from ionic liquids, John Wiley & Sons, 2017.

[3] A. Yakovlev, P. Bertrand, I. Smurov, Laser cladding of wear resistant metal matrix composite coatings, Thin Solid Films. 453–454 (2004) 133–138. doi:10.1016/j.tsf.2003.11.085.

[4] M. Schlesinger, M. Paunovic, Modern Electroplating, 4th ed., John Wiley & Sons, New York, 2000.

[5] G.A. DiBari, Plating and Surface Finishing, in: Nickel Electroplat. Appl. Trends, 1996: pp. 10–14.

[6] G.A. Di Bari, Electrodeposition of Nickel, Mod. Electroplat. Fifth Ed. (2011) 79–114. doi:10.1002/9780470602638.ch3.

[7] I. Gurrappa, L. Binder, Electrodeposition of nanostructured coatings and their characterization - A review, Sci. Technol. Adv. Mater. 9 (2008). doi:10.1088/1468-6996/9/4/043001.

[8] J.L. Stojak, J. Fransaer, J.B. Talbot, Review of Electrocodeposition, 2002.

[9] J.L. Stojak, J. Fransaer, J.B. Talbot, Review of Electrocodeposition, in: Adv. Electrochem. Sci. Eng. Vol. 7, 2001: pp. 193–223. doi:10.1002/3527600264.ch4.

[10] R. V. Williams, Electrodeposited composite coatings, Electroplat. Met. Finish. (1966) 92–96.

[11] V.P. Greco, A review of fabrication and properties of electrocomposites, Plat. Surf. Finish. 76 (1989) 68–72.

[12] P.R. Ebdon, The performance of electroless Nickel-PTFE Composites, Plat. Surf. Finish. 75 (1988) 65–68.

[13] R. Mévrel, State of the art on high-temperature corrosion-resistant coatings, Mater. Sci. Eng. A. 120–121 (1989) 13–24. doi:10.1016/0921-5093(89)90713-2.

[14] Y. Sofer, Y. Yarnitzky, S.F. Dirnfeld, Evaluation and uses of composite Ni-Co matrix coatings with diamonds on steel applied by electrodeposition, Surf. Coatings Technol. 42 (1990) 227–236. doi:10.1016/0257-8972(90)90155-6.

[15] G.A. Malone, Electrodeposition of dispersion-strenthened alloys, Plat. Surf. Finish. 78 (1991) 58–62.

[16] E.S. Güler, Effects of Electroplating Characteristics on the Coating Properties, in: A.M.A. Mohammed (Ed.), Electrodepos. Compos. Mater., IntechOpen, 2016: pp. 27–37. doi:10.5772/61745.

[17] Y.D. Gamburg, G. Zangari, Theory and Practice of Metal Electrodeposition, Springer Science & Business Media, 2011.

[18] D.A. MacInnes, The Principles of Electrochemistry, 2nd ed., Dover Publications, New York, 1961.

[19] A.J. Bard, L.R. Faulkner, Electrochemical Methods Fundamentals and Applications, 2nd ed., John Wiley & Sons, 2001.

[20] Z. Ahmad, Principles of Corrosion Engineering and Corrosion Control, Elsevier Ltd, Oxford, UK, 2006. doi:10.1016/B978-0-7506-5924-6.50008-8.

[21] F.A. Lowenheim, Modern Electroplating, John Wiley & Sons, Toronto, 1974.

[22] J.O.M. Bockris, A.K.N. Reddy, Modern Electrochemistry, New York, 1970.

[23] E. Mattsson, J.O. Bockris, Galvanostatic studies of the kinetics of deposition and dissolution in the copper + copper sulphate system, Trans. Faraday Soc. 55 (1959) 1586. doi:10.1039/tf9595501586.

[24] G. Bird, Observations on the Electro-Chemical Influence of Long-Continued Electric Currents of Low Tension, Philos. Trans. R. Soc. London. 127 (1837) 37–45.

[25] J. Shore, U.K. Patent, 8407, 1840.

[26] R. Bottger, Investigation of Nickel Plating on Metals, Erdmann's J. Prakt. Chemie. 30 (1843).

[27] O.P. Watts, Rapid Nickel Plating, Trans. Electrochem. Soc. 29 (1916) 395.

[28] L. Cambi, R. Piontelli, Italian Patent, 368,824, 1939.

[29] J.J. Kelly, N.Y.C. Yang, Electrodeposition of Ni from A Part I . Effect of a Stress Relief on Annealing Behavior and Film Metallurgy, 2001.

[30] G.A. Di Bari, Nickel Plating, in: Electroplat. Eng. Handb., Van Nostrand Reinhold Company, New York, 1984.

[31] ASM Handbook: Surface Engineering, 5th ed., American Society for Metals, 1994.

[32] J.K. Dennis, T.E. Such, Nickel and Chromium Plating, 3rd ed., Woodhead Publishing Ltd., Cambridge, UK, 1993.

[33] T.L.R. Char, S. Sathyanarayana, Electrodeposition from Sulphamate Solutions, J. Sci. Ind. Res. 16A (1957) 78–85.

[34] J.R. Davis, Nickel Coating, in: ASM Spec. Handb. Nickel, Cobalt Their Alloy., 2000.

[35] G.A. Prentice, C.W. Tobias, A Survey of Numerical Methods and Solutions for Current Distribution Problems, J. Electrochem. Soc. 129 (1982) 72. doi:10.1149/1.2123795.

[36] J. Kronsbein, Current and Metal Distribution in Electrodeposition, Am. Electroplat. Soc. 37 (1950).

[37] H.E. Haring, W. Blum, N, Trans. Am. Electrochem. Soc. 44 (1923).

[38] S.A. Watson, The Throwing Power of Nickel and Other Plating Solutions, Trans. IMF. 37 (1960) 28–39.

[39] Annual Book of ASTM Standards, Vol.02.05, American Society for Testing and Materials, West Conshohocken, PA, 1996.

[40] Y. Tsuru, M. Nomura, F.R. Foulkes, Effects of boric acid on hydrogen evolution and internal stress in films deposited from a nickel sulfamate bath, J. Appl. Electrochem. 32 (2002) 629–634. doi:10.1023/A:1020130205866.

[41] M. Surender, R. Balasubramaniam, B. Basu, Electrochemical behavior of electrodeposited Ni-WC composite coatings, Surf. Coatings Technol. 187 (2004) 93–97. doi:10.1016/j.surfcoat.2004.01.030.

[42] H.C. Rogers, Hydrogen Embrittlement of Metals: Atomic hydrogen from a variety of sources reduces the ductility of many metals, Science (80-.). 159 (1968) 1057–1064.

[43] C.T.J. Low, R.G.A. Wills, F.C. Walsh, Electrodeposition of composite coatings containing nanoparticles in a metal deposit, Surf. Coatings Technol. 201 (2006) 371–383. doi:10.1016/j.surfcoat.2005.11.123.

[44] V.P. Greco, Electrocomposites and their benefits, Plat. Surf. Finish. 76 (1989) 62–67.

[45] J.R. Roos, J.P. Celis, J.A. Helsen, Codeposition of Alpha- and Gamma-Alumina with Copper from Copper Sulphate Baths, Trans. IMF. 55 (1977) 113–116.

[46] C. White, J. Foster, Factors Affecting the Entrapment of Alumina Particles During the Electrodeposition of Copper, Trans. IMF. 59 (1981) 8–12.

[47] S.W. Watson, R.P. Walter, The Effect of Chromium Particles on Nickel Electrodeposition, J. Electrochem. Soc. 138 (1991) 3633–3637.

[48] P.R. Webb, N.L. Robertson, Electrolytic Codeposition of Ni-gamma/Al_2O_3 Thin Films, J. Electrochem. Soc. 141 (1994) 669–673.

[49] A.E. Grazen, Plating Process Co-deposits Oxides or Carbides, Iron Age. 183 (1959).

[50] M. Surender, B. Basu, R. Balasubramaniam, Wear characterization of electrodeposited Ni-WC composite coatings, Tribol. Int. 37 (2004) 743–749. doi:10.1016/j.triboint.2004.04.003.

[51] M.R. Vaezi, S.K. Sadrnezhaad, L. Nikzad, Electrodeposition of Ni-SiC nano-composite coatings and evaluation of wear and corrosion resistance and electroplating characteristics, Colloids Surfaces A Physicochem. Eng. Asp. 315 (2008) 176–182. doi:10.1016/j.colsurfa.2007.07.027.

[52] P. Baghery, M. Farzam, A.B. Mousavi, M. Hosseini, Ni-TiO_2 nanocomposite coating with high resistance to corrosion and wear, Surf. Coatings Technol. 204 (2010) 3804–3810. doi:10.1016/j.surfcoat.2010.04.061.

[53] N. Periene, A. Cesuniene, Taicas L., Nickel Electrodeposits with Improved Hot Oxidation and Corrosion Resistance by Codeposition of Submicron Powders, Plat. Surf. Finish. 80 (1993) 73.

[54] G.N.K. Ramesh Bapu, Electrocodeposition and characterization of nickel-titanium carbide composites, Surf. Coatings Technol. 67 (1994) 105–110. doi:10.1016/S0257-8972(05)80033-7.

[55] M. Mohammadi, M. Ghorbani, Wear and corrosion properties of electroless nickel composite coatings with PTFE and/or MoS_2 particles, J. Coatings Technol. Res. 8 (2011) 527–533. doi:10.1007/s11998-011-9329-y.

[56] P.A.I. Popoola, P.I. Odetola, O.M. Popoola, D. Delport, Parametric Variables in Electro-deposition of Composite Coatings, Electrodepos. Compos. Mater. (2016) 1–18.

[57] P.W. Martin, R. V. Williams, Electrodeposited Composite Coatings, Trans. IMF. 48 (1964) 182–188.

[58] D.W. Snaith, P.D. Groves, A Study of the Mechanisms of Cermet electrodeposition, Trans. IMF. 50 (1972) 95–101.

[59] E.A. Brandes, D. Goldthorpe, Electrodeposition of cermets, Metallurgia. 76 (1967) 195–198.

[60] E. V. Bezus, H. Brown, L.C. Tomaszewski, Codeposition of finely dispersed particles with metals, Plating. 59 (1969) 1234–1239.

[61] N. Guglielmi, Kinetics of the deposition of inert particles from electrolytic baths, J. Electrochem. Soc. 119 (1972) 1009–1012.

[62] C. Buelens, A Model for the Codeposition of Inert Particles with a Metal, PhD Thesis, Catholic University, Leuven, 1984.

[63] J.P. Celis, J.R. Roos, C. Buelens, A mathematical model for the electrolytic codeposition of particles with a metallic matrix, J. Electrochem. Soc. 134 (1984) 1402–1408.

[64] J.L. Valdes, Deposition of Colloidal Particles in Electrochemical Systems, PhD Thesis, Columbia University, New, York, 1987.

[65] Y. Eng, Electrodeposition of metal and colloidal particle composite films onto a rotating cylinder electrode, Columbia University, New York, 1991.

[66] J. Fransaer, Study of the behaviour of particles in the vicinity of electrodes, PhD Thesis, Catholic University, Leuven, 1994.

[67] J. Fransaer, J.P. Celis, J.R. Roos, Analysis of the Electrolytic Codeposition of Non-Brownian Particles with Metals, J. Electrochem. Soc. 139 (1992) 413–425.

[68] P. Bercot, E. Pena-Munoz, J. Pagetti, Electrolytic composite Ni–PTFE coatings: an adaptation of Guglielmi's model for the phenomena of incorporation, Surf. Coat. Technol. 157 (2002) 282–289.

[69] P.M. Vereecken, I. Shao, P.C. Searson, Particle Codeposition in Nanocomposite Films, J. Electrochem. Soc. 147 (2000) 2572. doi:10.1149/1.1393570.

[70] J.R. Roos, J.P. Celis, J. Fransaer, C. Buelens, The development of composite plating for advanced materials, JOM. 42 (1990) 60–63. doi:10.1007/BF03220440.

[71] I. Corni, R.J. Chater, A.R. Boccaccini, M.P. Ryan, Electro co-deposition of Ni–Al2O3 composite coatings, J. Mater. Sci. 47 (2012) 5361–5373. doi:10.1007/s10853-012-6381-7.

[72] M. Der Ger, Electrochemical deposition of nickel/SiC composites in the presence of surfactants, Mater. Chem. Phys. 87 (2004) 67–74. doi:10.1016/j.matchemphys.2004.04.022.

[73] M. Sabri, A.A. Sarabi, S.M. Naseri Kondelo, The effect of sodium dodecyl sulfate surfactant on the electrodeposition of Ni-alumina composite coatings, Mater. Chem. Phys. 136 (2012) 566–569. doi:10.1016/j.matchemphys.2012.07.027.

[74] L. Chen, L. Wang, Z. Zeng, J. Zhang, Effect of surfactant on the electrodeposition and wear resistance of Ni-Al_2O_3 composite coatings, Mater. Sci. Eng. A. 434 (2006) 319–325. doi:10.1016/j.msea.2006.06.098.

[75] S.T. Aruna, V.K. William Grips, K.S. Rajam, Synthesis and characterization of Ni–Al_2O_3 composite coatings containing different forms of alumina, J. Appl. Electrochem. 40 (2010) 2161–2169. doi:10.1007/s10800-010-0198-3.

[76] T. Borkar, S.P. Harimkar, Effect of electrodeposition conditions and reinforcement content on microstructure and tribological properties of nickel composite coatings, Surf. Coatings Technol. 205 (2011) 4124–4134. doi:10.1016/j.surfcoat.2011.02.057.

[77] B. Szczygieł, M. Kołodziej, Composite Ni/Al_2O_3 coatings and their corrosion resistance, Electrochim. Acta. 50 (2005) 4188–4195. doi:10.1016/j.electacta.2005.01.040.

[78] R.K. Saha, T.I. Khan, Effect of applied current on the electrodeposited Ni-Al_2O_3 composite coatings, Surf. Coatings Technol. 205 (2010) 890–895. doi:10.1016/j.surfcoat.2010.08.035.

[79] L. Chen, L. Wang, Z. Zeng, T. Xu, Influence of pulse frequency on the microstructure and wear resistance of electrodeposited Ni-Al_2O_3 composite coatings, Surf. Coatings Technol. 201 (2006) 599–605. doi:10.1016/j.surfcoat.2005.12.008.

[80] Q. Feng, T. Li, H. Teng, X. Zhang, Y. Zhang, C. Liu, J. Jin, Investigation on the corrosion and oxidation resistance of Ni-Al_2O_3 nano-composite coatings prepared by sediment co-deposition, Surf. Coatings Technol. 202 (2008) 4137–4144. doi:10.1016/j.surfcoat.2008.03.001.

[81] X. Wei, H. Dong, C.H. Lee, K. Jiang, Determination of young's modulus of electrochemically co-deposited Ni-Al_2O_3 nanocomposite, Mater. Lett. 62 (2008) 1916–1918. doi:10.1016/j.matlet.2007.10.053.

[82] A. Bund, D. Thiemig, Influence of bath composition and pH on the electrocodeposition of alumina nanoparticles and nickel, Surf. Coatings Technol. 201 (2007) 7092–7099. doi:http://dx.doi.org/10.1016/j.surfcoat.2007.01.010.

[83] D. Thiemig, A. Bund, Influence of ethanol on the electrocodeposition of Ni/Al_2O_3 nanocomposite films, Appl. Surf. Sci. 255 (2009) 4164–4170. doi:10.1016/j.apsusc.2008.10.114.

[84] D. Thiemig, A. Bund, J.B. Talbot, Influence of hydrodynamics and pulse plating parameters on the electrocodeposition of nickel-alumina nanocomposite films, Electrochim. Acta. 54 (2009) 2491–2498. doi:10.1016/j.electacta.2008.04.004.

[85] J.P. Celis, J.R. Roos, C. Buelens, A mathematical model for the electrolytic codeposition of particles with a metallic matrix, J. Electrochem. Soc. 134 (1987) 1402–1408.

[86] J.L. Stojak, Investigation of electrocodeposition using a rotating cylinder electrode, PhD thesis, University of California, San Diego, 1997.

[87] H. Hayashi, S. Izumi, I. Tari, Codeposition of α-Alumina Particles from Acid Copper Sulfate Bath, J. Electrochem. Soc. 140 (1993) 362–365.

[88] C. Buelens, J.P. Celis, J.R. Roos, Electrochemical aspects of the codeposition of gold and copper with inert particles, J. Appl. Electrochem. 13 (1983) 541–548.

[89] J.L. Stojak, J.B. Talbot, Investigation of electrocodeposition using a rotating cylinder electrode, J. Electrochem. Soc. 146 (1999) 4504–4513.

[90] N. Guglielmi, G. Icardi, Electrocombined Ni-TiO_2 Deposits, La Metall. Ital. 62 (1970) 420.

[91] E.S. Chen, G.R. Lakshminarayanan, F.K. Sautter, The codeposition of alumina and titania with copper, Metall. Trans. 2 (1971) 937–942.

[92] J.P. Celis, H. Kelchtermans, J.R. Roos, Properties of Electrodeposited Copper-Alumina Coatings, (n.d.).

[93] J.P. Celis, J.A. Helsen, P. Hermans, J.R. Roos, The determination of alumina in a copper matrix by atomic absorption spectrometry, Anal. Chim. Acta. 92 (1977) 413–416.

[94] M. Kimoto, A. Yakawa, T. Tsuda, R. Kammel, Zinc composite electrodeposition at high current densities, Met. Und Tech. 44 (1990) 1148–1152.

[95] C.E. Vest, D.F. Bazzarre, Co-Deposited Nickel-Molybdenum Disulfide a Self-Replenishing Solid Film Lubricant, Met. Finish. 65 (1967) 52–58.

[96] J. Zahavi, J. Hazan, Electrodeposited nickel composites containing diamond particles, Plat. Surf. Finish. 70 (1983) 57–61.

[97] A. Hovestad, L.J.J. Janssen, Electrochemical codeposition of inert particles in a metallic matrix, J. Appl. Electrochem. 25 (1995) 519–527. doi:10.1007/BF00573209.

[98] B. Reddy, Advances in Nanocomposites - Synthesis, Characterization and Industrial Applications, in: A. Gomes (Ed.), Electrodepos. Met. Matrix Nanocomposites Improv. Chem. Charact., InTech, 2011. doi:http://dx.doi.org/10.5772/46845.

[99] A.M.J. Kariapper, J. Foster, Further studies on the mechanism of formation of electrodeposited composite coatings, Trans. IMF. 52 (1974) 87–91.

[100] H. Takeuchi, Y. Tsunekawa, M. Okumiya, Formation of compositionally graded Ni–P deposits containing SiC particles by jet electroplating, Mater. Trans. JIM. 38 (1997) 43–48.

[101] J.P. Celis, J.R. Roos, Kinetics of the deposition of alumina particles from copper sulfate plating baths, J. Electrochem. Soc. 124 (1977) 1508–1511.

[102] J.H. Ouyang, X.S. Liang, J. Wen, Z.G. Liu, Z.L. Yang, Electrodeposition and tribological properties of self-lubricating Ni-$BaCr_2O_4$ composite coatings, Wear. 271 (2011) 2037–2045. doi:10.1016/j.wear.2010.12.035.

[103] Y.Z. Wan, Y.L. Wang, H.M. Tao, G.X. Cheng, X.H. Dong, Preparation and characterization of different particles - copper electrocomposites, J. Mater. Sci. Lett. 7 (1998) 1251–1253. doi:10.1023/A:1006539004598.

[104] S.W. Watson, Electrochemical study of SiC particle occlusion during nickel electrodeposition, J. Electrochem. Soc. 140 (1993) 2235–2238.

[105] F.K. Sautter, Electrodeposition of Dispersion-Hardened Nickel-Al_2O_3 Alloys, J. Electrochem. Soc. 110 (1963) 557–560.

[106] Y. Suzuki, M. Wajima, O. Asai, Cathodic Polarization Behavior of Ag-Al_2O_3 Electrode in Silver Thiocyanate Solution Containing Al_2O_3 Particles, J. Electrochem. Soc. 133 (1986) 259–262.

[107] P.J. Sonneveld, W. Visscher, E. Barendrecht, The influence of suspended particles on the mass transfer at a rotating disc electrode. Non-conducting particles, J. Appl. Electrochem. 20 (1990) 563–574.

[108] D.W. Gibbons, R.H. Muller, C.W. Tobias, Mass transport to cylindrical electrodes rotating in suspensions of inert microspheres, J. Electrochem. Soc. 138 (1991) 3255–3265.

[109] M. Verelst, J.P. Bonino, A. Rousset, Electroforming of metal matrix composite: dispersoid grain size dependence of thermostructural and mechanical properties, Mater. Sci. Eng. A. 135 (1991) 51–57.

[110] R. Narayan, B.H. Narayana, Electrodeposited Chromium-Graphite Composite Coatings, J. Electrochem. Soc. 128 (1981) 1704–1708.

[111] R. Narayan, S. Chattopadhyay, Electrodeposited Cr-Al_2O_3 composite coatings, Surf. Technol. 16 (1982) 227–234.

[112] G.N.K.R. Bapu, M.M. Yusuf, Electrodeposition of nickel-vanadium pentoxide composite and its corrosion behaviour, Mater. Chem. Phys. 36 (1993) 134–138.

[113] T. Tomaszewski, R. Clauss, H. Brown, Satin nickel by codeposition of finely dispersed solids, Tech. Proc. Am. Electroplat. Soc. 50 (1963) 169.

[114] E. Bezus, H. Brown, L. Tomaszewski, Codeposition of finely dispersed particles with metals, Plating. 56 (1969) 1234–1239.

[115] J. Man, S. Zhang, J. Li, B. Zhao, Y. Chen, Effects of electrolyte pH on morphologies and mechanical properties of α-Al_2O_3/Ni composite coatings and role of zeta potentials in co-deposition process, Surf. Coatings Technol. 249 (2014) 118–124. doi:10.1016/j.surfcoat.2014.03.054.

[116] S. Yeh, C. Wan, Codeposition of SiC powders with nickel in a Watts bath, J. Appl. Electrochem. 24 (1994) 993–1000.

[117] V.P. Greco, W. Baldauf, Electrodeposition of Ni-Al_2O_3, Ni-TiO_2 and Cr-TiO_2 Dispersion Hardened Alloys, Plating. 55 (1968) 250–257.

[118] C. Yee-Shyi, L.E.E. Jin-Yuan, Wear resistant nickel composite coating from bright nickel baths with suspended very low concentration alumina, Mater. Chem. Phys. 20 (1988) 309–321.

[119] R. Bazzard, P.J. Boden, Nickel-Chromium Alloys by Codeposition: Part I—Codeposition of Chromium Particles in a Nickel Matrix, Trans. IMF. 50 (1972) 63–69.

[120] Y. Suzuki, O. Asai, Adsorption-Codeposition Process of Al_2O_3 Particles onto Ag-Al2 O 3 Dispersion Films, J. Electrochem. Soc. 134 (1987) 1905–1910.

[121] J.W. Graydon, D.W. Kirk, Suspension electrodeposition of phosphorus and copper, J. Electrochem. Soc. 137 (1990) 2061–2066.

[122] R. Balaji, M. Pushpavanam, K.Y. Kumar, K. Subramanian, Electrodeposition of bronze-PTFE composite coatings and study on their tribological characteristics, Surf. Coatings Technol. 201 (2006) 3205–3211. doi:10.1016/j.surfcoat.2006.06.039.

[123] G. Sharma, R.K. Yadava, V.K. Sharma, Characteristics of electrocodeposited Ni-Co-SiC composite coating, Bull. Mater. Sci. 29 (2006) 491–496. doi:10.1007/BF02914080.

[124] G. Maurin, A. Lavanant, Electrodeposition of nickel/silicon carbide composite coatings on a rotating disc electrode, J. Appl. Electrochem. 25 (1995) 1113–1121.

[125] J. Sadowska-Mazur, M.E. Warwick, Electrodeposition and properties of tin-nickel/silicon carbide composite coatings, Trans. IMF. 64 (1986) 142–148.

[126] H. Abi-akar, C. Riley, G. Maybee, Electrocodeposition of Nickel - Diamond and Cobalt - Chromium Carbide in Low Gravity, Chem. Mater. 4756 (1996) 2601–2610. doi:10.1021/cm950483j.

[127] S.A. Watson, J. Edwards, An investigation of the mechanism of levelling in electrodeposition, Trans. IMF. 34 (1956) 167–198.

[128] N. Zhao-xia, F. CAO, W. Wang, Z. Zhang, J. Zhang, C. CAO, Electrodeposition of Ni-SiC nano-composite coating, Trans. Nonferrous Met. Soc. China. 17 (2007) 9–15.

[129] A. Fahami, B. Nasiri-tabrizi, M. Rostami, R. Ebrahimi-kahrizsangi, Influence of surfactants on the characteristics of nickel matrix nanocomposite coatings, ISRN Electrochem. (2013). doi:10.1155/2013/486050.

[130] N.K. Shrestha, M. Kawai, T. Saji, Co-deposition of B_4C particles and nickel under the influence of a redox-active surfactant and anti-wear property of the coatings, Surf. Coatings Technol. 200 (2005) 2414–2419. doi:10.1016/j.surfcoat.2004.08.192.

[131] F.C. Walsh, C. Ponce de Leon, A review of the electrodeposition of metal matrix composite coatings by inclusion of particles in a metal layer: an established and diversifying technology, Trans. IMF. 92 (2014) 83–98.

[132] Y. Chang, Y. Changb, C. Linb, Process aspects of the electrolytic codeposition of molybdenum disulfide with nickel, 43 (1998) 315–324.

[133] L.M. Wang, Effect of surfactant BAS on MoS_2 codeposition behaviour, J. Appl. Electrochem. 38 (2008) 245–249. doi:10.1007/s10800-007-9432-z.

[134] D.P. Weston, Y.Q. Zhu, D. Zhang, C. Miller, D.G. Kingerley, C. Carpenter, S.J. Harris, N.J. Weston, Co-electrodeposition of inorganic fullerene (IF-WS2) nano-particles with cobalt from a gluconate bath with anionic and cationic surfactants, Electrochim. Acta. 56 (2011) 6837–6846. doi:10.1016/j.electacta.2011.05.093.

[135] L. Wang, Y. Gao, H. Liu, Q. Xue, T. Xu, Effects of bivalent Co ion on the co-deposition of nickel and nano-diamond particles, Surf. Coatings Technol. 191 (2005) 1–6. doi:10.1016/j.surfcoat.2004.03.047.

[136] M. Pushpavanam, S.R. Natarajan, Nickel-boron nitride electrocomposites, Met. Finish. 93 (1995) 97–99. doi:10.1016/0026-0576(95)96247-L.

[137] A. Góral, E. Bełtowska-Lehman, P. Indyka, Structure Characterization of Ni/Al_2O_3 Composite Coatings Prepared by Electrodeposition, Solid State Phenom. 163 (2010) 64–67. doi:10.4028/www.scientific.net/SSP.163.64.

[138] S. Özkan, G. Hapçi, G. Orhan, K. Kazmanli, Electrodeposited Ni/SiC nanocomposite coatings and evaluation of wear and corrosion properties, Surf. Coatings Technol. 232 (2013) 734–741. doi:10.1016/j.surfcoat.2013.06.089.

[139] Y.J. Xue, J.S. Li, W. Ma, Y.W. Zhou, M. De Duan, Sliding wear behaviors of electrodeposited nickel composite coatings containing micrometer and nanometer La_2O_3 particles, J. Mater. Sci. 41 (2006) 1781–1784. doi:10.1007/s10853-006-3947-2.

[140] S.T. Aruna, S. Diwakar, A. Jain, K.S. Rajam, Comparative study on the effect of current density on Ni and Ni–Al_2O_3 nanocomposite coatings produced by electrolytic deposition, Surf. Eng. 21 (2005) 209–214. doi:10.1179/174329405X50037.

[141] X.J. Sun, J.G. Li, Friction and wear properties of electrodeposited nickel-titania nanocomposite coatings, Tribol. Lett. 28 (2007) 223–228. doi:10.1007/s11249-007-9254-5.

[142] M. Srivastava, V.K. William Grips, K.S. Rajam, Electrodeposition of Ni-Co composites containing nano-CeO_2 and their structure, properties, Appl. Surf. Sci. 257 (2010) 717–722. doi:10.1016/j.apsusc.2010.07.046.

[143] M. Karbasi, N. Yazdian, A. Vahidian, Development of electro-co-deposited Ni-TiC nano-particle reinforced nanocomposite coatings, Surf. Coatings Technol. 207 (2012) 587–593. doi:10.1016/j.surfcoat.2012.07.083.

[144] R. Weil, The Origins of Stress in Electrodeposition: Part 1, Plating. 57 (1970) 123.

[145] R. Weil, The Origins of Stress in Electrodeposition: Part 2, Plating. 58 (1971) 50, 137.

[146] A.T. Vagramyan, Z.A. Solov'eva, Technology of Electrodeposition, Robert Draper Ltd., Teddington, England, 1961.

[147] E. Raub, K. Muller, Fundamentals of Metal Deposition, Elsevier, New York, 1967.

[148] J.W. Dini, Stress, in: Mater. Sci. Coatings Substrates, Noyes, Westwood, New Jersey, 1993.

[149] J.L. Marti, The effect of some variables upon Internal stress of nickel as deposited from sulfamate electrolytes, Plating. 53 (1966) 61–71.

[150] J.B. Kushner, Stress in Electroplated Metals, Met. Prog. 81 (1962) 88.

[151] K. Parker, H. Shah, Residual Stress in Electroless Nickel Plating, Plating. 58 (1971) 230–236.

[152] J.B. Kushner, Factors Affecting Residual Stress in Electrodeposited Metals, Met. Finish. 56 (1958) 81.

[153] E.S. Güler, E. Konca, İ. Karakaya, Investigation of the tribological behaviour of electrocodeposited Ni-MoS2 composite coatings, Int. J. Surf. Sci. Eng. 11 (2017).

[154] COMSOL Multiphysics Reference Manual, (2018). www.comsol.com.

[155] ASTM-G99-95a, Standard Test Method for Wear Testing with a Pin-on-disk Apparatus, ASTM International, 2000.

[156] E.S. Güler, E. Konca, İ. Karakaya, Effect of Electrodeposition Parameters on the Current Density of Hydrogen Evolution Reaction in Ni and Ni-MoS_2 Composite Coatings, Int. J. Electrochem. Sci. 8 (2013) 5496–5505.

[157] A.M. Rashidi, A. Amadeh, The effect of current density on the grain size of electrodeposited nanocrystalline nickel coatings, Surf. Coatings Technol. 202 (2008) 3772–3776. doi:10.1016/j.surfcoat.2008.01.018.

[158] A. Góral, L. Lityńska-Dobrzyńska, M. Kot, Effect of Surface Roughness and Structure Features on Tribological Properties of Electrodeposited Nanocrystalline Ni and Ni/Al_2O_3 Coatings, J. Mater. Eng. Perform. 26 (2017) 2118–2128. doi:10.1007/s11665-017-2662-2.

[159] L. Du, B. Xu, S. Dong, H. Yang, Y. Wu, Preparation, microstructure and tribological properties of nano-Al_2O_3/Ni brush plated composite coatings, Surf. Coatings Technol. 192 (2005) 311–316. doi:10.1016/j.surfcoat.2004.06.008.

[160] H. Gül, M. Uysal, H. Akbulut, A. Alp, Effect of PC electrodeposition on the structure and tribological behavior of Ni-Al_2O_3 nanocomposite coatings, Surf. Coatings Technol. 258 (2014) 1202–1211. doi:10.1016/j.surfcoat.2014.07.002.

[161] Z. Pala, N. Ganev, X-ray Diffraction Study of Distribution of Macroscopic Residual Stresses in Surface Layers of Steels After Grinding, Mater. Struct. 14 (2007) 78–83.

[162] A.M. El-Sherik, J. Shirokoff, U. Erb, Stress measurements in nanocrystalline Ni electrodeposits, J. Alloys Compd. 389 (2005) 140–143. doi:10.1016/j.jallcom.2004.08.010.

[163] F. Erler, C. Jakob, H. Romanus, L. Spiess, B. Wielage, T. Lampke, S. Steinhäuser, Interface behaviour in nickel composite coatings with nano-particles of oxidic ceramic, Electrochim. Acta. 48 (2003) 3063–3070. doi:10.1016/S0013-4686(03)00380-3.

[164] J. Alexis, B. Etcheverry, J.D. Beguin, J.P. Bonino, Structure, morphology and mechanical properties of electrodeposited composite coatings Ni-P/SiC, Mater. Chem. Phys. 120 (2010) 244–250. doi:10.1016/j.matchemphys.2009.12.013.

[165] F. Cai, C. Jiang, Influences of Al particles on the microstructure and property of electrodeposited Ni-Al composite coatings, Appl. Surf. Sci. 292 (2014) 620–625. doi:10.1016/j.apsusc.2013.12.021.

[166] T.D. Ziebell, C.A. Schuh, Residual stress in electrodeposited nanocrystalline nickel-tungsten coatings, J. Mater. Res. 27 (2012) 1271–1284. doi:10.1557/jmr.2012.51.

[167] S. Pathak, M. Guinard, M.G.C. Vernooij, B. Cousin, Z. Wang, J. Michler, L. Philippe, Influence of lower current densities on the residual stress and structure of thick nickel electrodeposits, Surf. Coatings Technol. 205 (2011) 3651–3657. doi:10.1016/j.surfcoat.2011.01.012.

[168] M. Saitou, S. Oshiro, Y. Sagawa, Scaling behavior of internal stress in electrodeposited nickel thin films, J. Appl. Phys. 104 (2008). doi:10.1063/1.3009336.

[169] W. Gang, L. Ning, Z. Derui, M. Kurachi, Electrodeposited Co-Ni-Al_2O_3 composite coatings, Surf. Coatings Technol. 176 (2003) 157–164. doi:10.1016/S0257-8972.

[170] R.A. Shakoor, R. Kahraman, U. Waware, Y. Wang, W. Gao, Properties of electrodeposited Ni-B-Al_2O_3 composite coatings, Mater. Des. 64 (2014) 127–135. doi:10.1016/j.matdes.2014.07.026.

[171] M.H. Allahyarzadeh, M. Aliofkhazraei, A.R.S. Rouhaghdam, V. Torabinejad, Electrodeposition of Ni-W-Al_2O_3 nanocomposite coating with functionally graded microstructure, J. Alloys Compd. 666 (2016) 217–226. doi:10.1016/j.jallcom.2016.01.031.

[172] H. Gül, F. Kilic, S. Aslan, A. Alp, H. Akbulut, Characteristics of electro-co-deposited Ni-Al_2O_3 nano-particle reinforced metal matrix composite (MMC) coatings, Wear. 267 (2009) 976–990. doi:10.1016/j.wear.2008.12.022.

[173] A. Jegan, R. Venkatesan, Characterization and optimization of pulse electrodeposition of Ni/nano-Al_2O_3 composite coatings, Int. J. Miner. Metall. Mater. 20 (2013) 479–485. doi:10.1007/s12613-013-0754-z.

[174] Y. Tsuru, H. Imoto, R. Takamatsu, K. Hosokawa, Effects of boric acid and plating bath pH on the preferred crystal orientation and internal strain in electrically deposited nickel films, J. Surf. Finish. Soc. Japan. 45 (1994) 82–87.

[175] P. Gyftou, M. Stroumbouli, E.A. Pavlatou, P. Asimidis, N. Spyrellis, Tribological study of Ni matrix composite coatings containing nano and micro SiC particles, Electrochim. Acta. 50 (2005) 4544–4550. doi:10.1016/j.electacta.2004.10.090.

[176] E.A. Pavlatou, M. Stroumbouli, P. Gyftou, N. Spyrellis, Hardening effect induced by incorporation of SiC particles in nickel electrodeposits, J. Appl. Electrochem. 36 (2006) 385–394. doi:10.1007/s10800-005-9082-y.

[177] N.B. Brookes, A. Clarke, P.D. Johnson, Electronic and magnetic structure of bcc nickel, Phys. Rev. B. 46 (1992) 237–241. doi:10.1103/PhysRevB.46.237.

[178] W.M. Haynes, CRC Handbook of Chemistry and Physics, 97th ed., CRC Press, 2017.

[179] ICDD (2017). PDF-4+ 2017 (Database), edited by Dr. Soorya Kabekkodu, International Centre for Diffraction Data, Newtown Square, PA, USA.

APPENDIX A

Results of Properties of Composite Coatings

Table A.1 Overall results for hardness, wear rate and COF

Al_2O_3 Particle (g/l)	i (A/dm^2)	SLS (g/l)	ALS (g/l)	Hardness ($HV_{0.2}$)	COF	Wear rate x 10^3 ($mm^3/N/m$)
5	2	0	0	439 ± 17	0.475	41.95 ± 0.19
5	5	0	0	377 ± 10	0.436	32.81 ± 0.12
5	8	0	0	363 ± 9	0.514	33.42 ± 0.11
5	2	0	0.12	426 ± 12	0.456	27.13 ± 0.17
5	5	0	0.12	373 ± 11	0.539	27.8 ± 0.09
5	8	0	0.12	358 ± 14	0.407	29.1 ± 0.13
5	2	0	0.25	446 ± 13	0.526	25.35 ± 0.14
5	5	0	0.25	411 ± 19	0.472	25.52 ± 0.12
5	8	0	0.25	358 ± 14	0.519	24.67 ± 0.11
5	2	0.12	0	269 ± 5	0.375	26.48 ± 0.08
5	5	0.12	0	247 ± 8	0.361	26.37 ± 0.11
5	8	0.12	0	246 ± 9	0.525	24.48 ± 0.06
5	2	0.12	0.12	447 ± 19	0.596	23.82 ± 0.1
5	5	0.12	0.12	336 ± 10	0.544	27.7 ± 0.15
5	8	0.12	0.12	295 ± 9	0.391	27.51 ± 0.09
5	2	0.12	0.25	500 ± 14	0.414	24.25 ± 0.06
5	5	0.12	0.25	405 ± 23	0.661	21.78 ± 0.07
5	8	0.12	0.25	331 ± 7	0.392	28.86 ± 0.1
5	2	0.25	0	241 ± 5	0.411	23.77 ± 0.16
5	5	0.25	0	253 ± 14	0.453	26.51 ± 0.12
5	8	0.25	0	250 ± 7	0.444	28.74 ± 0.13
5	2	0.25	0.12	375 ± 5	0.419	27.22 ± 0.09
5	5	0.25	0.12	374 ± 7	0.419	30.14 ± 0.12
5	8	0.25	0.12	313 ± 15	0.483	27.05 ± 0.12
5	2	0.25	0.25	546 ± 16	0.413	29.13 ± 0.04
5	5	0.25	0.25	410 ± 4	0.478	26.38 ± 0.21
5	8	0.25	0.25	372 ± 5	0.561	23.09 ± 0.12
10	2	0	0	282 ± 7	0.447	25.77 ± 0.07
10	5	0	0	370 ± 13	0.425	25.53 ± 0.05
10	8	0	0	298 ± 15	0.361	25.19 ± 0.09
10	2	0	0.12	459 ± 26	0.457	37.02 ± 0.18
10	5	0	0.12	366 ± 10	0.489	32.5 ± 0.16

Table A.1 (continued) Overall results for hardness, wear rate and COF

10	8	0	0.12	329 ± 14	0.464	29.91 ± 0.14
10	2	0	0.25	560 ± 12	0.442	22.72 ± 0.1
10	5	0	0.25	406 ± 27	0.511	25.68 ± 0.13
10	8	0	0.25	344 ± 13	0.55	27.3 ± 0.07
10	2	0.12	0	285 ± 10	0.447	30.12 ± 0.17
10	5	0.12	0	260 ± 2	0.475	32.1 ± 0.13
10	8	0.12	0	259 ± 10	0.428	20.41 ± 0.08
10	2	0.12	0.12	429 ± 24	0.415	23.41 ± 0.08
10	5	0.12	0.12	331 ± 8	0.442	32.41 ± 0.11
10	8	0.12	0.12	329 ± 25	0.385	28.17 ± 0.1
10	2	0.12	0.25	557 ± 25	0.436	26.17 ± 0.12
10	5	0.12	0.25	405 ± 16	0.414	34.64 ± 0.13
10	8	0.12	0.25	315 ± 13	0.361	36.05 ± 0.06
10	2	0.25	0	311 ± 20	0.433	27.23 ± 0.09
10	5	0.25	0	266 ± 9	0.464	30.61 ± 0.17
10	8	0.25	0	285 ± 14	0.378	23.37 ± 0.08
10	2	0.25	0.12	557 ± 25	0.433	24.31 ± 0.06
10	5	0.25	0.12	389 ± 14	0.428	26.42 ± 0.12
10	8	0.25	0.12	303 ± 17	0.475	27.27 ± 0.11
10	2	0.25	0.25	597 ± 18	0.481	20.97 ± 0.08
10	5	0.25	0.25	371 ± 14	0.431	24.53 ± 0.11
10	8	0.25	0.25	336 ± 12	0.456	25.19 ± 0.09
15	2	0	0	348 ± 9	0.439	26.5 ± 0.21
15	5	0	0	405 ± 14	0.425	30.68 ± 0.18
15	8	0	0	362 ± 13	0.469	28.14 ± 0.13
15	2	0	0.12	442 ± 15	0.475	29.98 ± 0.11
15	5	0	0.12	374 ± 10	0.492	26.85 ± 0.12
15	8	0	0.12	319 ± 8	0.375	25.93 ± 0.18
15	2	0	0.25	513 ± 34	0.483	26.18 ± 0.12
15	5	0	0.25	401 ± 15	0.528	21.93 ± 0.07
15	8	0	0.25	374 ± 17	0.369	29.68 ± 0.1
15	2	0.12	0	274 ± 7	0.493	37.59 ± 0.22
15	5	0.12	0	283 ± 8	0.453	32.58 ± 0.16
15	8	0.12	0	273 ± 9	0.461	22.73 ± 0.09
15	2	0.12	0.12	371 ± 5	0.443	29.61 ± 0.1
15	5	0.12	0.12	289 ± 15	0.411	32.56 ± 0.11
15	8	0.12	0.12	274 ± 12	0.409	34.05 ± 0.07
15	2	0.12	0.25	493 ± 7	0.442	31.13 ± 0.12
15	5	0.12	0.25	363 ± 10	0.45	26.62 ± 0.05
15	8	0.12	0.25	310 ± 5	0.356	25.77 ± 0.12
15	2	0.25	0	300 ± 5	0.406	32.18 ± 0.12
15	5	0.25	0	279 ± 9	0.425	28.35 ± 0.04

Table A.1 (continued) Overall results for hardness, wear rate and COF

15	8	0.25	0	268 ± 14	0.427	29.72 ± 0.07
15	2	0.25	0.12	426 ± 13	0.444	30.92 ± 0.06
15	5	0.25	0.12	324 ± 21	0.443	26.06 ± 0.14
15	8	0.25	0.12	293 ± 13	0.442	32.77 ± 0.06
15	2	0.25	0.25	479 ± 5	0.415	31.89 ± 0.11
15	5	0.25	0.25	349 ± 11	0.456	29.54 ± 0.23
15	8	0.25	0.25	318 ± 15	0.517	33.67 ± 0.06

APPENDIX B

Counter Plots of Properties

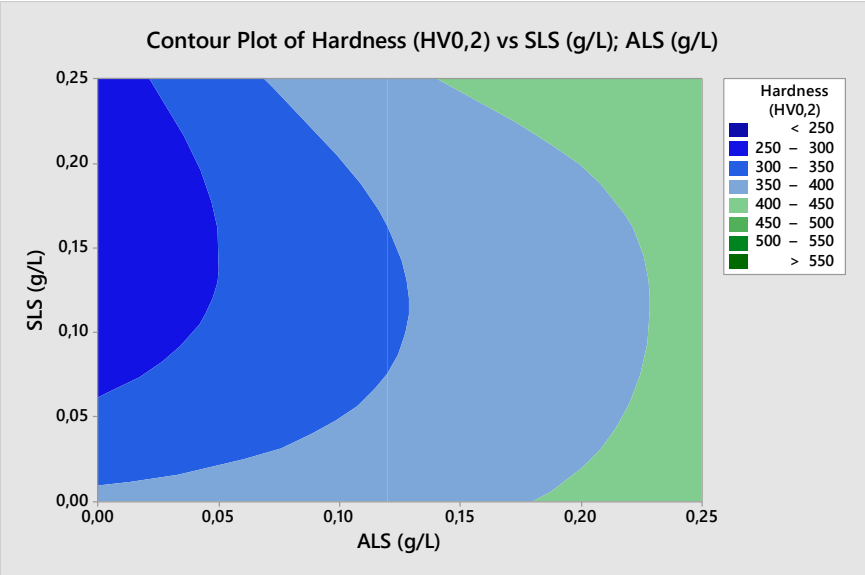

Figure B.1 The counter plot for hardness values for different SLS and ALS addition

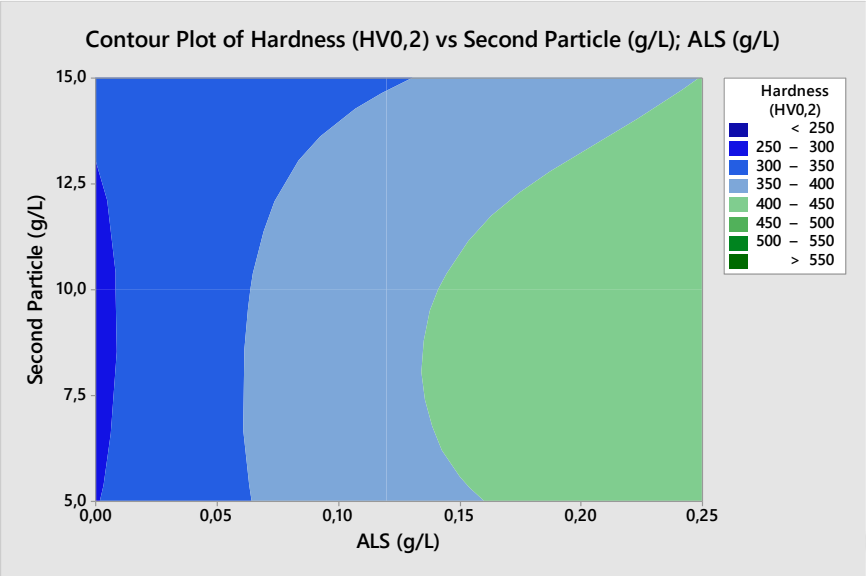

Figure B.2 The counter plot for hardness values for different ALS and the second phase particles in the electrolye

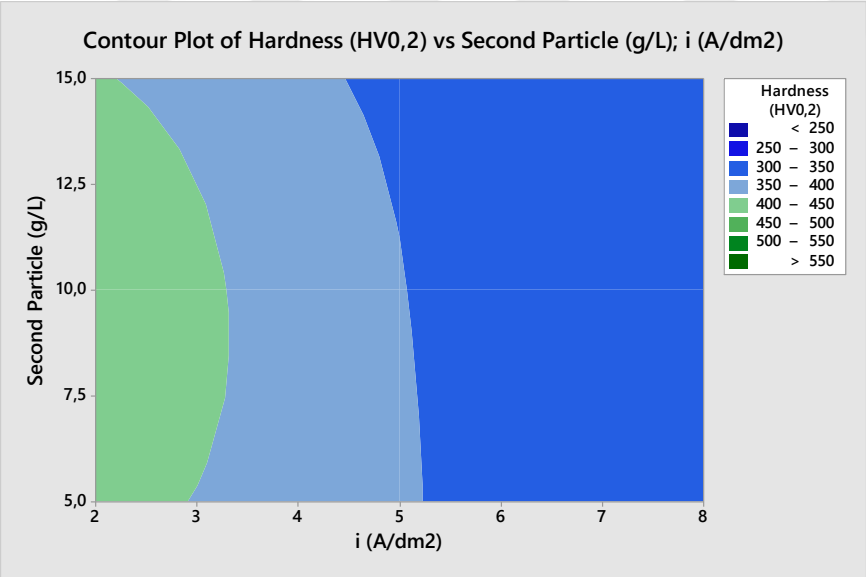

Figure B.3 The counter plot for hardness values with respect to the amount of second phase particle and current density

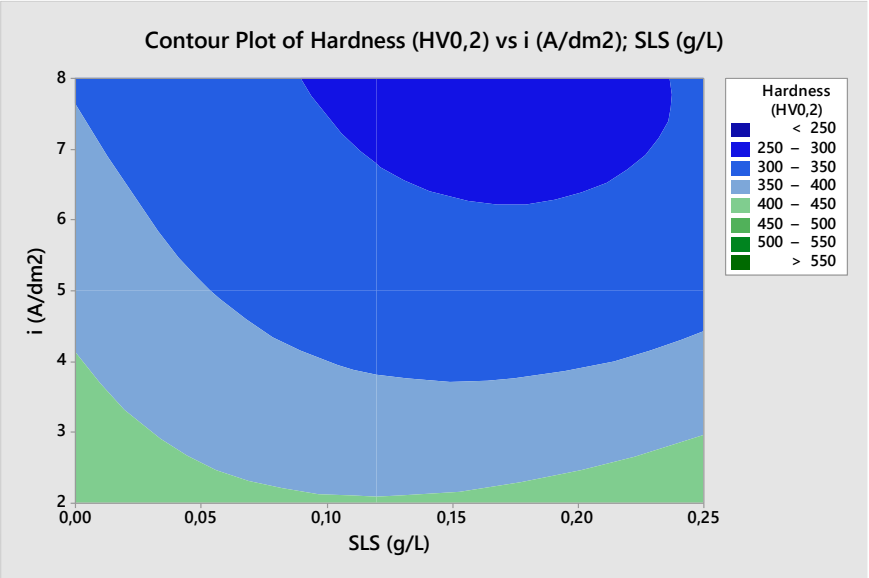

Figure B.4 The counter plot for hardness values with respect to the amount of SLS and current density

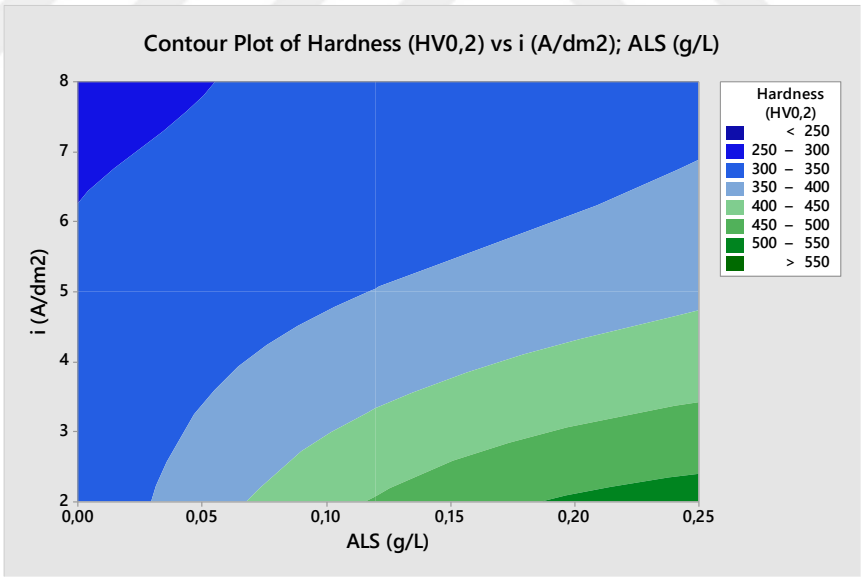

Figure B.5 The counter plot for hardness values with respect to the amount of ALS and current density

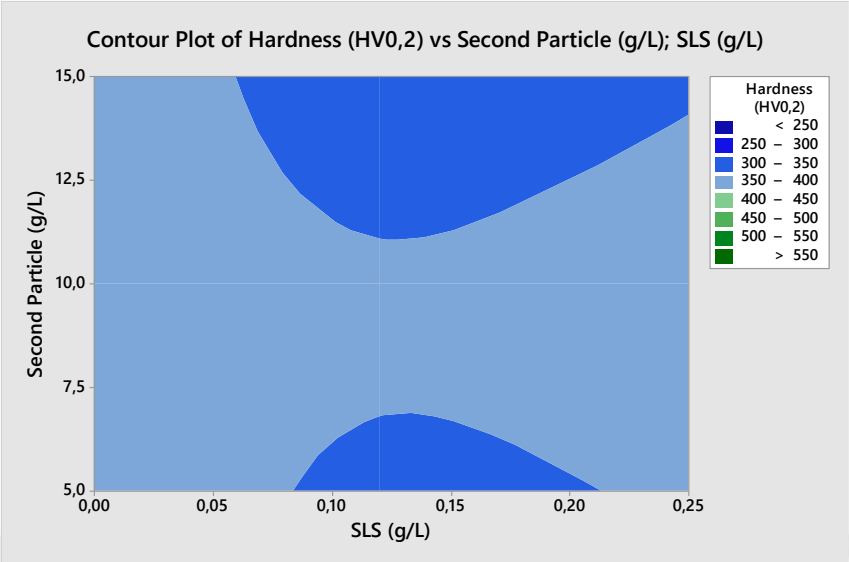

Figure B.6 The counter plot for hardness values with respect to the amount of second phase particles and SLS

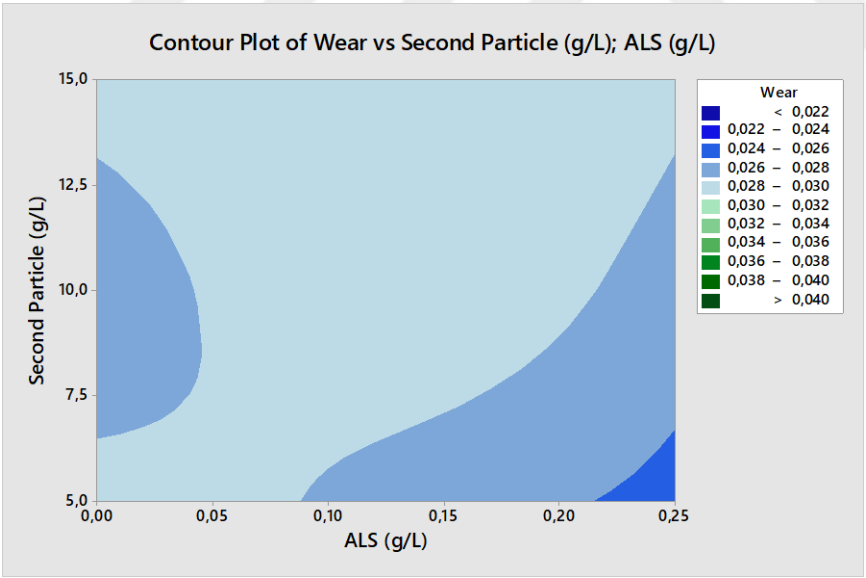

Figure B.7 The counter plot for wear rate with respect to the amount of second phase particle and ALS in the electrolyte

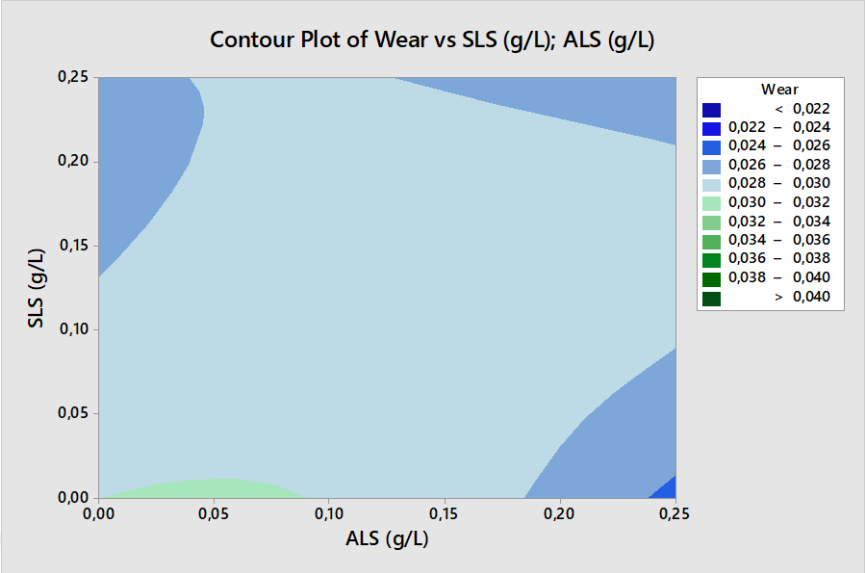

Figure B.8 The counter plot for wear rate with respect to the amount of SLS and ALS

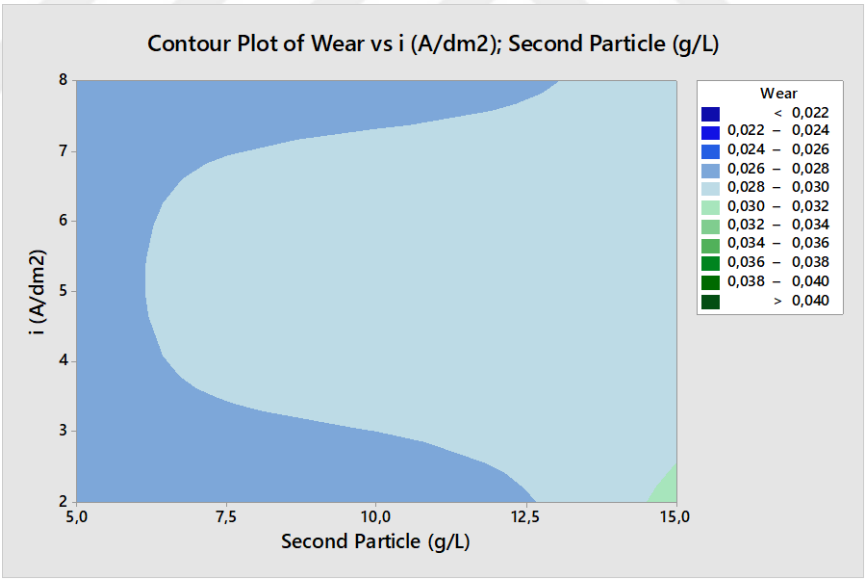

Figure B.9 The counter plot for wear rate with respect to current density and the amount of second phase particle

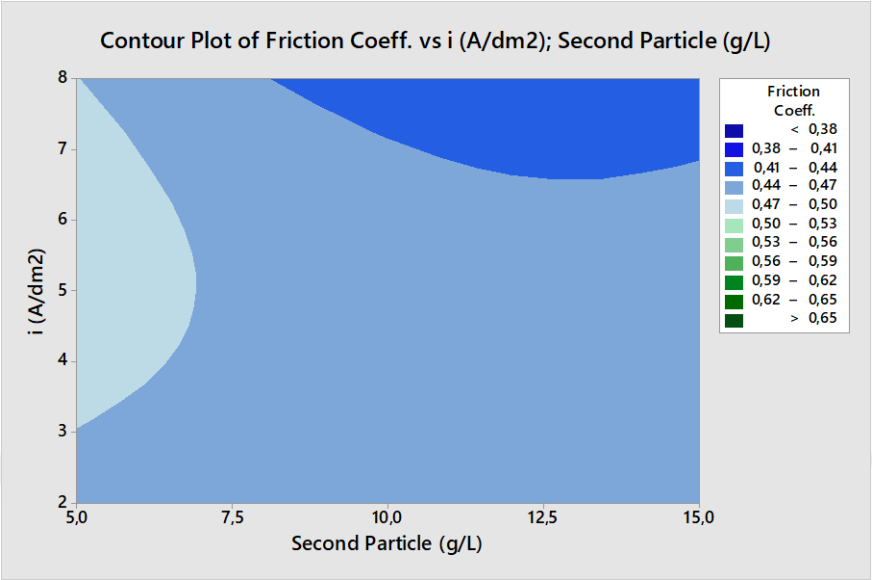

Figure B.10 The counter plot for COF with respect to current density and second phase particle amount in the electrolyte

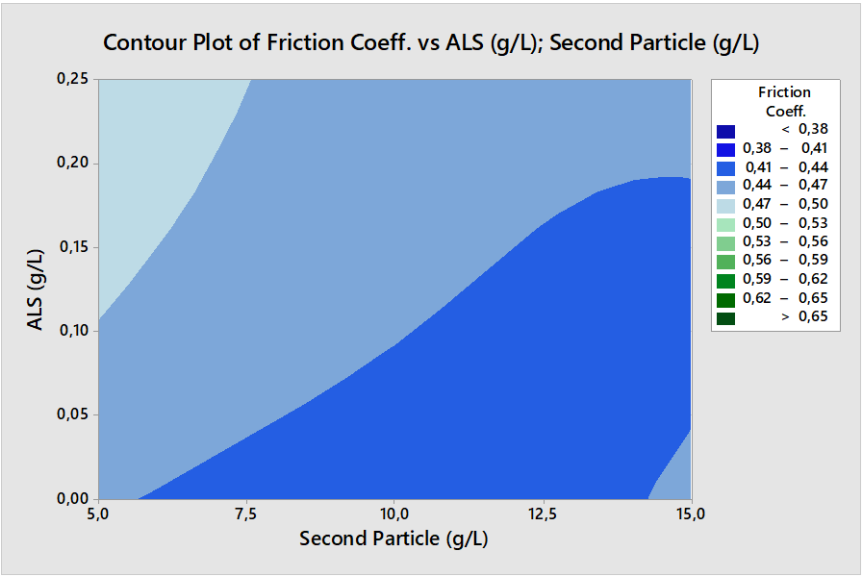

Figure B.11 The counter plot for COF with respect to the amount of ALS and Al_2O_3

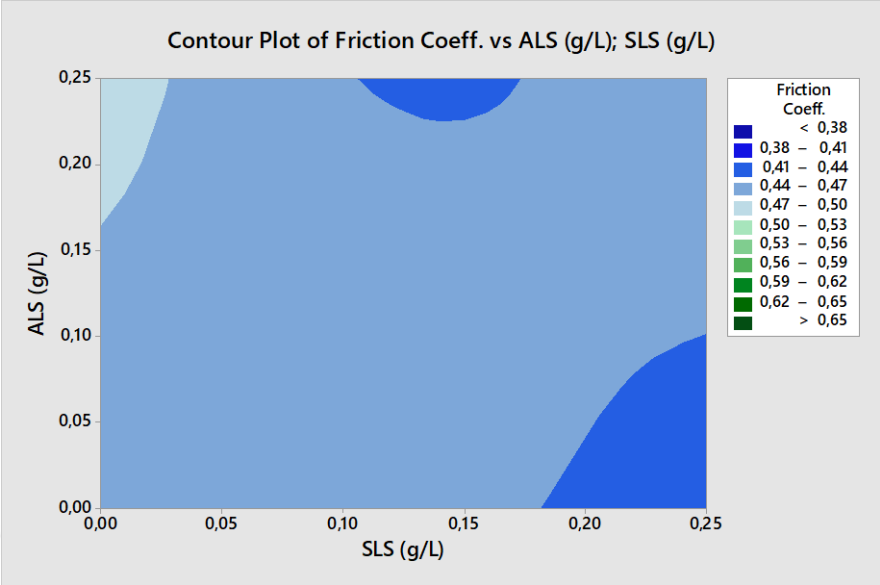

Figure B.12 The counter plot for COF with respect to the amount of ALS and SLS

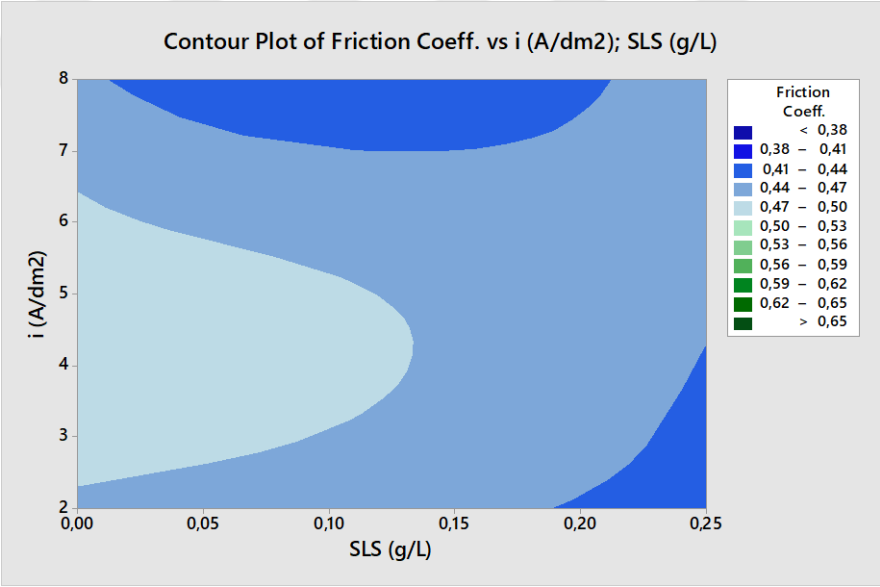

Figure B.13 The counter plot for COF with respect to the current density and SLS amount

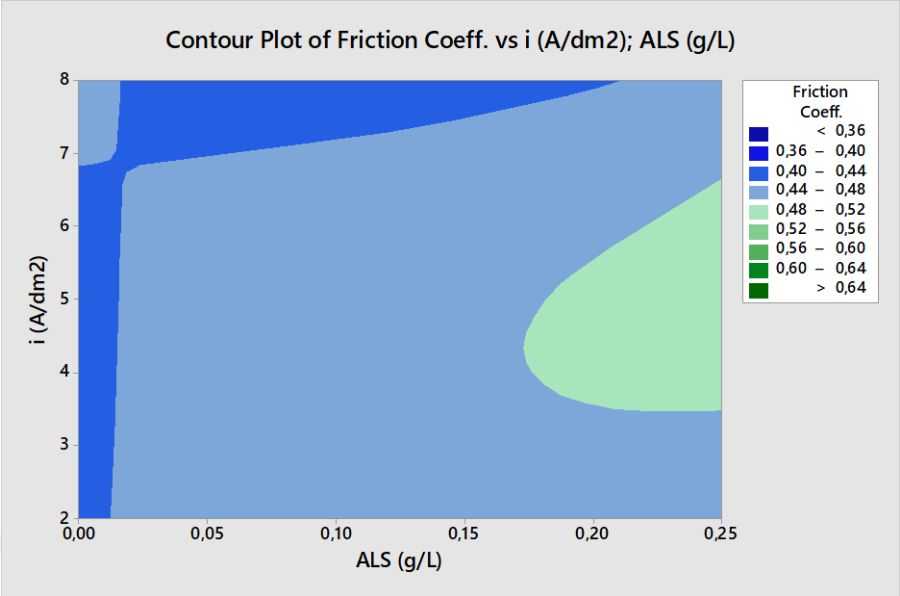

Figure B.14 The counter plot for COF with respect to the current density and the amount of ALS in the electrolyte

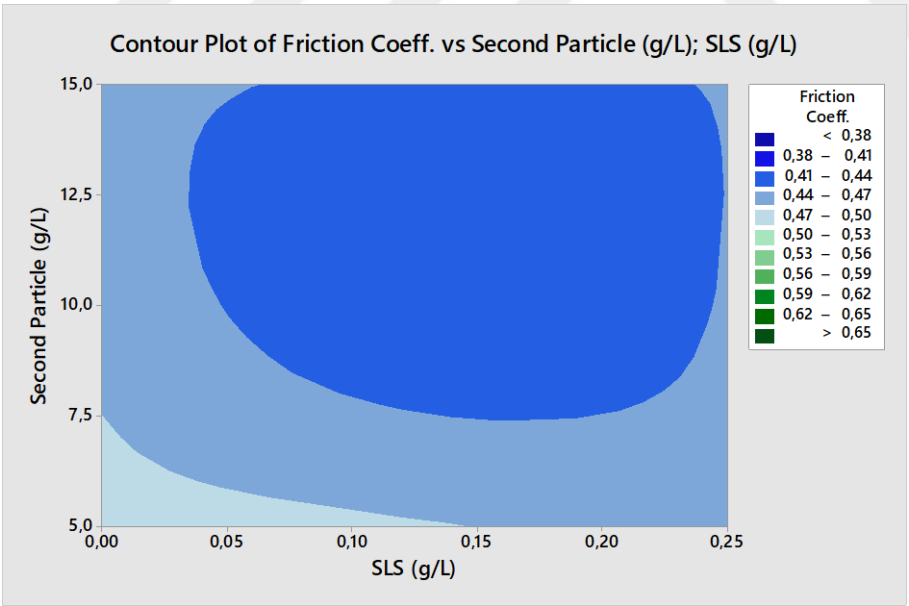

Figure B.15 The counter plot for COF with respect to amount of SLS and Al_2O_3

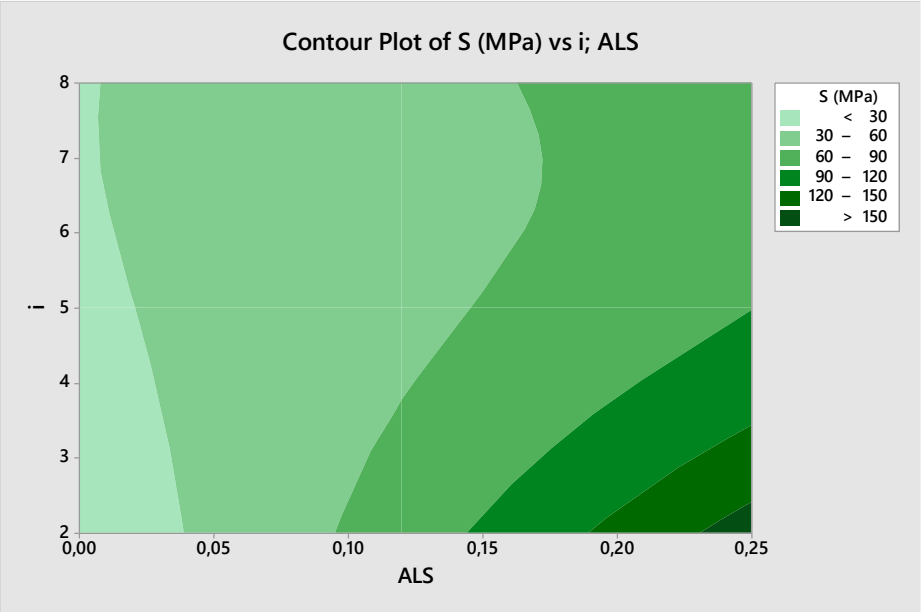

Figure B.16 The counter plot for internal stress with respect the current density and ALS amount

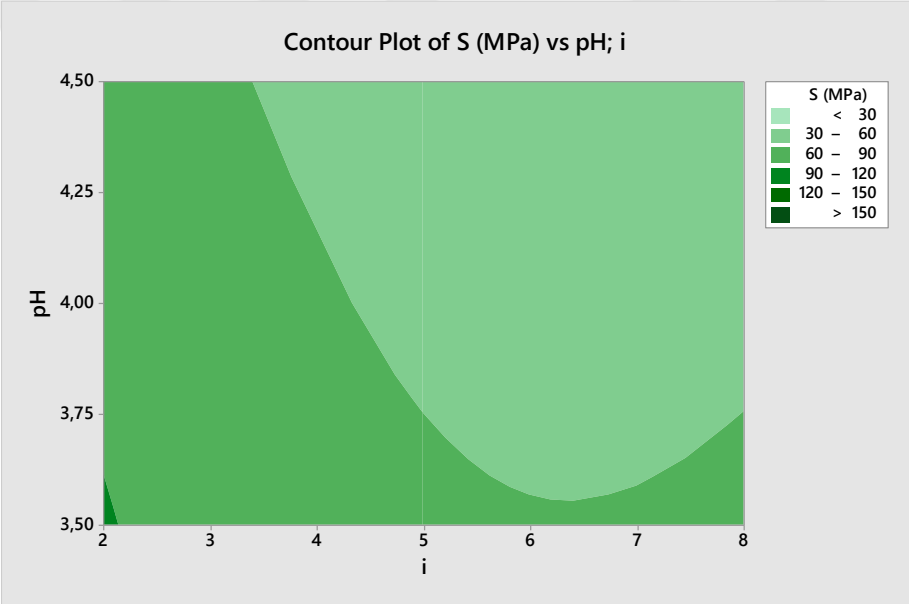

Figure B.17 The counter plot for internal stress with respect to pH and current density

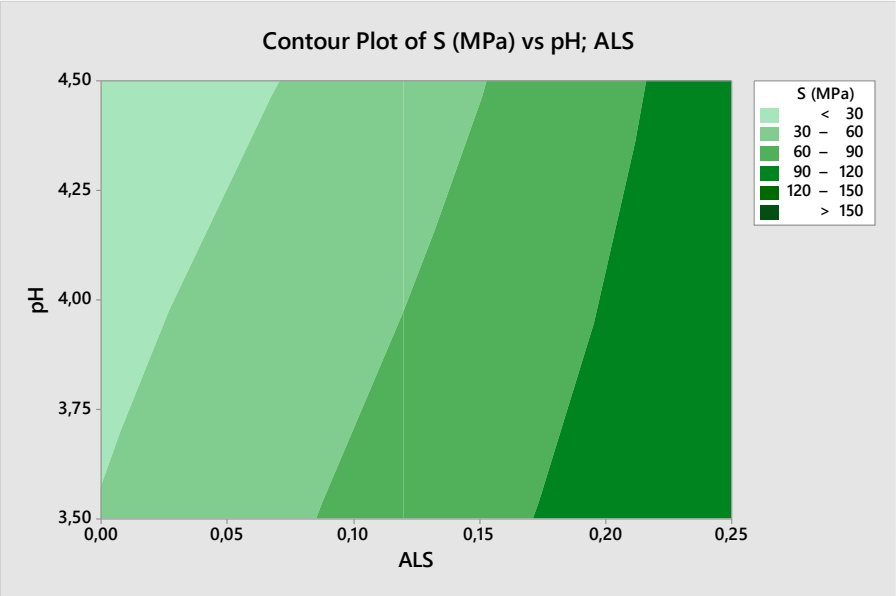

Figure B.18 The counter plot for internal stress with respect to pH and ALS amount

APPENDIX C

Interaction Plots and COF Measurements

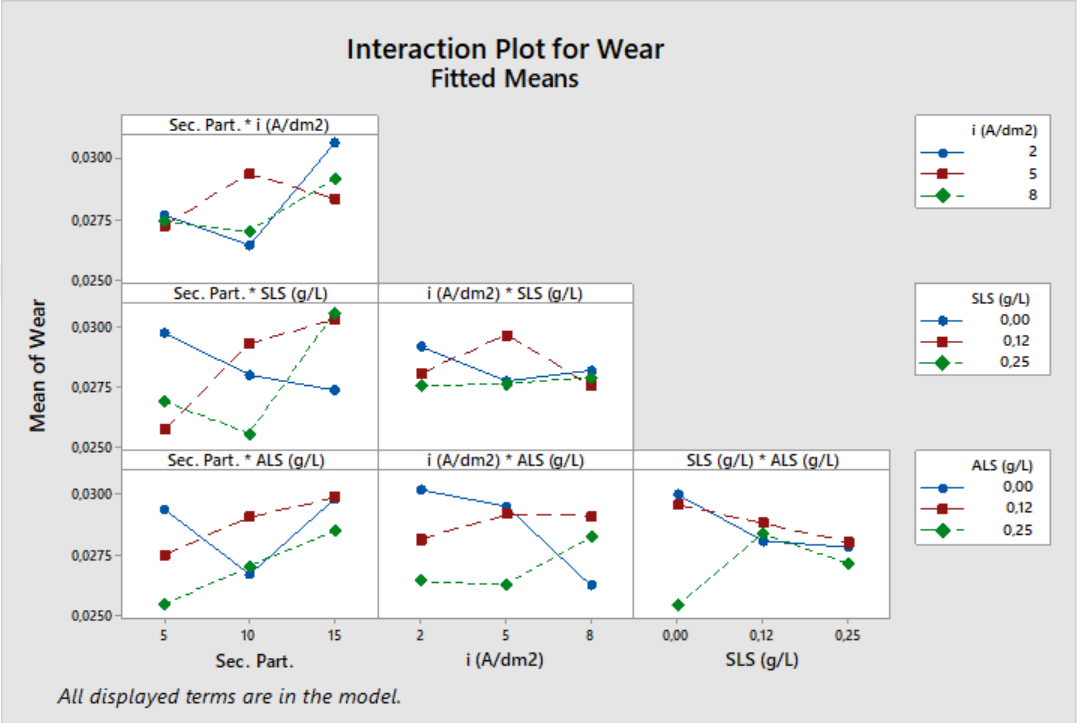

Figure C.1 Interaction plot for wear rate

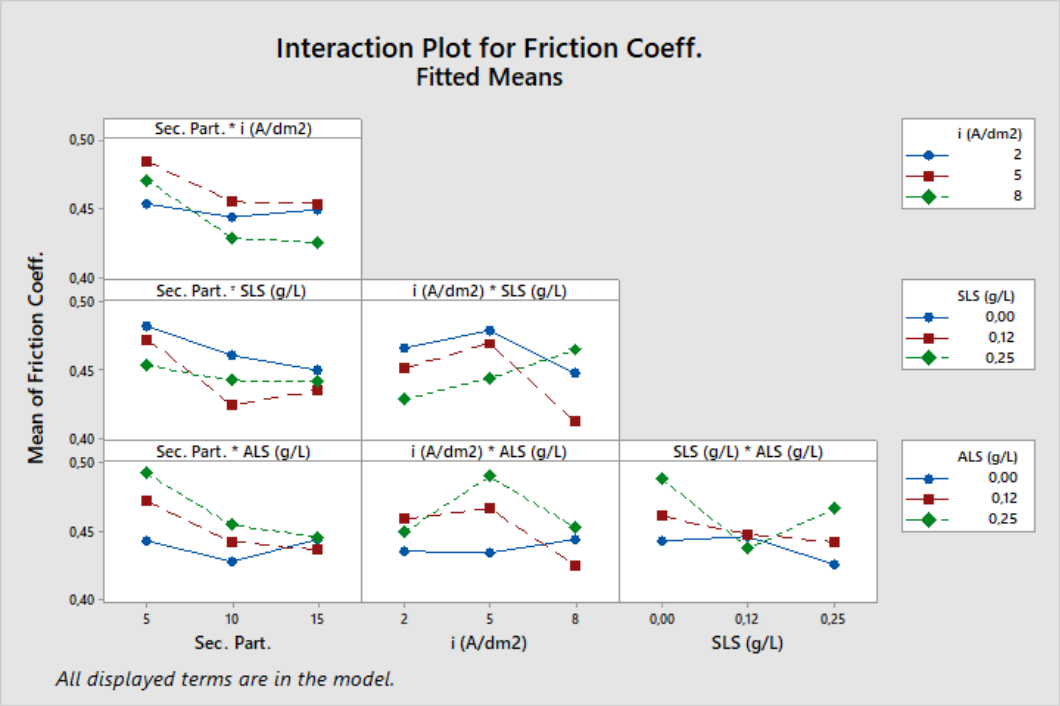

Figure C.2 Interaction plot for COF

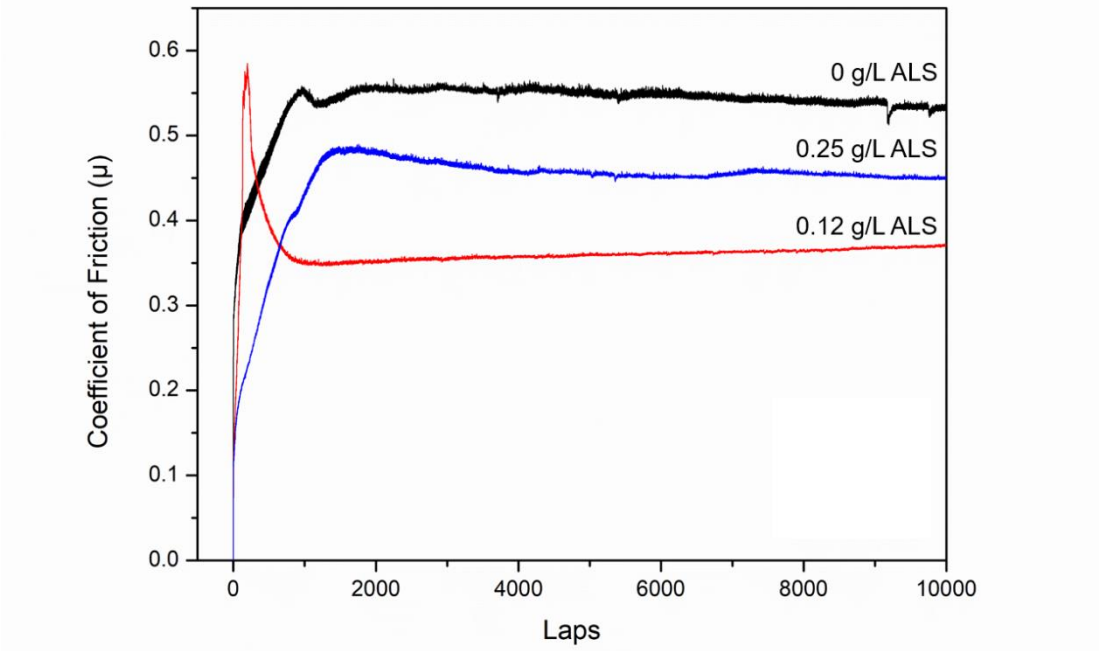

Figure C.3 COF measurements at three different ALS amount

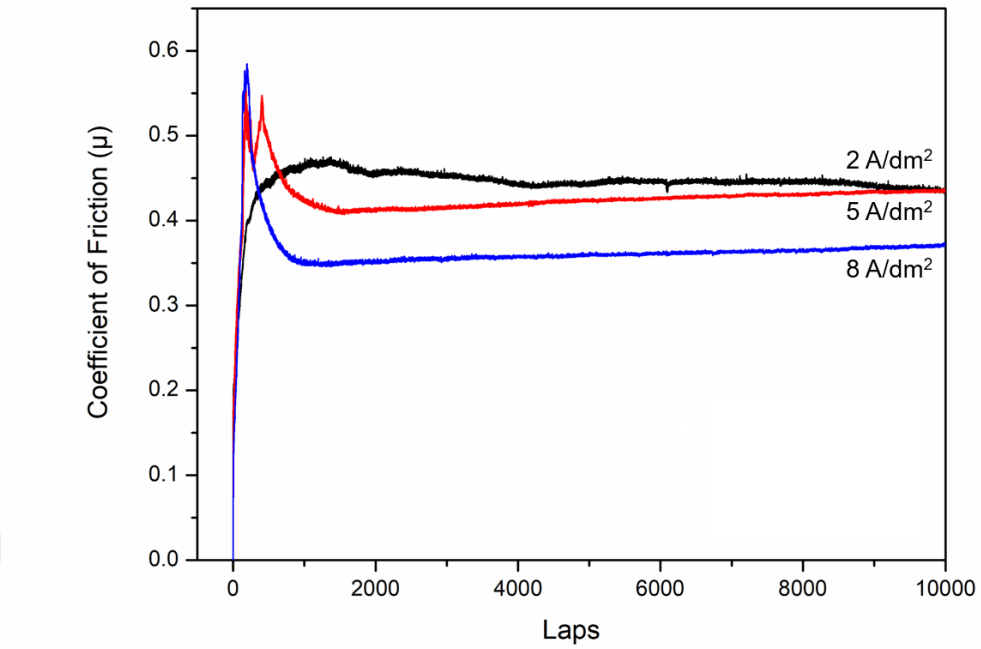

Figure C.4 COF measurements at three different current densities